TESTING OF NOVEL ANTIFOULING CONCEPTS

A DISSERTATION

Submitted in partial fulfilment of the
requirements for the award of the degree
of

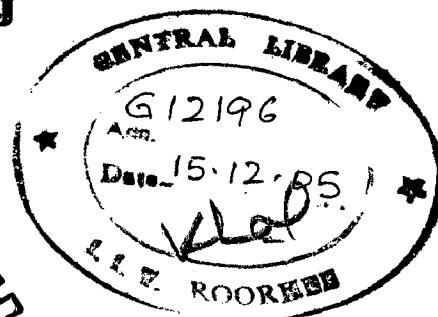MASTER OF TECHNOLOGY

in

CHEMICAL ENGINEERING

(With Specialization in Industrial Pollution Abatement)

By

S. NATARAJ

DEPARTMENT OF CHEMICAL ENGINEERING
INDIAN INSTITUTE OF TECHNOLOGY ROORKEE
ROORKEE-247 667 (INDIA)

JUNE, 2005

CANDIDATE'S DECLARATION

I hereby declare that the work which is being presented in thesis Entitled "**Testing of Novel Antifouling Concepts** " in partial fulfilment of the requirements for the award of the degree of Master of Technology in Chemical Engineering with specialization in "Industrial Pollution Abatement", submitted in the Department of Chemical Engineering, Indian Institute of Technology, Roorkee, India is an authentic record of my own work carried out during the period from September 2004 to May 2005, under the kind guidance of Prof. Dr. R. Schomäcker, Technische Universität, Berlin, Germany and Dr. I.M.Mishra, Professor, Department of Chemical Engineering, Indian Institute of Technology, Roorkee, India.

The matter embodied in this thesis has not been submitted for the award of any other degree.

Place : Roorkee
Date : 27/06/2005

(S.Nataraj)

This is to certify that the above statement made by the candidate is correct to the best of our knowledge. We have read this dissertation and that, in our opinion, it is fully adequate in scope and quality as a dissertation for the degree of Master of Technology.

(Prof. Dr. R. Schomäcker)
Technical Chemistry Department
Technische Universität, Berlin.

Prof. Dr. I.M.Mishra
Dept. of Chemical Engineering
IIT Roorkee, India.

Technische Universität Berlin
Prof. Dr. Reinhard Schomäcker
Institut für Chemie - Sekr. TC 8
Straße des 17. Juni 124, D-10623 Berlin

Technische Universität Berlin
Institut für
Verfahrenstechnik
Sekr. MA 5 -7
Str. des 17. Juni 135
10623 Berlin
Fornruf : 314 - 237 01

ABSTRACT

Extracellular polymeric substances (EPS) are viewed as major fouling components during filtration of biological feeds in industry. However, very few studies investigated the fouling mechanisms of polysaccharides, one major group of macromolecules in EPS. In this work, cross flow filtration of Xanthan, Actigum CS 11 and Glucan, model polysaccharides, were carried out and analyzed using "resistance in series model" and "classical filtration laws". The Xanthan and Actigum CS 11 polysaccharide were obtained as powders and Glucan was obtained as concentrated aqueous suspension directly after fermentation step during manufacturing. The cake filtration model appears to fit the entire range of the ultrafiltration data for the polysaccharide solution at low concentration of 20 mg/l with both "resistance in series model" and "classical filtration laws". It was difficult to detect/identify the predominant fouling mechanism with higher concentration of polysaccharide feed suspension with the use of above models. This indicates that the fouling could be the result of combination of two or more fouling mechanisms. For the two types of polysaccharide suspension it was observed that (i) the investigated model polysaccharides contained micro aggregates and the concentration of micro aggregates decreased during filtration runs and it is more pronounced with the aqueous polysaccharide suspension; (ii) viscosity analysis of polysaccharide in the retentate showed that the polysaccharide accumulated in the retentate and removed from the membrane surface and (iii) concentration measurements showed that the major portion of the polysaccharide remained in suspension.

ACKNOWLEDGEMENT

TABLE OF CONTENTS

LIST OF FIGURES

LIST OF TABLES

NOMENCLATURE

Symbol	Description	Unit
ΔP	transmembrane pressure difference	bar
P_{feed}	pressure on feed side of membrane	bar
$P_{permeate}$	pressure on permeate side of membrane	bar
$P_{concentrate}$	pressure on concentrate side of membrane	bar
J	transmembrane flux	l/m^2h
Q_p	permeate flow rate	m^3/s
A_m	membrane surface area	m^2
V	the volume of filtrate that passes through the filter	m^3
t	filtration time	sec
μ	fluid viscosity	cP
R_a	resistance due to adsorption	$1/m$
R_p	resistance due to pore blocking	$1/m$
R_m	hydraulic resistance of the membrane in pure water	$1/m$
R_i	internal irreversible fouling resistance (pore plugging and adsorption)	$1/m$
R_c	resistance due to particle deposit at membrane surface, cake resistance	$1/m$
Q_o	flow rate through unfouled membrane	m^3/h
N_o	number of pores per unit membrane surface area	m^{-2}
d_o	diameter of each pore	nm
C_{PBM}	pore blocking constant, number of pores per unit membrane surface area that become plugged per unit filtrate volume	-
C_{PBM}	pore blocking constant, number of pores per unit membrane surface area that become plugged per unit filtrate volume	-
C_{CFM}	cake filtration resistance constant	-

ρ_o	mass of cake deposited per volume of filtrate	mg/ml
C	mass of particles per volume of filtrate	kg/m^3
L	membrane thickness	m
r_p	average pore radius	m
K_2	he number of plugging particles per volume of filtrate	m^{-3}
N_p	number of pores still open	-
N^0_p	number of pores in a clean filter	-
N'_{po}	number of pores/unit a mrea in a clean filter	m^{-2}
ΔP_o	the initial pressure drop across the membrane	bar
M_o	initial system flow rate	m^3/s
ΔP_o	the initial pressure drop across the membrane	bar
α	specific resistance of the cake that forms on the membrane surface	m/kg
ρ_s	mass density of the plugging particles	kg/m^3
K	Boltzmann constant	
T	absolute temperature	K
η	solvent viscosity	cP
q	scattering vector	-
$\tilde{n}$	solvent refractive index	-
λ_0	vacuum wavelength of the laser	nm
θ	scattering angle	[^{0}]
D	diffusion coefficient	cm^2/s
R_H	hydrodynamic radius	nm
$2c/b^2$	polydispersity index	-
L_0	path length of the sample	cm
A_b	absorbance	-
ε	molar absorbtivity (extinction coefficient)	mol/lcm
c	concentration of the compound in solution	mol l^{-1}
$G(\Gamma)$	correlation coefficients	-
Γ	delay time	μs
$I(t_0)$	intensity at time initial time t_0	
$I(t_0+\Gamma)$	intensity after delay time Γ	

LIST OF ABBREVIATIONS

ATR-FTIR	: Attenuated Total reflectance-Fourier Transform Infrared Spectroscopy
BAP	: Biomass Associated Products
CFV	: Crossflow Velocity
DLS	: Dynamic Light Scattering
ECPs	: Extracellular Polymers
EPS	: Extracellular Polymeric Substances
HRT	: Hydraulic Retention Time
IR	: Infra Red Spectroscopy
IRE	: Internal Reflection Element
IUPAC	: International Union for the Pure and Applied Chemistry
MBR	: Membrane Bioreactor
MF	: Microfiltration
MLSS	: Mixed Liquor Suspended Solid
MWCO	: Molecular Weight Cutoff
NNLS	: Non Negative Least Squares
NOM	: Natural Organic Matter
PCS	: Photon Correlation Spectroscopy
PMT	: Photo Multiplier
PSD	: Particle Size Distribution
QELS	: Quasi Elastic Light Scattering
SMP	: Soluble Microbial Products
SRT	: Solid Retention Time
TMP	: Transmembrane pressure
TOC	: Total Organic Carbon
TUB	: Technical University Berlin
UAP	: Utilization Associated products
UF	: Ultrafiltration
UV-VIS	: Ultraviolet-Visible
VSS	: Volatile Suspended Solids

INTRODUCTION

1.1 INTRODUCTION

Membrane processes are becoming increasingly attractive to conventional water and wastewater treatment. A major obstacle in applying membrane processes for wastewater treatment is the permeate flux decline. During Membrane filtration some constituents of the feed water deposit on the membrane surface and/or in the membrane matrix. The International Union for the Pure and Applied Chemistry (IUPAC) defines fouling as "*the sum of all processes leading to a loss of membrane performances due to the deposition of suspended or dissolved substances on its external surfaces, at its pore openings or within pores*"[1]. The most phenomenal aspect of fouling is that, either it increases the transmembrane pressure (TMP) or reduces the flux, respectively, depending on whether the system is operated at constant flux or constant pressure. In conjunction with the flux reduction or TMP rise a shift in the effective pore size/MWCO to smaller diameters is oftentimes observed.

If in a conventional wastewater treatment system the settleability of the sludge is poor, the system will perform less than optimum, but it is still functioning. If on the other hand the filtration of an MBR system is not performing properly, it might lead to zero production[2]. Series problem will occur if membrane fouling cannot be controlled, leading to replacement of membranes, which is quite costly. Thus controlling membrane fouling is absolutely essential in the operation of an MBR system. This is usually accomplished by applying a crossflow along the membrane wall, providing shear stress to remove accumulated material. The crossflow can be caused by recirculation of feed suspension through the membrane module chosen or by air scour.

Understanding the mechanisms of permeate flux decline and usage of models for the behavior of permeate flux in crossflow membrane filtration are therefore of paramount importance to the design and successful applications of this technology. Thus far, strategies concerning fouling control and membrane cleaning are primarily based on trial-and-error. A more in depth knowledge is needed about the substances causing

organic fouling in low-pressure membrane filtration as well as on the relevant fouling mechanisms. This would enable better choice concerning membrane selection as well as cleaning strategies, thereby reducing chemicals and extending membrane life. A considerable amount of research effort has been directed towards better understanding membrane fouling by particular materials.

Particles may deposit on the membrane surface leading to fouling externally or internally that may reduce membrane permeability. In this work, we consider the role of *"polysaccharides"* as it may differentially influence membrane fouling in constant transmembrane pressure operation. Experimental crossflow filtration studies involving polysaccharide suspensions clearly show that permeate flux varies with time once a polysaccharide suspension is introduced to the filtration system. Typical flux versus time curves shows a relatively rapid flux decline rate at the start the filtration, followed by a more gradual decrease, until a steady-state (or a pseudo-steady-state) flux is approached. Depending on system variables, the transient stage in crossflow filtration of polysaccharide suspensions can last from minutes to several hours. At the present time, it is not clear how system variables, such as particle concentration and size, applied pressure, and crossflow (shear) rate influence the transient behavior of permeate flux.

Understanding of filtration phenomenon can be gained by using a standard protocol and hence a batch apparatus but at the same time operate as closely to reality as possible on different polysaccharide streams. Next to that, a standardised filtration experiment can be used to quantify the filterability of a given polysaccharide obtained from different biological source. In this way, the applied method serves two goals: gaining knowledge and quantifying filterability. With the method to quantify filterability it is possible to identify whether polysaccharide may influence the filterability.

Here the topic of this research is the fouling potential of polysaccharides in low-pressure membrane filtration (UF). The aim of this project is to systematically investigate the dynamic behavior of permeate flux in the transient stages of crossflow membrane filtration of polysaccharide suspension before a steady-state flux is attained. Crossflow filtration experiments were conducted with three different polysaccharide suspensions under well-controlled physical conditions. Resistance in series model and Classical Blocking Filtration Laws were used to examine the fouling mechanism. The effects of

feed particle concentration, transmembrane pressure and particle size, on the dynamics of permeate flux decline are elaborated and discussed. The basic aim of this study is to identify the influence of polysaccharides in low-pressure membrane filtration of wastewater treatment plant. Furthermore, the underlying fouling mechanisms are investigated.

1.2 OBJECTIVES AND AIM OF THE RESEARCH

➤ To identify fouling phenomenon and compare different Polysaccharides in terms of their fouling and phenomenon.

➤ To identify the variation in particle size distribution of polysaccharides during crossflow filtration in the retentate phase by Dynamic Light Scattering (DLS).

➤ To evaluate the basic values of polysaccharide content in a crossflow membrane filtration operations using UV absorbance and colorimetric determination method.

➤ To identify the change in surface properties of membrane after filtration experiments by Attenuated Total reflectance-Fourier Transform Infrared Spectroscopy (ATR-FTIR).

➤ To evaluate the change in viscosity of polysaccharide during filtration experiments.

LITERATURE REVIEW & THEORETICAL BACK GROUND

2.1 EXTRACELLULAR POLYMERIC SUBSTANCES (EPS)

2.1.1 Extracellular polymeric Substances in Activated Sludge

Important point to be considered in membrane based wastewater treatment is to identify substance causing organic fouling and relevant fouling mechanism. Depending on membrane application, organic substances produced by microorganisms are referred to as soluble microbial products (SMP, wastewater effluent membrane filtration) or extracellular polymeric substances (EPS, MBR applications). However, Laspidou and Rittmann (2002)[3] indicated that SMP and soluble EPS are referring to the same group of compounds. EPS are composed of utilization association products (UAP) and biomass associated products (BAP), the former of which is associated with substrate metabolism and growth of bacteria, and the latter of which is associated with the decay of biomass[4].

EPS is a main constituent of activated sludge. Activated sludge flocs are complex systems composed of microbial cells embedded in a polymeric matrix. The exopolymer matrix has been defined as materials which can be removed from microorganisms without disrupting the cells and without which the microorganism still viable[5]. Since EPS provide a highly hydrated gel matrix in which microorganisms are embedded, they provide a significant barrier to permeate flow in the MBR. Microbial EPS are high molecular-weight mucous secretions from microbial cells. They can play an important role for floc formation in activated sludge liquors[6]. The extracellular matrix of the biofilm is often termed "biopolymers" or "polysaccharides". Polysaccharides predominate and represent approximately 65 % of extracellular material but other substances are also present such as proteins, nucleic acids and lipids [5]. The EPS matrix is very heterogeneous, with polymeric materials arising including polysaccharides, proteins, lipids, and nucleic acids [7]. Recently, many MBR studies have identified EPS as the most significant biological factor responsible for membrane fouling. Chang and Lee[8] correlated the EPS levels and membrane fouling quantitatively. These authors examined the EPS levels in activated sludge in various physiological states, and found there to be a

linear relationship between membrane fouling and EPS levels[9,10,11]. Similarly linked hydraulic resistance to EPS levels in the aeration tank, including empirical parameters for EPS production and degradation, developing a phenomenological model to predict fouling and to evaluate the effects of loading rate, flux, and shear stress on bioreactor performance. Huang et al.[6] found soluble organic substances with high molecular weights, mostly attributable to metabolic products, to accumulate in the bioreactor. These had a negative influence on membrane permeability: accumulation of 50 mg TOC (total organic carbon) L^{-1} resulted in 70% decrease in flux. In addition, EPS levels of 23 mg L^{-1} have been found to produce a six- to sevenfold increase in the internal fouling resistance[6]. The fouling propensity of specific EPS components has also been studied. Shin et al.[6] attributed 90% of the cake resistance to EPS and found resistance to vary with the ratio of protein and carbohydrate in the EPS. Mukai et al.[6] found the protein to sugar ratio of the EPS to influence permeate flux during ultrafiltration, the permeate flux decreasing with an increasing protein content. In a study illustrating the effects of EPS on membrane fouling carried out by Kim et al[12], addition of powdered activated carbon to the MBR was shown to increase permeability by reducing dissolved EPS levels from 121–196 to 90–127 mg/gVSS. Most studies of the effect of EPS on membrane fouling rely on extraction of EPS from the sludge flocs. However, relatively large amounts of EPS can originate from unmetabolized wastewater components and bacterial products arising either from cell-lysis or cell-structural polymeric components[13]. Thus, the quantitative expression of flux as a function of EPS concentration has an inherent limitation.

Little information is currently available on EPS membrane fouling mechanisms. For the membrane filtration of marine bacteria SW8, Hogdson et al.[14] proposed that EPS and cells were co-deposited during membrane filtration, with EPS filling the voids between the cells, forming a barrier of high hydraulic resistance. Since most resistance is attributed to the cake layer on the membrane surface rather than internal fouling.

These Extracellular polymers substances (EPS) also play an essential role in biofilm structure, activity and performance in biological waste water treatment. They mediate the transport of chemicals to and from the microorganisms, creating diffusional resistance to the movement of material carried by water. They also have ion exchange

properties due to negatively charged surface functional groups[15] which allow them to bind cationic species such as heavy metal. EPS in activated sludge occur as a capsule surrounding the bacterial cell wall which enhances flocculation ("extractable EPS") and in solution in the supernatant as slime polymers ("suspended EPS"). Mikkelsen and Keiding[16] state that sludges with higher extractable EPS concentration have a tendency to form larger flocs and thus a better filterability. Kim et al.[17] and Nagaoka et al.[10] report a decrease of filterability with increasing suspended and extractable EPS concentration, respectively.

2.1.2 EPS and Crossflow Filtration

Pressure-driven membrane filtration can operate at either crossflow or dead-end flow configuration. It is generally accepted that separation of colloids and suspended matter in a crossflow mode is advantageous over dead-end operation[18]. Crossflow membrane filtration may be performed under conditions of either constant transmembrane pressure or constant flux. In contrast with dead end filtration, the feed stream is directed tangentially to the membrane surface and a portion of "concentrate" remains in the module while the rest of the fluid exits as permeate. The goal of the tangential flow is to arrest the growth of the fouling layer and thereby retain a higher permeate flux[19]. The more complex of a crossflow filtration module entail a suite of particle transport mechanisms that are sensitive to the type of suspension to be filtered. During crossflow membrane filtration, suspended particles are transported to the membrane surface by permeate flow due to the imposed pressure drop. Because of the finite size of colloidal particles, particle concentration on the membrane surface reaches its maximum value after a short period of time, and a cake layer starts to form[20]. The resulting cake layer on the membrane surface increases the hydraulic resistance to permeate flow and, thus, reduces permeate flow through the membrane.

The particles of size range from the nominal membrane pore size up to approximately 0.5 m play an important role in the process of crossflow filtration depending on the crossflow velocity[2] these particles can escape the influence of the crossflow and enter the boundary layer near the membrane. In the water phase EPS can be found in the mentioned size range and indeed contribute to the process of membrane

fouling[8]. EPS in the water phase is quite small compared to microbial flocs. This implies that microbial flocs are not involved in membrane fouling as much.

2.2 PRESSURE DRIVEN MEMBRANE FILTRATION

2.2.1 Membrane Filtration

The basic principle of all membrane operations is the separation of a mixture of substances with a selective thin film. Each membrane has the ability to transport one component more readily than other because of differences in physical and/or chemical properties between the membrane and the permeating components. Furthermore, some components can freely permeate through the membrane, while others will be retained. The stream containing the components that permeate through the membrane are called permeate and the stream containing the retained components is called retentate. The separation of components is based on the differing transport resistance of the single components. The transport of matter through the selective barrier is caused by a chemical potential difference between the two phases i.e., feed and permeate. The driving force of the chemical potential difference can be either a difference as shown in table 2-1.

Table 2-1: Classification of membrane processes according to their driving forces[21].

Driving Force	Pressure Difference	Concentration Difference	Temperature Difference	Electrical potential difference
Membrane process	Microfiltration Ultrafiltration Nanofiltration Reverse Osmosis	Pervaporation Gas Separation Dialysis Liquid-membranes	Thermo-Osmosis Membrane Distillation	Electrodialysis Electro osmosis

These different membrane operations are used to concentrate, fractionate or purify waste wastewater solutions. In the wastewater treatment plant, the solution of interest is raw wastewater that has been pretreated to varying degrees and needs further purification. Pressure-driven membrane filtration is an important process for separation of colloids and

particulate matter from liquid suspensions in many fields of engineering and applied science. In general, pressure driven membranes are employed for this purification step i.e. microfiltration, Ultrafiltration, Nanofiltration or reverse osmosis membranes. In this research work membrane filtration based on pressure difference with Ultrafiltration membranes is taken into consideration.

2.2.2 Membrane Fouling

One of the most important parameters in the viability of a membrane process is its capacity to treat a sufficient wastewater flux. This flux should be stable over time. It is influenced by the sensibility of the membrane with fouling phenomenon. Introducing Membrane filtration also means introducing membrane fouling. During membrane filtration some constituents of the feed water deposit on the membrane surface and/or in the membrane matrix. The most phenomenal aspect of fouling is that, either it increases the transmembrane pressure (TMP) or reduces the flux, respectively, depending on whether the system is operated at constant flux or constant pressure. In conjunction with the flux reduction a shift in the effective pore size/MWCO to smaller diameters is oftentimes observed. This can result in MF process to display characteristics of UF membrane filtration[22].

On a brief review of membrane fouling, it can be distinguished into four types: scaling, biofouling, organic fouling and particulate fouling. *"Scaling"* occurs on the membrane surface if dissolved salts exceed their solubility product. Scaling is not of concern in low-pressure membrane operation (MF and UF) as the salts pass the membrane freely. *"Biofouling"* involves adhesion and growth of microorganism on the membrane surface, i.e. the formation of a biofilm, which results in a loss of membrane performance. Because bacteria have developed elaborate adhesion mechanism biofilm can occur on all kinds of materials, natural and synthetic[22]. Generally adhesion to surfaces is achieved by extracellular polymeric substances (EPS).

"Organic Fouling" on the other hand is defined as reduction in flux due to adsorption of dissolved organic substances on the membrane surface or in its pores. The adhesion depends primarily on the chemical and electrostatic characteristics of the organic material. Organic fouling can be due to natural organic matter (NOM)[22],

9

synthetic organic compounds (SOC) which are added by the consumer and soluble microbial products (SMP) produced during the biological wastewater treatment process[22]. The term dissolved substances normally refers to any compounds that passes a 0.45 m filter. Anything that is retained by this filter is categorised as particulates. This operational definition of dissolved/particulate material does not account for colloids. Colloids are defined as organic or inorganic substances with sizes between 1nm and 1 m and therefore can occur in both fractions. The following compounds are colloidal in nature; $CaCO_3$, iron hydroxides, micro organisms and microbial debris, polysaccharides, humic substances, amorphous silica, and clay. Particulate fouling is defined as the fouling caused by particulates, which accumulate on the membrane surface thereby forming a filtration cake.

Soluble microbial products are indeed identical with soluble EPS. Both EPS and SMP are substances produced by microorganisms that are released into the liquid phase as part of the metabolism and due to biological or mechanical stress. This implies that the extracellular polymeric substances can have a fouling potential by themselves outside of a biofilm. Thus polysaccharides, proteins and lipids may play an important role in organic fouling of membrane applications to wastewater treatment. The emphasis in this research is put on the investigation of organic fouling due to polysaccharides in its soluble suspended state.

2.2.3 Permeate Flux and Solute Transport

In pressure driven membrane filtration operation the pressure difference (P) or transmembrane pressure difference (TMP) between the feed (P_{feed}) and permeate ($P_{permeate}$) side is given by [Eqn.1]

$$\Delta P = P_{feed} - P_{permeate}$$
<div align="right">Eqn. 1</div>

The above equation holds true for dead- end filtration or direct filtration membrane operation. For membrane modules that are operated in the crossflow mode only an average TMP can be calculated due to pressure drop across the module. In this case [Eqn 2] can be used

$$\Delta P = \frac{P_{feed} - P_{concentrate}}{2} - P_{permeate} \qquad \text{Eqn.2}$$

For the efficient operation of membrane filtration the permeate flux J is of most importance. It is defined as the permeate flow rate Q_p (= permeate volume V per filtration time t) divided by the membrane area A_m.

$$J = \frac{Q_p}{A_m} = \frac{V}{A_m t} \qquad \text{Eqn.3}$$

The relationships between pure water permeate flux J of a clean MF or UF membrane is Darcy's law:

$$J = \frac{\Delta P}{\mu R_m} \qquad \text{Eqn.4}$$

Where   is the viscosity of water and R_m is the hydraulic resistance of the clean membrane. The advantage is that additional resistance due to fouling can be accounted and is explained briefly in the following section.

2.2.4 Factors Influencing Membrane Filtration

The performance of the membrane operations is a function of various parameters such as

- ➢ Membrane material and module construction
- ➢ Hydrodynamic conditions (flux, transmembrane pressure (TMP), crossflow velocity)
- ➢ Operational conditions (temperature, solid retention time (SRT), hydraulic retention time (HRT), inflow and oxygen concentration)
- ➢ Characteristics of feed water (e.g., temperature, viscosity, mixed liquor suspended solids (MLSS), extracellular polymeric substances (EPS) attached to the micro organism or to the liquid phase, etc.)

The above key factors impact upon or contribute to fouling, most of which are interrelated (figure 2-1)

Factors affecting fouling

Membrane | Biomass | Operating conditions

Membrane:
- Configuration
- Material
- Hydrophobicity
- Porosity
- Pore size

Biomass:
- MLSS
- EPS
- Floc structure
- Dissolved matter
- Floc size

Operating conditions:
- Configuration
- CFV
- Aeration
- HRT/SRT
- TMP
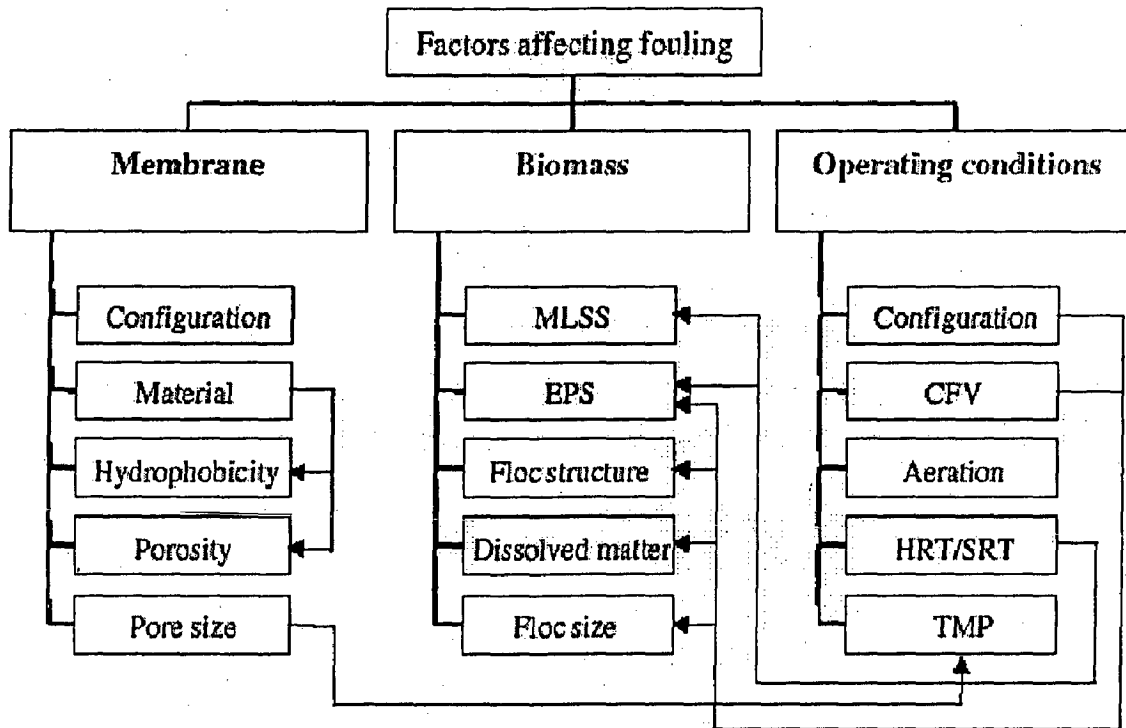
Figure 2-1: Factors influencing membrane fouling in MBR process[24].

2.2.5 Fouling Mechanisms and Models

A number of fouling models exist in order to describe different fouling mechanisms encountered during membrane filtration. In most references that review fouling phenomena the focus is on cross-flow systems and/or reverse osmosis of single-solute feed water solutions. Bowen and Jenner[26] reviewed the theoretical filtration models for colloidal and fine particle dispersions, in both cross-flow and dead-end operational mode. In the gel polarization model it is suggested that when the concentration at the membrane surface increases, the macro-solute reaches its solubility limit and precipitates on the membrane surface and forms solid gels. Solutes that do not precipitate are not taken into account. The osmotic pressure model describes flux behavior when solutes do no not precipitate or gelate. However, in Ultrafiltration processes the osmotic pressure is negligible. These two models can be modified in various ways, but are still only applicable for well defined solutions. Particle interactions

are taken into account by a different group of filtration models. Of special interest is the work by Wessling[27] on stochastic modelling, in which fouling of microfiltration membranes were described as a function of nanoparticles (like proteins). Although these particles are much smaller than the membrane pores, it was found that these particles could foul the membrane heavily. The stochastic modelling showed that interaction of the particles might lead to the formation of agglomerates of particles forming bridges over a pore. Verification of the theoretical results was found to be very difficult. In the current research the resistance in series model and approach introduced by Hermia (1982) are used for the description of filtration phenomena in cross flow Ultrafiltration.

2.2.5.1 Resistance in Series Model

According to this model total hydraulic resistance is divided in several hydraulic resistances. Each of those resistances corresponds to physical phenomenon. The resistance in series model is schematically drawn in figure 2-2.
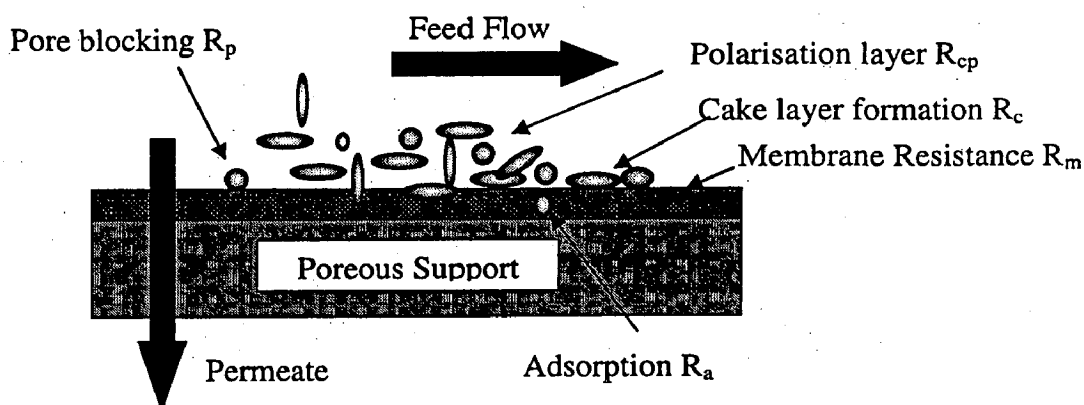
Figure 2-2: The Resistance of fouled membrane by various fouling mechanisms, the driving force is from upstream to downstream side of membrane, R_p= pore blocking, R_a = pore constriction (adsorption, R_m = initial membrane resistance, R_c = cake filtration R_{cp}= concentration polarization[25].

During membrane filtration these mechanisms may occur simultaneously. The initial membrane resistance is mainly determined by the average pore diameter and porosity of the membrane. Ultrafiltration performance can also be interpreted by a resistance in series relationship[26]. This resistance in series model is based on Darcy's

13

law, each deposition layer (inside, outside the membrane pores, adsorption, etc.,) relates to an additional resistance. Applying Darcy's law to this relationship between transmembrane pressure and the permeate flux

$$J = \frac{\Delta P}{\mu(R_m + R_i + R_c)} = \frac{Q}{A_m} = \frac{1}{A} \cdot \frac{dV}{dt} = \frac{Q}{A_m}$$ Eqn.5

With ·

R_m: hydraulic resistance of the membrane in pure water (1/m)

R_{cp}= resistance due to concentration polarization (1/m)

R_i: $R_a + R_p$: internal irreversible fouling resistance (1/m)

R_c: resistance due to particle deposit at membrane surface, cake resistance (1/m)

Three main fouling mechanisms for flux decline can be identified for Ultrafiltration of colloidal species as: standard pore blocking, pore blocking and cake buildup[28] and these can be respectively described by the following resistance models.

The standard pore blocking model (pore narrowing/pore constriction) assumes that the foulants deposit evenly on along the pore walls, causing the pore diameter to decrease, while the number of pores per unit area remains constant. It is also assumed that the change in pore volume due to fouling is proportional to the filtrate volume. With the above assumptions and integration of [Eqn 5] yields

$$R_i + R_m = R_m (1 + K_{SBM} Q_o . t)^2$$ Eqn.6

Where

$$K_{SBM} = 4C_{SBM} / (A N_o \Pi l d_o^2)$$

Q_0 : flow rate through unfouled membrane (m^3/h)

l: pore length (m)

C_{SBM}: standard blocking constant, polysaccharide volume that deposit on pore wall per unit filtrate volume.

N_o: number of pores per unit membrane surface area

14

d_o: diameter of each pore (nm)

The resistance increases with time with an increasing slope when fouling is described by this standard blocking model.

The pore blocking model (Pore plugging/complete blocking/pore sealing assumes that the number of pores that become plugged increases proportionally to the filtrate volume, while pore diameter remains constant. The pore plugging model of the membrane resistance as a function of time is given by [Eqn 7]

$$R_i + R_m = R_m e^{K_{PBM} \cdot t}$$ Eqn.7

Where

$$K_{PBM} = (\Pi d_o^4 \Delta P A_m C_{PBM})/(128 \mu l)$$

C_{PBM}: pore blocking constant, number of pores per unit membrane surface area that become plugged per unit filtrate volume.

The resistance also increases with time with an increasing slope when fouling follows the pore plugging model.

In the cake build up (or cake filtration) model, internal membrane fouling due to pore plugging or standard blocking does not occur i.e., (R_m+R_i) remains constant and only R_c increases with time. The cake filtration model in terms of total resistance as a function of time [Eqn.8]

$$R_t = R_m (1 + 4.t.K_{CFM} Q_o^2)^{0.5}$$ Eqn.8

Where

$$K_{CFM} = (\mu C_{CFM} \rho_o)/(2A^2 \Delta P)$$
C_{CFM}: specific cake resistance

$_o$: mass of cake deposited per volume of filtrate (mg/l)

Unlike the pore plugging model and standard blocking model, the resistance increases with time with a decreasing slope. Briefly, the irreversible resistance R_i creates an additional resistance to the filtration depending on several causes such as membrane

15

porosity, its structure, its pore form, its chemical affinity and chemical composition of the solution filtered. This resistance is generally due to adsorption (R_a) of soluble organic or mineral compounds or to a mechanical pore blockage (R_p) made by minor molecules. This resistance increases continuously depending on permeate volume filtered and time of filtration. The cake layer filtration is a function of filtered solution composition and characteristics but also the hydraulic conditions of membrane operation. If those conditions do not change this resistance value reaches its maximum in few minutes. It is now clear that the fouling phenomenon depends on several parameters, which impact more or les on the filtration performance

2.2.5.2 Classical Filtration Laws

Polysaccharide fouling in ultrafiltration and microfiltration may be occurring via a number of mechanisms. Internal deposition, pore blocking, and cake formation may occur depending on polydispersity of model polysaccharides molecular weight and aggregation. In addition, the filter cake may be heterogeneous with mixtures of large aggregates infiltrated with smaller molecular weight components. Four classic filtration laws, originally developed by Hermia[29], are widely used to explain the flux behaviour under constant pressure filtration. All models imply a dependence of flux decline on the ratio of the particle size to the pore diameter.

2.2.5.2.1: Cake Filtration Model

Cake formation normally occurs when particles larger than the average pore size accumulate on the membrane surface, forming a "cake" (fig 2-3). This cake then provides an additional porous surface through which the liquid must pass. As a result, the cake may increase the particle removal efficiency of the filter; however, it also increases the filter's resistance. Typical performance curves that characterize cake formation are shown in figure 2-4. Curves are shown for both constant pressure and constant flow rate processes. For constant flow, the increase in pressure drop is linear with time. For constant pressure, the flow decreases most early in the process. To obtain a better understanding, data like that in figure 2-4 must be replotted using characteristic equations derived from Darcy's equation. The derivation of the equation is described in Appendix I.
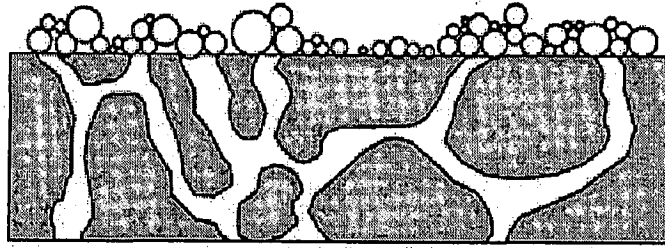
Figure 2-3: Pictorial view of cake formation

$$\frac{dV}{dt} = \frac{\Delta PA}{\mu\left(\frac{\alpha CV}{A_m} + R_m\right)}$$

Eqn.9

Darcy's equation states that the flow rate is proportional to the membrane area and pressure drop, but it is inversely proportional to the viscosity and membrane resistance. So, as the system resistance increases due to particulate loading and cake formation, either the pressure drop or low rate will be affected.

For constant pressure systems, Darcy's equation can be solved to yield the following characteristic equation (Appendix I, Equation 5).

$$\frac{t}{V} = C_1 V + C_2$$

Eqn.10

This equation states that the time required to flow a unit volume is directly proportional to the volume of fluid passing through the membrane multiplied by a constant.

2.2.5.2.2: Complete Pore Blocking Model

Figure 2-5 depicts complete pore plugging. It typically occurs when the particle sizes are similar to the mean pore size. In this model, particles seal individual pores. As individual pores are plugged, flow is diverted to other pores that plug successively. Eventually, this reduces the available membrane area and increases the membrane's resistance. Figure 2-6 provides examples of typical complete pore plugging curves. Curves are shown for both constant pressure and constant flow process. Unlike in cake formation the curves are not

17
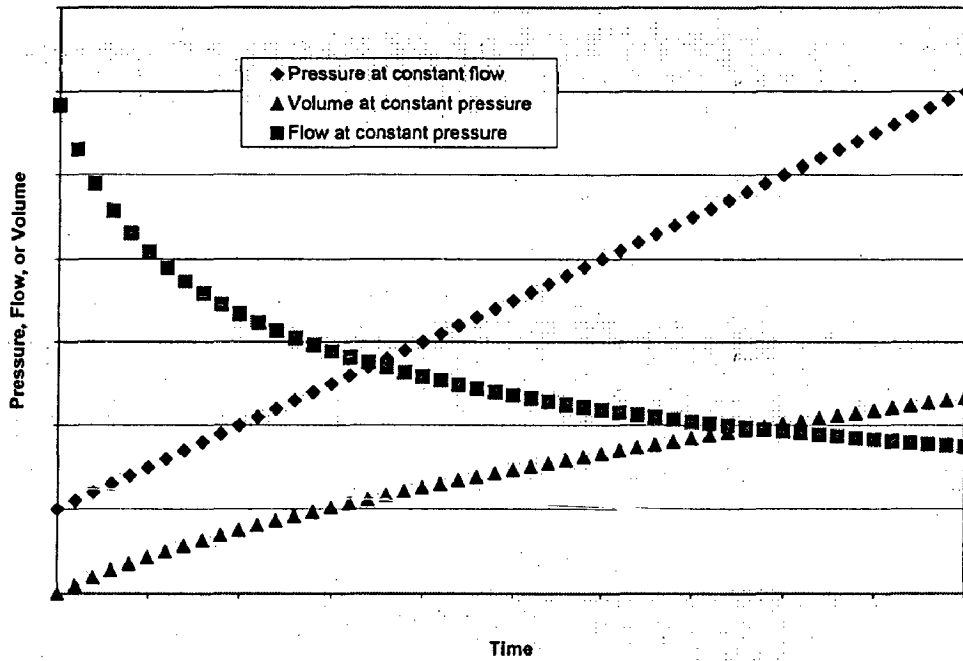
Figure 2-4: Typical cake formation system curves
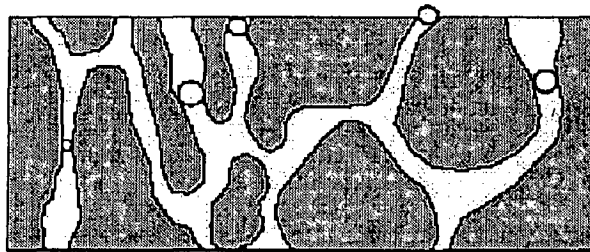
Figure 2-5: Pictorial view of Complete Pore Blocking

linear. At the end of the filter life, pressure drop increases dramatically. Data like that shown in Figure 2-6 must be re-plotted in a form dictated by characteristic equations to confirm the plugging method.

$$\frac{dV}{dt} = \frac{\Pi \Delta PA}{8\mu L} r_p^4 N^1{}_{po} - \frac{\Pi \Delta P}{8\mu L} r_p^4 K_2 V$$

Eqn.11

For complete pore plugging, the characteristic equations are derived from Poiseuille's law. Poiseuille's law states that the flow rate is proportional to the pressure drop, pore size to the 4th power, and the number of open pores, but, it is inversely proportional to viscosity and membrane thickness. In this case, as pores plug, the number of open pores is reduced. As a result, either the flow rate is reduced or the pressure drop increases. For constant pressure systems, solving Poiseuille's law yields a very difficult to use characteristic equation (Appendix I, Equation 9). An intermediate step in the solution of Poiseuille's law yields a much easier equation to understand (Appendix I, Equation 8).

$$\frac{dV}{dt} = C_3 - C_4 V \qquad\qquad \text{Eqn.12}$$

This equation states that the flow rate is a linear decreasing function of volume filtered.
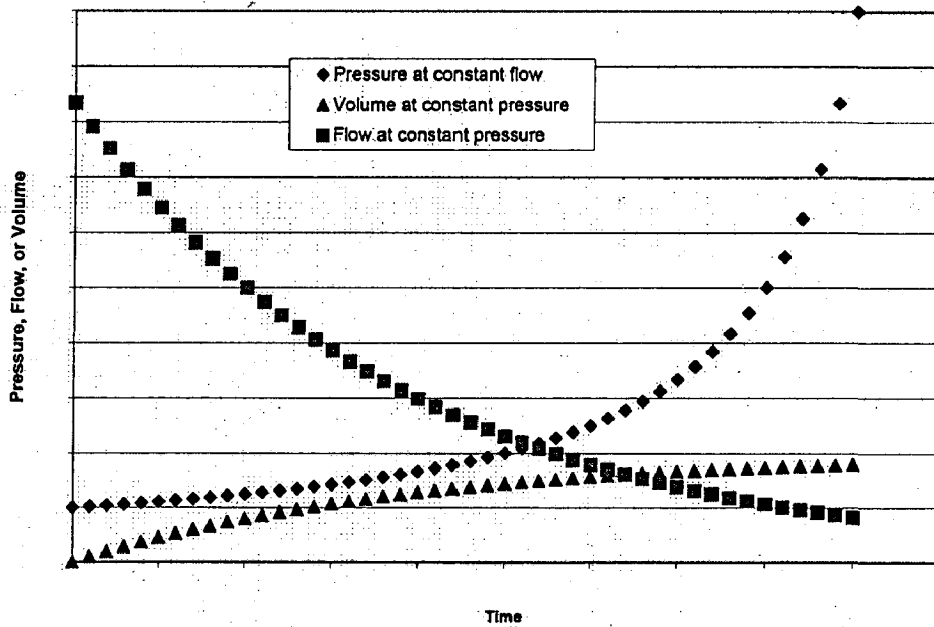
Figure 2-6: Typical Complete Pore Blocking system curves

2.2.5.2.3: Gradual Pore Plugging Model

Gradual pore plugging is most dominant when retained particles are smaller than the pores. It is often called adsorptive fouling. In this case, particles in the fluid approach the

19

membrane, enter the pores, and adhere to the pore walls. This mechanism is illustrated in figure 2-7. Unlike the complete pore plugging model, there is no complete blocking of pores. In this case, the adhesion of particles to the walls decreases the available pore diameter and increases the resistance of the membrane.
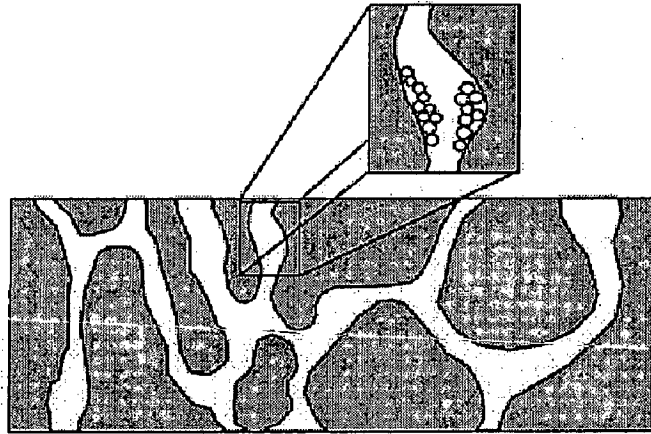
Figure 2-7: Pictorial view of Gradual Pore Blocking

From typical test data shown in figure 2-8, it is very difficult to determine if a filter is plugging due to complete or gradual pore plugging as these curves are also non-linear. Like complete pluggage, pressure drop increases dramatically at the end of filter life. To obtain a better understanding, data like that shown in figure 2-8 must be re-plotted using characteristic equations.

$$\frac{dV}{dt} = \frac{\Pi \Delta PA}{8\mu L} r_p^4 N_p^1$$ Eqn.13

$$CV = \rho_s \Pi LAN_p^1 (r_o^2 - r_p^2)$$ Eqn.14

law. However, as pores plug in gradual pore plugging model, the number of pores available for flow remains constant while the pore diameter decreases.

The decrease in the cross-section of the pore can be calculated based on the volume of plugger being carried into the pore. Pore size appears in Poiseuille's law to the fourth power. As a result, small changes in the pore diameter can result in large changes to either the flow rate or the pressure drop.
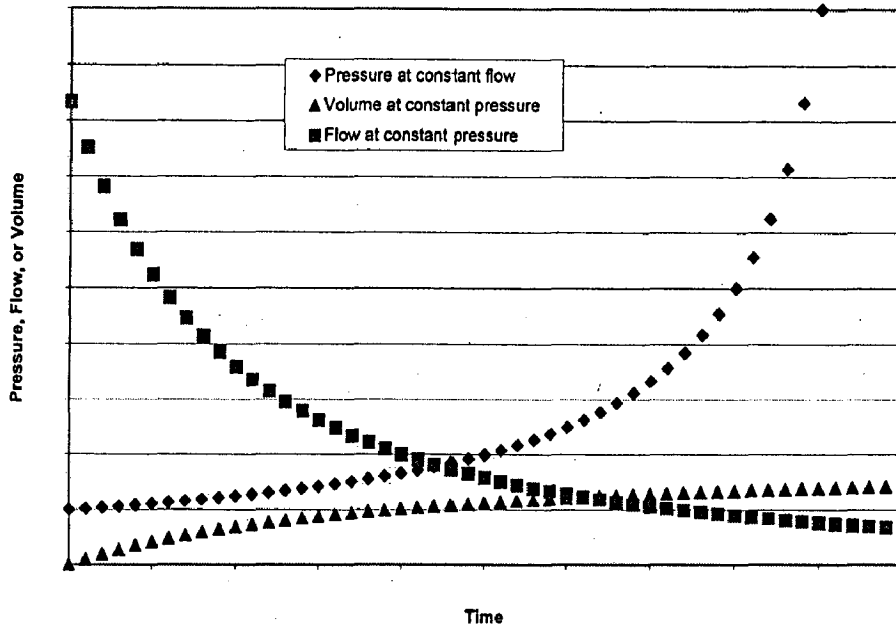
Figure 2-8: Typical Gradual Pore Blocking system curves

For constant pressure systems, solving Poiseuille's law using the gradual pore plugging assumptions leads to the following characteristic equation (Appendix I, Equation 13):

$$\frac{t}{V} = C_5 t + C_6 \qquad\qquad \text{Eqn.15}$$

This equation states that the time required to flow the total volume (inverse of average flow rate) is directly proportional to time.

2.2.5.2.4: Summary of Characteristic Equations

The characteristic equations for the three different models are shown in Table 2-2. The definitions of the constants in individual characteristics equations are shown in Appendix A. The equations in table 2-2 will be used in the following section for data analysis. For constant pressure drop systems (1) both the Cake Formation and Gradual Pore Plugging characteristic equations are linear. By plotting t/V versus both Volume and Time, it can be determined which of the two models more accurately reflects the actual

21

process. Normally, a visual examination of the curves will determine which method produces the straightest line. However, a linear regression would provide more confidence. If a regression is performed, it may be necessary to delete the first few points if it can be determined that measurement error is involved. (2) The complete pore plugging characteristic equation is also linear. To determine if this model more accurately reflects the process, plot flow rate (dV/dt) versus Volume. If complete pore plugging is the dominant method, then flow rate versus Volume should be linear with a decreasing slope.

Ye et al.,[23] investigated the fouling mechanisms of polysaccharides, dead end unstirred filtration of sodium alginate, a model polysaccharide, was carried out and analyzed using classical filtration laws and the combined pore blockage and cake formation model. It was found that the cake model appears to fit the entire range of the ultrafiltration data while the consecutive standard pore blocking model and cake model are more applicable to microfiltration membranes (0.2 μm track-etched and 0.22 μm PVDF membranes). Madaeni[30] used the standard blocking law and the cake filtration law successfully to distinguish between particle deposition within the membrane and cake filtration on the membrane surface in unstirred and stirred batch microfiltration of virus suspensions. Unstirred operation was related to dead-end filtration. The stirred cell operation was done at 400 rpm, resulting in similar results as a thin channel cross-flow cell at a Reynolds number of about 2200. The microfiltration membranes were hydrophobic Millipore (GVHP) membranes (0.22 μm). The Ultrafiltration membranes were polysulfone Amicon (PM30) membranes (MWCO 30 KDa). The bacteria created a much higher fouling layer resistance, indicating blocking and pore obstruction. The viruses probably adsorbed on and inside the membrane. Lojkine et al. (1992) reviewed cross-flow microfiltration of cell suspensions, focusing mainly on models for flux prediction, emphasizing on particle size effects. The main focus was the application of the standard blocking filtration law and the cake filtration law. Various models based on the film theory were also reviewed, but these were mainly useful for cross-flow systems. Lojkine et al. (1992) stated that models have various drawbacks. They are often derived for dilute solutions of rigid, spherical and neutrally buoyant particles. According to Lojkine[31], most reviewed research suggested that flux decreases with decreasing particle

size (for polystyrene lattices, kaolin clay), although also the opposite has been found (colloidal silica, ~ *Aspergillus Niger* (reduction of particle size distribution)).

Table 2-2: Summary of characteristic Equation

Model	Characteristic Equation	Constant Pressure	constants
Cake Formation	$\dfrac{dV}{dt} = \dfrac{\Delta PA}{\mu\left(\dfrac{\alpha CV}{A_m} + R_m\right)}$	$\dfrac{t}{V} = C_1 V + C_2$	$C_1 = \dfrac{\alpha C \mu}{2\Delta p a^2}$ $C_2 = \dfrac{\mu R_m}{\Delta PA}$
Complete Pore Plugging	$\dfrac{dV}{dt} = \dfrac{\Pi \Delta PA}{8\mu L}r_p^4 N^1_{po} - \dfrac{\Pi \Delta P}{8\mu L}r_p^4 K_2 V$	$\dfrac{dV}{dt} = C_3 - C_4 V$	$C_4 \dfrac{\Pi \Delta P}{8\mu L}r_p^4 K_2$ $C_3 = \dfrac{\Pi \Delta PA}{8\mu L}r_p^4 N_{po}$
Gradual Pore Plugging Model	$\dfrac{dV}{dt} = \dfrac{\Pi \Delta PA}{8\mu L}r_p^4 N^1_p$	$\dfrac{t}{V} = C_5 t + C_6$	$C_5 = \dfrac{C}{\Pi L\rho_s}\left(\dfrac{\Pi}{8\mu L}\right)^{\frac{1}{2}}\left(\dfrac{\Delta P}{M_o N_p}\right)^{\frac{1}{2}}$ $C_6 = \dfrac{\mu R_m}{\Delta PA}$

2.3 CHARACTERIZATION METHOD

2.3.1 Dynamic Light Scattering

When a monochromatic and coherent light is focused into a dilute macromolecule solution, and if solvent molecules and macromolecules have different refractive indices, the incident light will be scattered by each illuminated macromolecule to all directions. The scattered light waves from different macromolecules mutually interfere, or combine at a distant and fast photomultiplier tube detector to product a net scattering intensity I(t) or photon counts n(t). If all macromolecules are stationary, the scattered light intensity at each given direction would be constant i.e. independent of time. However, in reality, all macromolecules in solution are undergoing constant Brownian motion, which leads to translational diffusion. The faster the diffusion the faster the fluctuation will be[32].

Dynamic light scattering (DLS), also known as photon correlation spectroscopy (PCS) or quasi-elastic light scattering (QELS), provides many advantages as a particle

size analysis method. DLS is a noninvasive technique that measures a large population of particles in a very short time period, with no manipulation of the surrounding medium. Because of the sensitivity to trace amounts of aggregates and the ability to resolve multiple particle sizes, DLS is ideally suited for macromolecular applications necessitating low sample concentration and volume. Particles and macromolecules in solution undergo Brownian motion. Brownian motion arises from collisions between the particles and the solvent molecules. As a consequence of this particle motion, light scattered from the particle ensemble will fluctuate with time. In DLS, these fluctuations are measured across very short time intervals to produce a correlation curve, from which the particle diffusion coefficient (and subsequently the particle size) is extracted. In contrast to separation techniques, where particles are separated and then counted, in the DLS technique, all of the size information for the ensemble of particles is contained within a single correlation curve. As such, particle size resolution requires a deconvolution of the data contained in the measured correlation curve. While standard algorithms exist for transforming the correlation curve to a particle size distribution, an understanding of the precision and accuracy of the distribution necessitates a solid understanding of the underlying principles behind the DLS technique itself.

2.3.1.1 Theory

Light scattering is a consequence of the interaction of light with the electric field of a particle or small molecule. This interaction induces a dipole in the particle electric field that oscillates with the same frequency as that of the incident light. Inherent to the oscillating dipole is the acceleration of charge, which leads to the release of energy in the form of scattered light. For a collection of solution particles illuminated by a light source such as a laser, the scattering intensity measured by a detector located at some point in space will be dependent on the relative positions of the particles within the scattering volume. The scattering volume is defined as the crossover section of the light source and the detector optics shown in figure 2-4 (a).

The position dependence of the scattering intensity arises from constructive and destruction interference of the scattered light waves. If the particles are static or frozen in space, then one would expect to observe a scattering intensity that is constant with time,

as described in figure 2-4 (b). In practice, however, the particles are diffusing according to Brownian motion, and the scattering intensity fluctuates about an average value equivalent to the static intensity. As detailed in figure (2-4(a) and (b)), these fluctuations are known as the dynamic intensity.

(a)   (b)
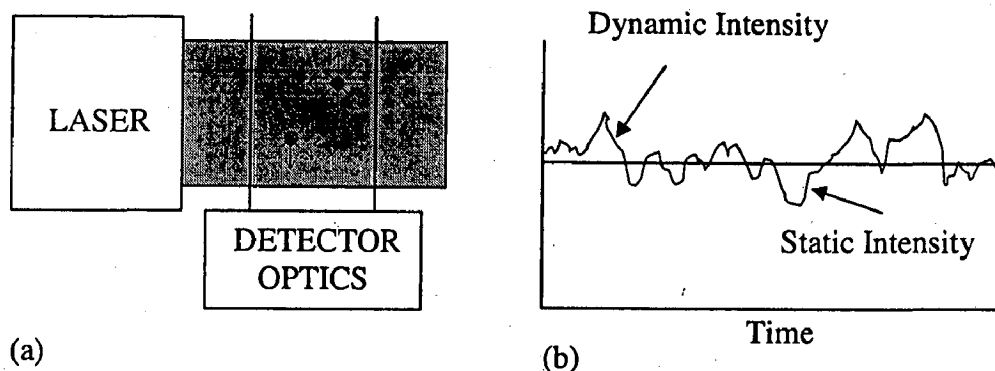
Figure 2-9: schematic detailing (a) the scattering volume and (b) subsequent static and dynamic light scattering intensities

Across a long time interval, the dynamic signal appears to be representative of random fluctuations about a mean value. When viewed on a much smaller time scale, it is evident that the intensity trace is in fact not random, but rather comprises a series of continuous data points. This absence of discontinuity is a consequence of the physical confinement of the particles in a position very near to the position occupied a very short time earlier. In other words, on short time scales, the particles have had insufficient time to move very far from their initial positions, and as such, the intensity signals are very similar. The net result is an intensity trace that is smooth, rather than discontinuous. Correlation is a second-order statistical technique for measuring the degree of nonrandomness in an apparently random data set. When applied to a time-dependent intensity trace, as measured with DLS instrumentation, the correlation coefficients, $G(\Gamma)$, are calculated as shown in equation (16), where t is the initial (start) time and Γ is the delay time.

$$G(\Gamma) = \int_0^\infty I(t_o)I(t_o + \Gamma)dt \qquad \text{Eqn. 16}$$

As a summation, the correlation equation can be expressed as shown in Equation (17).

$$G_k(\Gamma_k) = \sum_{i=0} I(t_{oi})I(t_{oi} + \Gamma_k)$$
<div align="right">Eqn. 17</div>

Typically, the correlation coefficients are normalized, such that $G(\infty)=1$. In DLS instrumentation, the correlation summations are performed using an integrated digital correlator, which is a logic board comprising operational amplifiers that continually add and multiply short time scale fluctuations in the measured scattering intensity to generate the correlation curve for the sample.

2.3.1.2 Hydrodynamic size

All of the information regarding the motion or diffusion of the particles in the solution is embodied within the measured correlation curve. For monodisperse samples, consisting of a single particle size group, the correlation curve can be fit to a single exponential form as given in [Eqn.18] where B is the baseline, A is the amplitude, and D is the diffusion coefficient. The scattering vector (q) is defined by [Eqn.19] where $\bar{n}$ is the solvent refractive index; $_0$ is the vacuum wavelength of the laser, and   is the scattering angle.

$$G(\Gamma) = \int_0^\infty I(t).I(t + \Gamma)dt = B + A.e^{-2.q^2D\Gamma}$$
<div align="right">Eqn. 18</div>

$$q = \frac{4\Pi\bar{n}}{\lambda_o}\sin\left(\frac{\theta}{2}\right)$$
<div align="right">Eqn. 19</div>

The hydrodynamic radius is defined as the radius of a hard sphere that diffuses at the same rate as the particle under examination. The hydrodynamic radius is calculated using the particle diffusion coefficient and the Stokes- Einstein equation given in Equation (20) where k is the Boltzmann constant, T is the absolute temperature, and η the solvent viscosity.

$$R_H = \frac{KT}{6\Pi\eta D}$$
<div align="right">Eqn.20</div>

A single exponential or Cumulant fit of the correlation curve is the fitting procedure recommended by the International Standards Organization (ISO). The simplest way of obtaining a size from this curve is to use the cumulants analysis as described in ISO 13321. A third order fit of a polynomial to a semi-log plot of the correlation function is performed as given in [Eqn.21].

$$\ln[G] = a + b\Gamma + c\Gamma^2 \qquad \text{Eqn. 21}$$

A plot of ln [G] vs time (figure 2-5) and the third order fit to the curve will give the diffusion coefficient value, where b is the Z average diffusion coefficient; $2c/b^2$ is the polydispersity index (width of the distribution)

ln[G]

b = Z-avg diffusion coefficient

$2c/b^2$ = polydispersity index

time (μs)
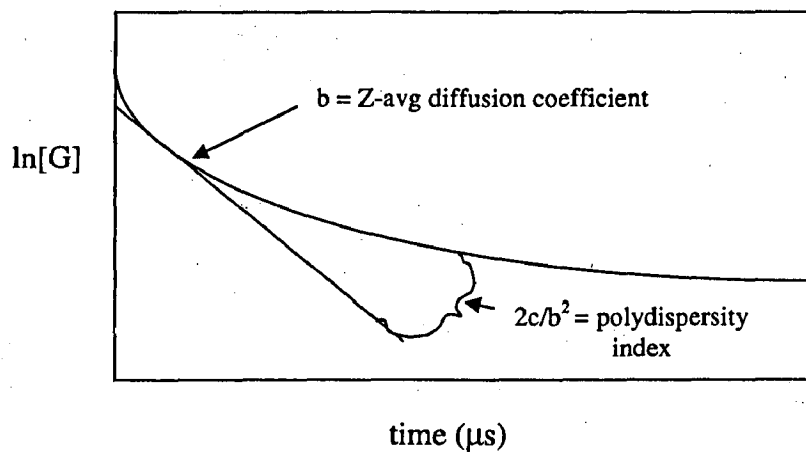
Figure 2-10: Cumulant analysis for determination of Z-average diffusion coefficient.

The hydrodynamic size extracted using this method is an average value, weighted by the particle scattering intensity. Because of the intensity weighting, the Cumulant size is defined as the Z average or intensity average. While the Cumulant algorithm and the Z average are useful for describing general solution characteristics, for multimodal solutions, consisting of multiple particle size groups, the Z average can be misleading. For multimodal solutions, it is more appropriate to fit the correlation curve to a multiple exponential form, using common algorithms such as CONTIN or Non Negative Least Squares (NNLS).

2.3.2 ANALYTICAL MEASUREMENTS

2.3.2.1 Attenuated Total Reflectance Fourier Transform Infra Red Spectroscopy

Internal Reflection Spectrometry or Attenuated Total Reflectance Infrared (ATR/IR) Spectrometry provide valuable information related to the chemical structure of separations membranes. Mid-infrared spectra are obtained by pressing small pieces of membrane against an internal reflection element (IRE), e.g., zinc selenide (ZnSe) or germanium (Ge). IR radiation is focused onto the end of the IRE. Light enters the IRE and reflects down the length of the crystal. At each internal reflection, the IR radiation actually penetrates a short distance (~1 m) from the surface of the IRE into the polymer membrane (Figure 2-6 (top)). It is this unique physical phenomenon that enables one to obtain infrared spectra of samples placed in contact with the IRE.

Molecular vibrations and rotations are excited by absorption of light in the infrared region between 4000 and 400 cm^{-1}. In IR spectra, many functional groups of organic molecules show characteristic oscillations, which can be attributed to absorption bands in defined regions. These oscillations are essentially localized to the functional groups and do not span over the whole molecule. Hence, IR spectroscopy is well suited, and indeed mainly used, for organic structure determination and verification. The basic idea of FTIR is the simultaneous acquisition of all frequencies of the entire IR spectrum. The whole excitation spectra, which are irradiated at all times at constant intensity, are transferred in an interferometer into an interferogram, which then is not a function of frequency but time. After the transformed radiation passed through the sample, the interferogram is analyzed by the Fourier transformation, i.e. retranslated into its reciprocal, which is the dependent spectrum. The schematic representation of FTIR instrument is shown in figure 2-6 (bottom). The heart of the FTIR is the "interferometer", which contains a semi-transparent germanium coated KBr mirror and is first hit by the incident beam of the glow bar. This mirror separates the beam into two parts, one part is directed onto a static mirror and the other part is directed onto a movable mirror, whose distance to the semitransparent mirror is varied as spectrum is produced. Varying the distance, between movable mirror and variable-transparent mirror, results in constructive
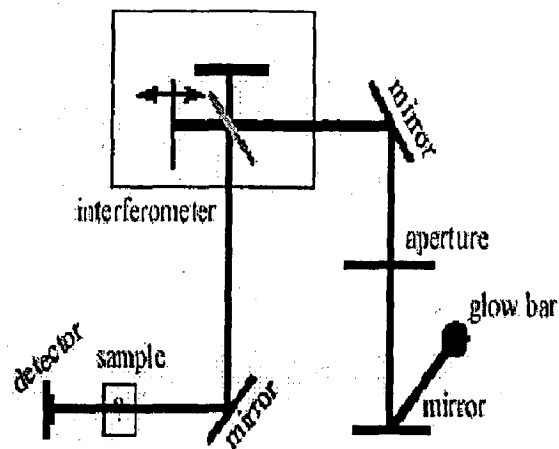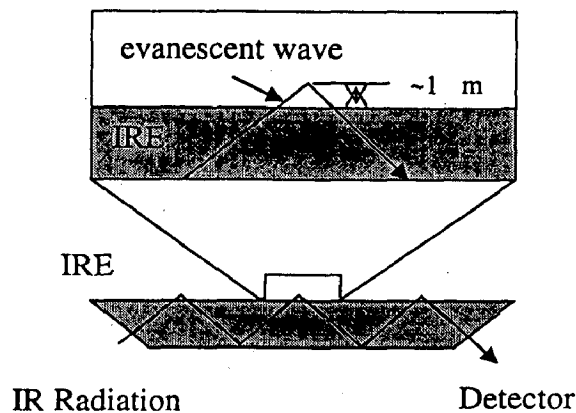
Figure 2-11: Total internal reflection at the interface of an internal reflection element and depth of penetration of the evanescent wave is approximately 1μm (top), Schematic representation of FTIR Spectrometer (bottom).

or destructive interference. The modulated radiation is then passed through the sample, where absorption takes place according to the excited vibrations in the sample. The detector transfers the optical signals into electrical signals, which are then Fourier analyzed by the computer.

2.3.2.2 Photometric Measurements

2.3.2.2.1 Colorimetric Determination

Simple sugars, oligosaccharides, polysaccharides, and their derivatives, including the methyl ethers with free or potentially free reducing groups, give an orange - yellow color when treated with phenol and concentrated sulfuric acid. Thus phenol in the presence of sulfuric acid can be used for the quantitative colorimetric micro determination of sugars and their methyl derivatives, oligosaccharides, and polysaccharides. The method is simple, rapid, and sensitive, and gives reproducible results. The reagent is inexpensive and stable, and a given solution requires only one standard curve for each sugar. The color produced is permanent and it is unnecessary to pay special attention to the control of the conditions[33].

2.3.2.2.2 UV/VIS Spectroscopy:

Ultraviolet-Visible Spectroscopy or Ultraviolet-Visible Spectrophotometry involves spectroscopy of photons. It uses light in the visible and in adjacent near ultraviolet (UV) and near Infrared (IR) ranges. In this region of energy space molecules undergo electronic transitions. The UV-VIS spectra have broad features that are of limited use for sample identification but are very useful for quantitative measurements. The concentration of an analyte in solution can be determined by measuring the absorbance at some wavelength using the Beer Lambert Law given by

$$A_b = cL_0$$

A_b is absorbance, has no units-it is the logarithm of the ratio of light intensity incident on the sample divided by the light intensity leaving the sample.

is the molar absorbtivity (extinction coefficient), $mol^{-1} l cm^{-1}$

L_0 is the path length of the sample, cm

MATERIALS AND EXPERIMENTATION

3.1 CROSSFLOW MEMBRANE FILTRATION SYSTEM

3.1.1 Model Polysaccharide Suspension

Three different polysaccharides denoted as Xanthan, Actigum CS 11 and Glucan by the supplier (Bioprocess Engineering Department, TUB, Berlin) were selected as model polysaccharides for the membrane filtration experiments. Dynamic light scattering (DLS) measurements were used to verify the size and polydispersity of the polysaccharides. The Xanthan and Actigum CS 11 polysaccharides were received as powders and Glucan was received as concentrated aqueous suspension and it contained little biomass in it. According to the supplier, the Glucan aqueous suspension was obtained directly after fermentation during manufacturing. The stability of the polysaccharide suspensions investigated in the crossflow membrane filtration experiments was determined by measuring changes in particle size distribution with time using Dynamic light scattering. The DLS results showed all the polysaccharide samples are polydisperse in nature.

3.1.1.1 Xanthan Polysaccharide

Xanthan gum is a high molecular weight extracellular polysaccharide produced by bacteria of the genus Xanthomonas. According to the supplier the Xanthan polysaccharide molecular weight was approximately 3 MD. Commercial Xanthan gum is extracted from Xanthomonas campestris[34,35,36]. Xanthan gum may be chemically considered as an anionic polyelectrolyte, with a backbone chain consisting of (1-4) β-d-glucan cellulose. The polymer backbone is substituted at C-3 on alternate glucose residues with a trisaccharide side chain. The side chain consists of β-d-mannopyranosyl-(1-4)-(α-d-glucuropyranosyl)-(1-2)-β-d-mannopyranoside 6-acetate. A pyruvic acid residue is linked to the 4 and 6 positions between 31–56% of the terminal d-mannose residues[34,35,36,37]. Acetyl and pyruvate substituents are linked in variable amounts to the

side chains, depending upon which X.campestris strain the Xanthan isolated from. The pyruvic acid content also varies with the fermentation conditions. On average about half of the terminal mannoses carry a pyruvate, with the number and positioning of the pyruvate and acetate residues conferring a certain irregularity to otherwise very regular structure. The structure of the repeating unit of Xanthan polysaccharide is given in figure 3-1. The Xanthan molecule undergoes a conformation transition from an ordered double helix to a random coil when heated to above, between 40 and 80°C depending on the ionic strength of solution[34]. Previous studies of Xanthan gum in solutions posses an ordered secondary structure. One possible model for this structure is a 5-fold single helix suggested by X-ray scattering studies of Xanthan fibers; electron micrographs, by contrast suggest that the native structure is multi-stranded with either 2 or perhaps 3
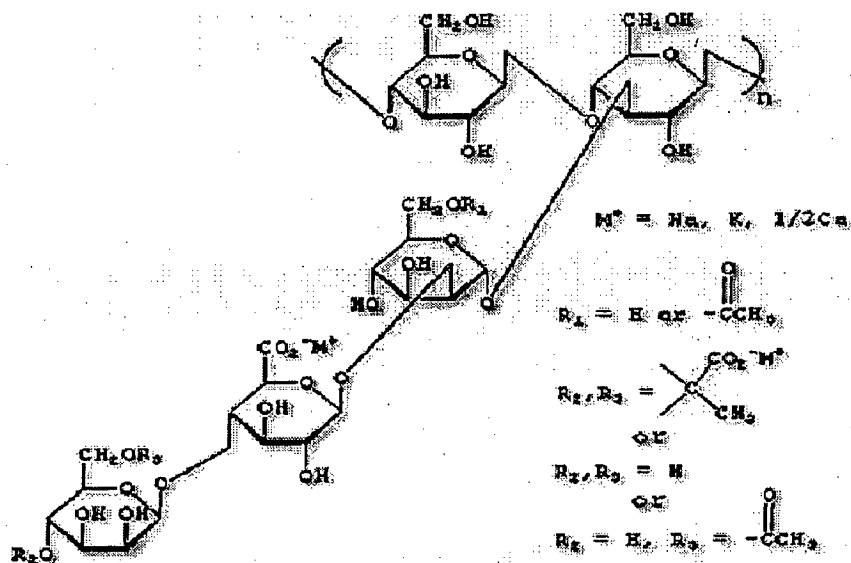
Figure 3-1: Repeating unit of Xanthan polysaccharide[37,39].

strands arranged in a right-handed twist[38]. These Xanthan molecules can easily forms a double-stranded helix and has a high tendency to aggregate, but it does not form gels by itself[35]. Xanthan is widely used as a viscosifier in the food and paint industries. The interesting rhelogical properties of Xanthan solutions arise from its ordered helical structure, which produces a rigid rod-like molecule. The backbone structure and high molecular weight of Xanthan result in rheological properties that are insensitive to ionic strength in solution as compared with other polyelectrolyte and create a molecule that is

32

resistant to mechanical degradation. Techniques that have been used to study the molecular size of Xanthan include electron microscopy, light scattering, viscometry, and ultracentrifugation. Electron Micrographs show native Xanthan to have contour length of 2-10 m. Using classical light scattering methods, Xanthan was found to exhibit M= $2*10^6$ for solutions heated for 3 hr at 90^0 in 4M Urea and M = $13*10^6$ and $50*10^6$ for two native samples that were not heated[38]. Dynamic light scattering studies at < 0.01 % have diffusion coefficients of D^0_t = 2.4-2.7 * 10^{-8} cm^2/s for freshly filtered Xanthan in deionized water and for Xanthan in 4M Urea. Upon ageing for one week, the diffusion coefficient in water alone decreased to D^0_t = 1.1 * 10^{-8} cm^2/s but did not increase with time in Urea. This difference was interpreted as being due to aggregation caused by hydrogen bonding and inhibited by the addition of Urea. Using the value of the diffusion coefficient for Xanthan in Urea and a measured value of the intrinsic viscosity [η] = 212 mL/g, they calculated a molecular weight of M = 2.16 * 10^6. From sedimentation and intrinsic viscosity measurements, Holzwarth obtained weight-average molecular weights of M_w = 2.8 * 10^6 for native, commercial Xanthan and M_w = 62 * 10^6 for native culture-broth.

3.1.1.2 Actigum CS 11

Scleroglucan is a natural polysaccharide, produced by fungi of the genus *Sclerotium*. Sclg is a general term used to designate a class of glucans of similar structure produced by fungi, especially those of the genus Sclerotium. The commercial product is termed Scleroglucan, but it is also known with other names according to the company that produces the polysaccharide (e.g., Actigum, Clearogel, Polytetran, Polytran FS, Sclerogum). Because of its peculiar rheological properties and its resistance to hydrolysis, temperature and electrolytes, Sclg has various industrial applications, especially in the oil industry for thickening, drilling muds and for enhanced oil recovery. Sclg is a branched homopolysaccharide that gives only D-glucose upon complete hydrolysis. The polymer consists of a main chain of (1-3)-linked ß-D-glucopyranosyl units; every third unit it bears a single ß-D-glucopyranosyl unit linked (1-6) shown in figure 3-2.
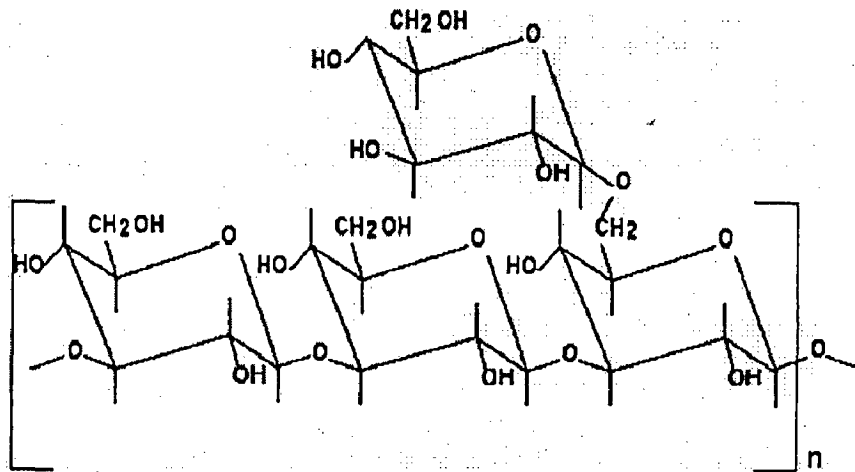
Figure 3-2: Molecular structure of scleroglucan consists of -1,3 linked glucose units in the main chain with -1, 6 linked glucose units branching out on every third unit of the main chain[40,41].

Oriented-fiber X-ray diffraction indicates that Sclg has a triple-helical backbone conformation and also that dissolved Sclg chains assume a rod-like triple helical structure[40], in which the Dglucosidic side groups are on the outside and prevent the helices from coming close to each other and aggregating. In dimethyl sulfoxide, or in solutions of pH=12.5 or higher, the reduced viscosity, the specific rotation and the sedimentation coefficient indicate, in each case, that Sclg molecules are monodispersed in a single-chain random coil.

3.1.2 Crossflow Membrane Filtration Unit

For the investigation of polysaccharide fouling phenomenon special membrane test cell suitable for highly suspensions was used. The schematic diagram of the laboratory-scale crossflow membrane filtration system is shown in figure 3-3. The aim of this project is to use a standard protocol and hence a batch apparatus but at the same time operate as closely to reality as possible. This includes crossflow conditions and as little impact on the suspended particle structure as possible. The main unit of the membrane test cell shown in figure 3-4. The flow region of the membrane test cell used in the experiments can be decomposed into five sub regions: inlet and outlet tubes, narrow flat slit (channel) directing the flow normal to the axis of the inlet and outlet tubes, and two ducts connect inlet and outlet tubes with the channel.
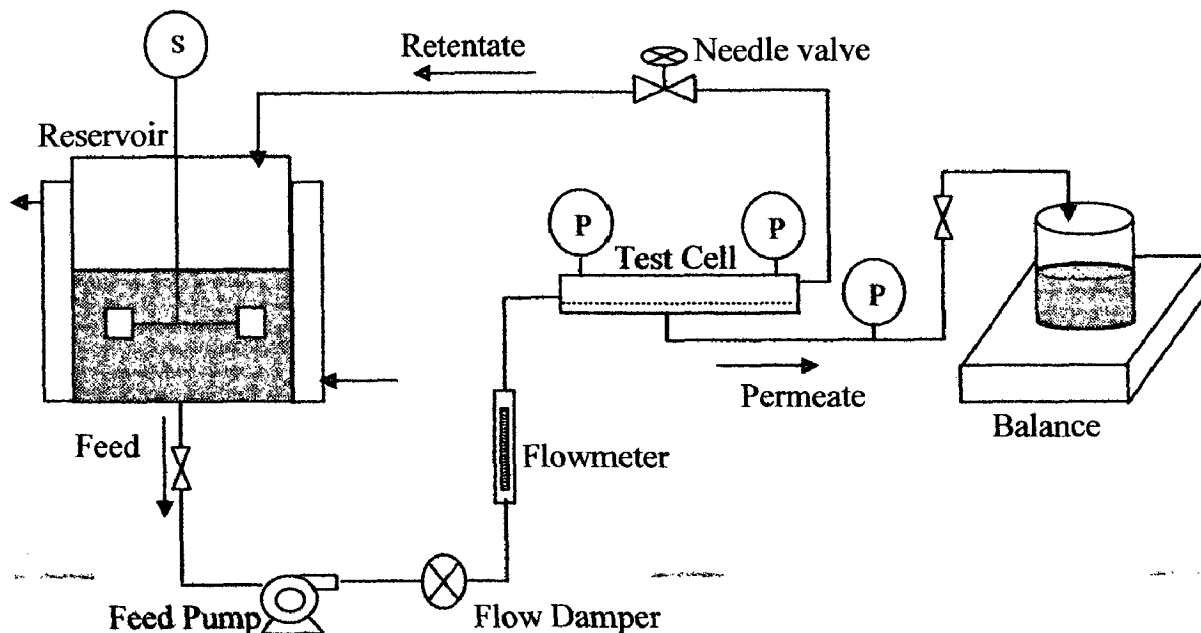
Filtration Membrane Characteristics

Filtration Membrane Characteristics	
MWCO	: 10 KDa and 30 KDa
Material	: Regenerated Cellulose
Filtration area:	0.0088m^2

Operating Conditions	
Stirring rod	: 200 rpm
TMP	: 1.2 and 1.4 bar
Temperature :	20°C

P-Pressure sensors, S-Stirrer

Figure 3-3: Schematic description of the laboratory-scale crossflow membrane filtration unit.
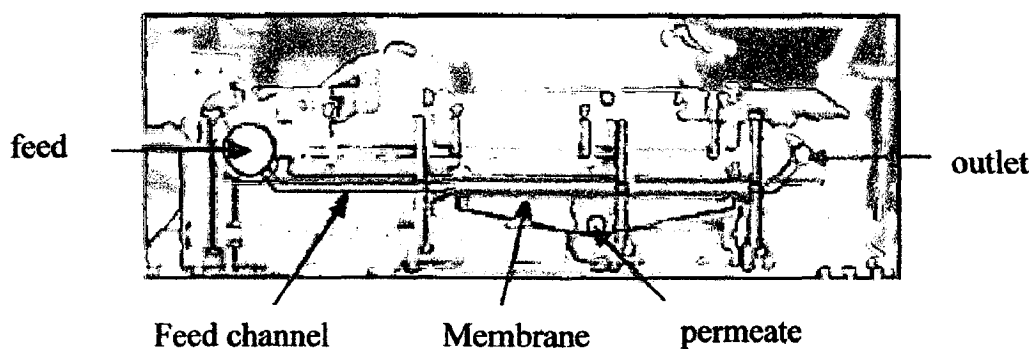
Figure 3-4: Picture of crossflow membrane test cell

35

The feed, polysaccharide suspension after entering the channel of the membrane test cell through the inlet tubes, passes over the membrane, makes 90 degree turn to enter the outlet tube and exits the system. The length, the width and height of the filtration channel in the crossflow membrane test cell are 160, 55 and 1 mm correspondingly. The dimensions translate to a cross-sectional flow area of 0.0055 m^2 and 0.008 m^2 respectively.

The polysaccharide suspension was held in 8 liter feed tank/reservoir equipped with stirrer rotating at 200 rpm and was fed to the inlet port of the membrane module by a Centrifugal pump (Cole-Palmer Instruments Co. Nile). The feed flow rate was measured by a digital flow meter connected to the inlet of the membrane module. The transmembrane pressure was set by a stainless steel needle valve installed on the outlet side of the membrane module. The transmembrane pressure was measured by a transducer (Model DPI 5-44, Validyne Engineering corp. Northbridge, CA) connected to the inlet of the membrane module. The transducer measures pressure ranging from 0 to 32 psi (220 KPa) with a reported accuracy of 0.5%. Temperature was controlled at 20^0C by circulating chilled water surrounding the container holding the feed suspension. The permeate flux through the membrane was measured by collecting the permeate at predetermined time intervals in a preweighed beaker and weighing the sample to determine the permeate volume. This was done by an electronic balance and recorded using a computer.

3.1.3 Model Membrane and Crossflow Filtration Experiments

All experiments were performed using regenerated Cellulose membrane. Membranes with a molecular weight cut off 10000 Daltons and 30000 Daltons were chosen. The details of the membrane used are shown in Table (3-1). The sample membrane sheet was cut into membrane sheets of appropriate size (16* 5.5 cm, with rounded corners) to fit the crossflow membrane test cell). Before each experiment, the filtration system was cleaned thoroughly using deionized water for half an hour and the water remained in the damper, inlet and outlet tubes were discarded carefully. Filtration experiments were performed for different polysaccharides at various feed particle concentrations. The polysaccharide feed suspension was prepared by dissolving defined

36

amount (respective to specific polysaccharide concentration) of polysaccharide in 7 liters of deionized water taken in the feed tank. The value at the bottom of the feed tank was closed and the feed suspension was stirred for a time period of 1 hour for all polysaccharides in all experiments.

Table 3-1: characteristics of flat sheet membrane used in crossflow membrane test cell

Membrane Material	MWCO (Daltons)	Manufacturer	Applied Pressure
Regenerated Cellulose	30000	Sartotius	1.4 bar
Regenerated Cellulose	10000	Sartotius	1.2 bar

The membrane was then conditioned by pumping the prepared feed suspension at zero transmembrane pressure and moderate flow rate for approximately half an hour to ensure stable performance. Then the transmembrane pressure was set by the needle valve on the outlet side of the membrane module. To ensure analogous fouling conditions for all membrane, the initial transmembrane pressure was adjusted to yield the same initial permeate flux for all experiments. But still the initial permeate flux showed different values because of the inherent property of the membrane.

The experiments were conducted to study the fouling tendency of polysaccharides when they are taken in different concentrations. All the operating conditions were maintained constant: crossflow velocity 0.5 m/s and transmembrane pressure 1.2 bars and 1.4 bars in some cases. For every experiment a new membrane sheet was used. A flow meter and transducer measured the flow rate and transmembrane pressure respectively. The suspension flowing out of the crossflow membrane test cell i.e. retentate was recycled back to the feed tank and circulated along the surface of the flat-sheet membrane in the membrane module. Flux measurements for all experiments were taken over a period of 130 minute and each permeate sample was collected over a period of 20 seconds. The experiments conducted with Xanthan polysaccharide were repeated more than twice and the transmembrane flux results were very reproducible. At the end of each

5

experiment membrane was removed from the membrane test cell and any presence of cake layer was inspected by Attenuated Total Reflectance-Fourier Transform Infrared Spectroscopy (ATR-FTIR) measurements. Then the feed suspension was discarded, deionized water was introduced into the feed tank and pumped to flow through the crossflow membrane filtration system.

3.1.4 Polysaccharide Suspension Analysis

Several experiments were conducted to determine any change in stability of polysaccharide suspension during crossflow filtration for all the experiments. A feed sample was collected just before the start of the filtration run by a 25ml volumetric pipette and then every 20 minute for the remainder of the run up to 100 minute. The final sample was collected at 130 minute.

The collected samples were subsequently analyzed for

> ➤ concentration by the UV Absorbance of the sample and by colorimetric determination

> ➤ viscosity by capillary viscometer measurements

> ➤ particle size distribution by Dynamic Light Scattering (DLS)

3.2 Dynamic Light Scattering

Dynamic light scattering measurements were carried out in a Autosizer S4700 (128 channel Series 7032 Multi-8 correlator, Malverns Instrument GmbH) equipped with a Argon Laser (Lexel, Model 95 Ion Laser) emitting a wavelength of 488nm operating between 50 mW-160mW and coupled to a series 7032 Multi-8 correlator (Technical Chemistry Department, TUB, Berlin). The correlograms were evaluated using PCS for Windows V1.41 original software by Malvern. Auto mode and cumulant analysis were used by default. Latter Contin analysis was used for particle size distribution analysis. All measurements were performed at an angle of 90^0.

3.2.1 Experimental Set Up

The experimental set up is shown in figure 3-5. The light from Argon Laser with wavelength 488nm after passing through a focusing lens (L) enters a temperature

controlled vat in which the polysaccharide sample in a 10 mm inner diameter cylindrical scattering glass cell is positioned at the center and so that the cell is perpendicular to the incident beam. The scattered light beam leaves the cylindrical glass cell at an angle 90^0 to that of incident radiation. The glass outside of the temperature controlled vat is cylindrical in shape so the incident beam always has an angle of 0^0 to the normal. This causes no refraction at the interface.
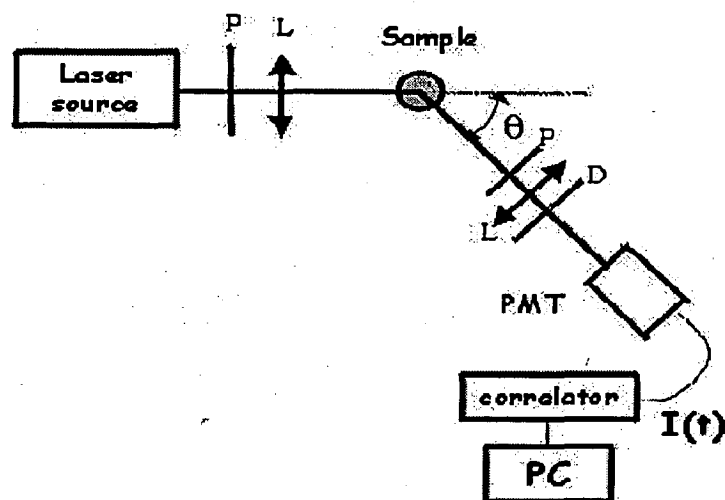
Figure 3-5:Experimental setup of Dynamic Light Scattering, L-lens, PMT- Photomultiplier Detector, PC-Personal computer, -Scattering angle, I(t)-Intensity at time t.

It is also necessary to enclose the scattering cuvette/cylindrical cells in a transparent container filled with a refractive index matching fluid that minimizes the change in index at the edge of the cuvette and pushes the air interface further away from the detector's optical axis. Hence the sample cell was surrounded by water to reduce the amount of stray light that reached the detector. A water bath attached to the Goniometer controlled the temperature of the water at 25^0C and a micro pump was equipped to remove dust. The controlling of the temperature in vat is done for two reasons. The first is that the sample is then stable and there are no temperature gradients. Secondly, the sample is kept at a specific temperature because the refractive index is depending on the temperature and by controlling the refractive index the amount of multiple scattering can be controlled. The scattering angle was set at 90^0 by adjusting the rotating rigid arm.

The scattered radiation was focused by another lens (L) after which a pinhole arrangement images a small scattering volume onto the photomultiplier (PMT). The pinhole arrangement minimizes spatial averaging and maximizes intensity fluctuations. The second lens (L), the pinhole arrangement and the detector are mounted on a movable computer controlled arm. The signal of the photomultiplier/detector (PMT) is fed into a purpose build correlator to compute the normalized time-average intensity correlation functions. In DLS instrumentation, the correlation summations as mentioned in Eqn.18 do performed using an integrated correlator, which is a logic board comprise operational amplifiers that continually add and multiply short time scale fluctuations in the measured scattering intensity to generate the correlation curve. The picture of the experimental set up is shown in figure 3-6. The correlator used in our experiments contained 128 channels, working in parallel mode. In parallel mode the correlator was split into four sub-correlators over which the 128 channels were distributed evenly. Each sub-correlator then samples linearly across a number of channels with a different initial sample time. The sample times vary as Γ_1, $d\Gamma_1$, $d^2\Gamma_1$, $d^3\Gamma_1$.....$d^7\Gamma_1$ depending on the number of sub correlators used. Γ_1 is the shortest sampling time and d is the dilation factor by which the samples times in the other correlators are varied, typically set to between 2 and 6. In all experiments the dilation factor was set to 2 by default. The sample or delay time was assumed automatically dependent in the correlator settings and in this work it varied between 50 s and 200 s. The correlator stores the data in channels. Each channel corresponds for different delay times. These are the channels to which references are made later. Each polysaccharide samples taken from feed tank at different time was recorded 5 times using 10 sub run measurements and appropriate sample viscosity was assumed as measured by viscometer analysis. Before measurement all samples were allowed to settle for approximately half an hour in order to remove any large particles that would cause much higher intensity value during DLS measurements. In order to avoid number fluctuations and multiple scattering effects the count rate was adjusted between 50-100 Kcounts/sec by adjusting pinhole between 50 to 500 m.
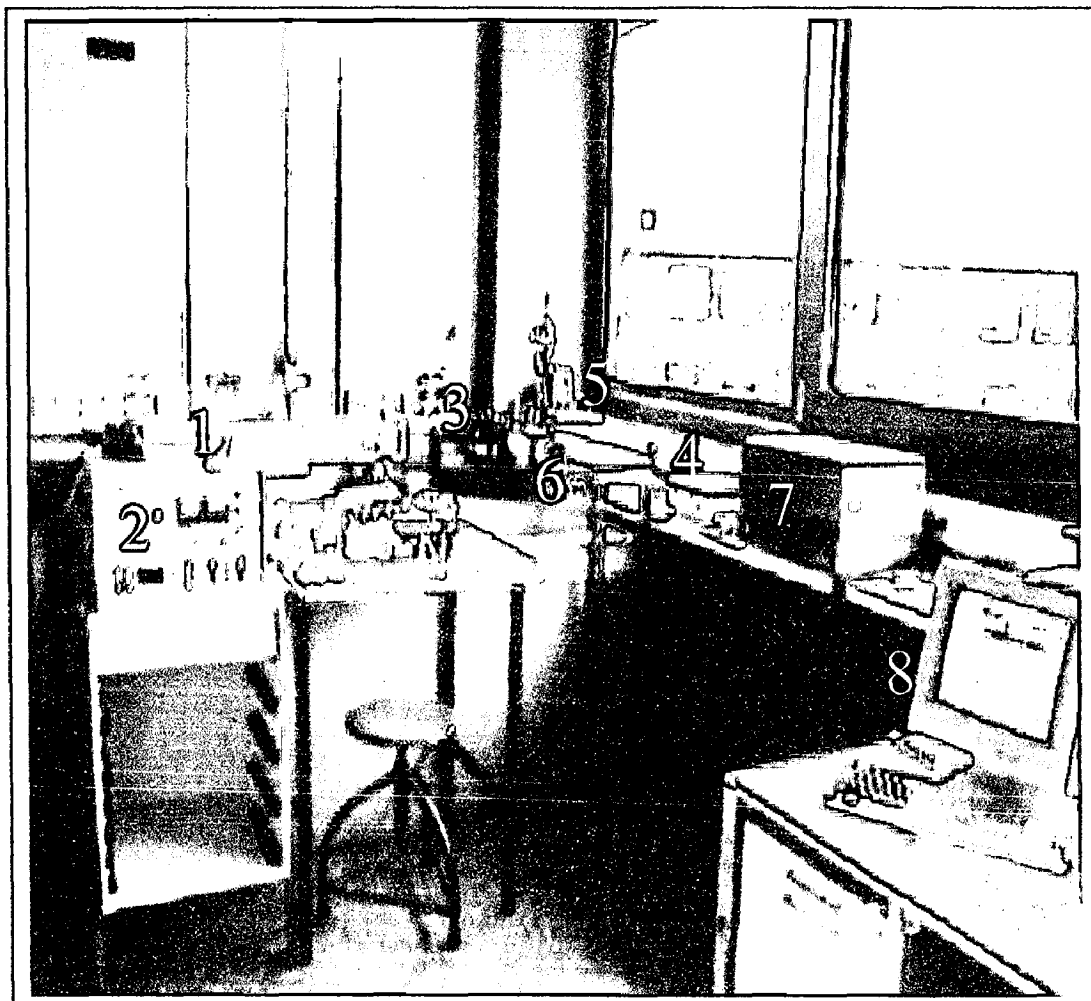
1. Laser 2.Power Supply 3. Sample cell assembly 4.temperature controller
5.Micropump 6.detector 7. Correlator 8. Computer

Figure 3-6: picture of dynamic Light scattering experimental set up.

42

3.3 VISCOSITY MEASUREMENTS

The kinematic viscosity measurements were performed at room temperature with an Ubbelohde capillary viscometer equipped with an automatic Schott-Gerate Model AVS300 GmbH viscometry system (Technical Chemistry Department, TUB, and Berlin). The Ubbelohde capillary viscometers with inner diameters 63 mm were chosen for measurements. In this instrument, efflux time measurements were fully automatic and were determined on a digital display (4-digit print out) within an uncertainty of ±0.01 s. Approximately 15ml of polysaccharide sample was placed in viscometer and the efflux time measurements were made four times for each sample and average time was considered for kinematic viscosity estimation.

During the initial period of work viscosity measurements were conducted with Rotational viscometer VT550 (Geb Haake GmbH, verfahrenstechnik, TUB, Berlin). In order to include low viscosities, the viscometer was supplied with the double gap measurement device. The width of the annular gap was 0.4 mm. Through a RS232 port the viscometer was connected to a computer supplied with the Haake application software 2.3. However, the results obtained were not reliable (viscometer is reliable as such but detection limit is > 2 mPa.s) when compared with capillary viscometer measurements. Then onwards viscosity measurements were conducted with capillary viscometer.

3.4 ANALYTICAL MEASUREMENTS

3.4.1 Photometric measurements

3.4.1.1 UV absorption at 280 nm

The calibration was done with Xanthan polysaccharide sample. The Xanthan polysaccharide of concentrations (2-100 mg/l) was prepared and all found to exhibit maximum absorbance value at a wavelength of 280 nm (shown in section 4.4.1). The calibration curve is shown in figure 3-7. Calibration curve for the Xanthan showed that the UV absorbance is linearly proportional to polysaccharide concentration. The UV absorbance at a wavelength of 280 nm (UV_{280}) was measured with UVIKON 943 Double

Beam UV/VIS spectrophotometer (Technical Chemistry Department, TUB, Berlin). For all samples Hellma 10 mm precision cuvettes made of quartz glass Suprasil was used. The concentration of the polysaccharide sample collected at different times during filtration experiments was calculated from UV absorbance value at 280 nm (UV_{280}) and the linear equation for concentration obtained from calibration.

3.4.1.2 Polysaccharide Analysis/Colorimetric Determination

Polysaccharide concentrations were analyzed according to the method of Dubois et al[33]. The procedure is presented in appendix 1. The calibration curve is shown in figure 3-8. D-Glucose Monohydrate was used for calibration (5-100 mg/l). Each polysaccharide was analyzed twice at 490 nm with SPECORD 200 UV/VIS Spectral photometer (Verfahrenstechnik, TUB, Berlin).

3.4.2 Attenuated Total Reflectance- Fourier Transform Infrared Spectroscopy (ATR-FTIR)

Fourier Transform Infrared Spectroscopy (ATR-FTIR) is useful in detecting representative functional groups in organic samples. However, an identification of specific substances is not possible due to complex matrix of organic matter. Attenuated total reflectance – Fourier transform infrared spectra are measured using a Spectrum One FTIR Spectrometer from Perkins Elmer (Technical Chemistry department, TUB, Berlin) with composite Zinc Selenide and Diamond flat plate crystal. The system is set to use an IR light source, a KBr beam splitter and a Mercury Cadmium Telluride (MCT) detector. During the spectrum acquisition the measuring chamber is purged with purified air (without CO_2, and water) in order to minimize interferences by CO_2 and water. ATR/FTIR analyses were performed on fouled membrane samples of about 10 by 10 mm. All the measurements were made the next day after filtration experiments. The fouled membrane sample was pressed against flat plat Zinc Selenide/Diamond internal reflection element. The pressure plates of the Universal ATR accessory were adjusted to 130 to 140 gauges with a torque wrench. A series of 4 scans were collected at $4 cm^{-1}$ resolution.

$y = 0.0012x + 0.001$
$R^2 = 0.9931$

◆ Abs Xanthan
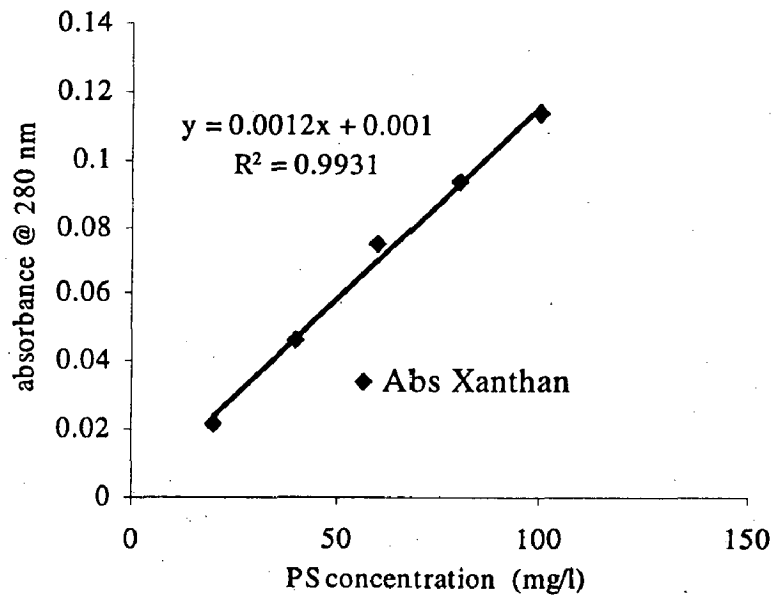
• *Measured data* --- *linear fit over all points*

Figure 3-7: Calibration curve for UV/VIS spectrophotometer measured with Xanthan polysaccharide

$y = 0.0106x + 0.0095$
$R^2 = 0.9993$

◆ Abs D Glucose Monohydrate
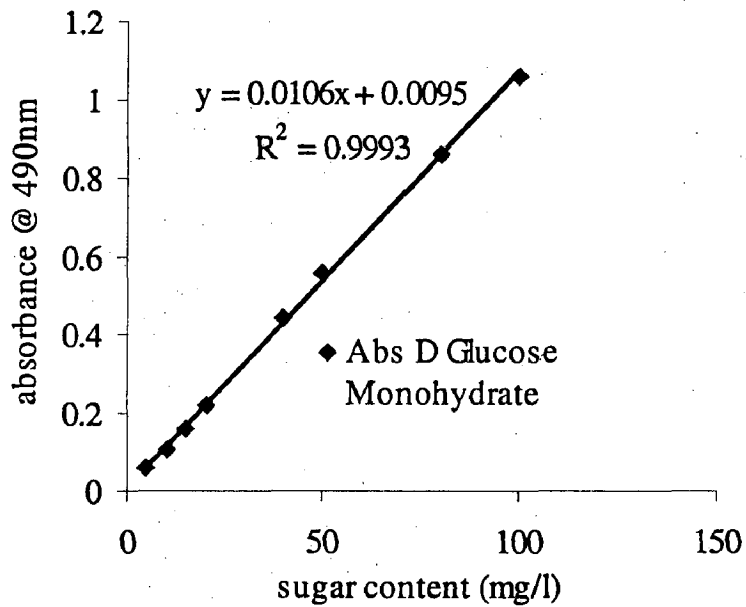
• *Measured data* --- *linear fit over all points*

Figure 3-8: Calibration curve for UV/VIS spectrophotometer measured with D-Glucose Monohydrate.

45

The sample spectra were ratioed against a bare zinc Selenide/Diamond background spectrum and converted to absorbance with Spectrum one B software, version 3.01 (Perkin Elmer Limited 1998). Spectra were corrected to take into account the wavelength dependence of ATR and baseline corrected. Difference spectra were obtained by digital subtraction with the Spectrum one B software. The resulting bands and peaks at different wave numbers can be attributed to specific chemical bonds[22].Different substances and respective wave numbers are shown in table (3-2).

Table 3-2: wave numbers of functional groups of polysaccharides, proteins and humic substances[22].

Wave numbers	Chemical bond	Compound recognition
1080-1100	C-O bond of carbohydrates	
2940	-CH stretch	Polysaccharides
3400	-OH stretch	
1636-1660	C = O bond	
1380-1390	-NH bond	Proteins
1550	-C-N bond	
1620	Aromatic group	
1720	Carboxylic group	Humic substances
3400	Alcohol group	

48

RESULTS AND DISCUSSION

4.1 FOULING ANALYSIS/CROSSFLOW MEMBRANE FILTRATION RESULTS

4.1.1 Raw Flux Data

Insight into the possible fouling mechanism and dependency of the polysaccharide layer can be obtained by evaluating transient flux decline and membrane resistance including fouling and cake resistance during filtration of solutions of the individual polysaccharide samples. Figure 4-1 shows typical experimental data for the filtrate flux as a function of time during constant transmembrane pressure crossflow filtration for polysaccharides at different concentration.

The results demonstrate that the permeate flux declines much faster with increasing polysaccharide feed concentration. The stronger decline of permeate flux at higher feed polysaccharide concentration is attributed to the increased particle transfer rate to the cake layer. The phenomenon behind this is described in following section. The initial flux ranged from 180 to 260 l/m^2h for cellulose membrane with MWCO 30 KDa. This variation in initial flux is due to inherent membrane variability and variation in polysaccharide concentration. The flux declined quite rapidly at the start of the filtration, with the rate of the flux decline increasing with increasing bulk polysaccharide concentration. The extent of flux decline was significantly different from one another; the degree of flux decline was intimately related with membrane pore size. At long times at about 130 minute of filtration time, the transmembrane flux does not approach a constant value for all polysaccharide conducted with 30 KDa membrane (Actigum CS 11(20mg/l), Xanthan (20mg/l), Glucan). The transmembrane flux data for Xanthan (40mg/l) and Actigum CS 11 (20 mg/l) solutions conducted with 10 KDa appeared to approach a nearly constant value which was slightly smaller than the initial flux. Immediate fouling of cellulose membrane with 10 KDa was manifested by a rapid initial permeate flux decline for both Xanthan (40mg/l) and Actigum CS 11 (20mg/l) polysaccharide. This rapid initial flux decline clearly shows that these polysaccharide particles were

significantly larger than the membrane pore size i.e., very low porosity therefore rejection was high and a result their accumulation increased near the membrane surface.

4.1.2 Volume of Permeate vs. Time of Filtration

Figure (4-2) shows typical experimental data for the total collected filtrate volume as a function of time during constant transmembrane pressure crossflow filtration for polysaccharides at different concentration. The filtrate volume increases nearly independent of the bulk polysaccharide concentration at earlier stages of operation where J is similar to J_0 for all polysaccharide except Actigum CS 11 (20 mg/l) with 10 KDa membranes. The curve diverges after about 10 minute, with the total collected volume increasing with decreasing polysaccharide concentration. Table (4-1) shows the total filtrate volume collected for different polysaccharide after about 130 minute of operation.

Table 4-1: Total volume of permeates data collected after 130 minute of filtration time.

Polysaccharide	Concentration (mg/l)	Membrane (MWCO)	Total volume after 130 minute of operation (l)
Xanthan	20	30	2.727
Xanthan	40	10	1.631
Xanthan	60	30	2,169
Glucan	55	30	2.219
Actigum CS 11	20	30	1.124
Actigum CS 11	20	10	0.432

Crossflow filtration of all polysaccharide sample conducted with 30 KDa membranes does not show linearity during the initial stages of operation, rather linearity exists at longer time. Although the data at long times look nearly linear, the filtrate (permeate) flux continues to decline with time leading to a gradual reduction in the rate at which volume increases. This is discussed in more detail subsequently. Crossflow filtration of polysaccharide conducted with 10 KDa membranes shows a slightly different behavior than that of 30 KDa. The curve shows linearity throughout the entire experiment. The
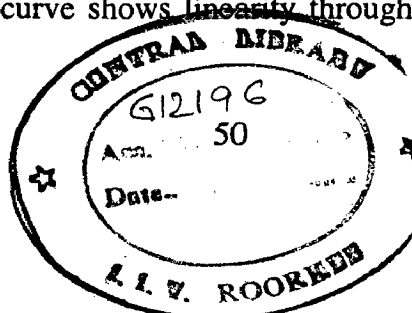
larger reduction in total filtrate volume for Actigum CS 11 polysaccharide (20 mg/l) at the 10 KDa membrane is due to smaller pore size of membrane, the polysaccharide is large enough to pass through the membrane pores. The difference in total filtrate volume collected for Actigum CS 11 polysaccharide with two different membrane of MWCO 10 KDa and 30 KDa of same material clearly reveals the dependency of permeate flux on pore size of membrane.

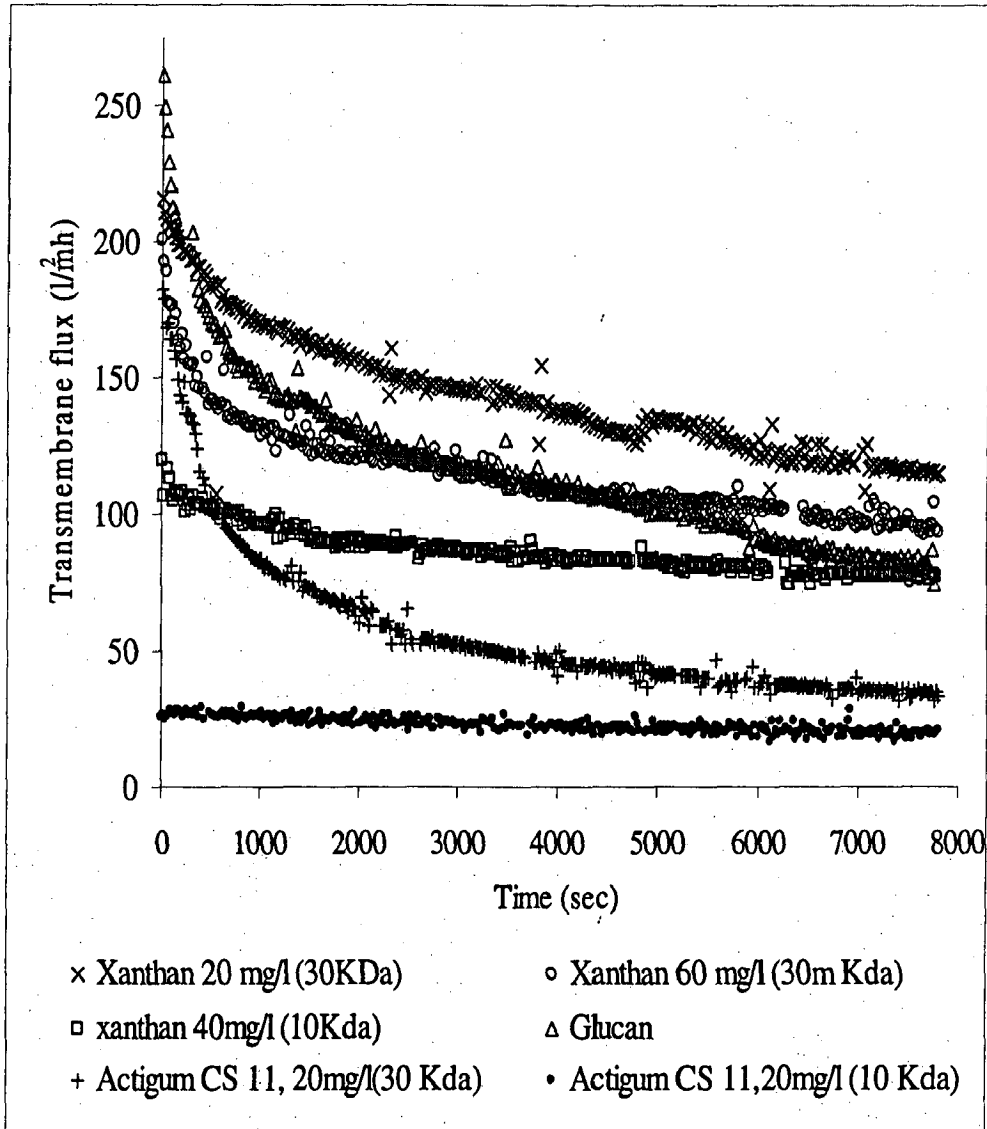
Figure 4-1: Flux decline curves of crossflow membrane test cell experiments for Xanthan (20, 40, 60 mg/l), Actigum (20 mg/l) and Glucan with cellulose membrane of 30 KDa and 10 KDa.
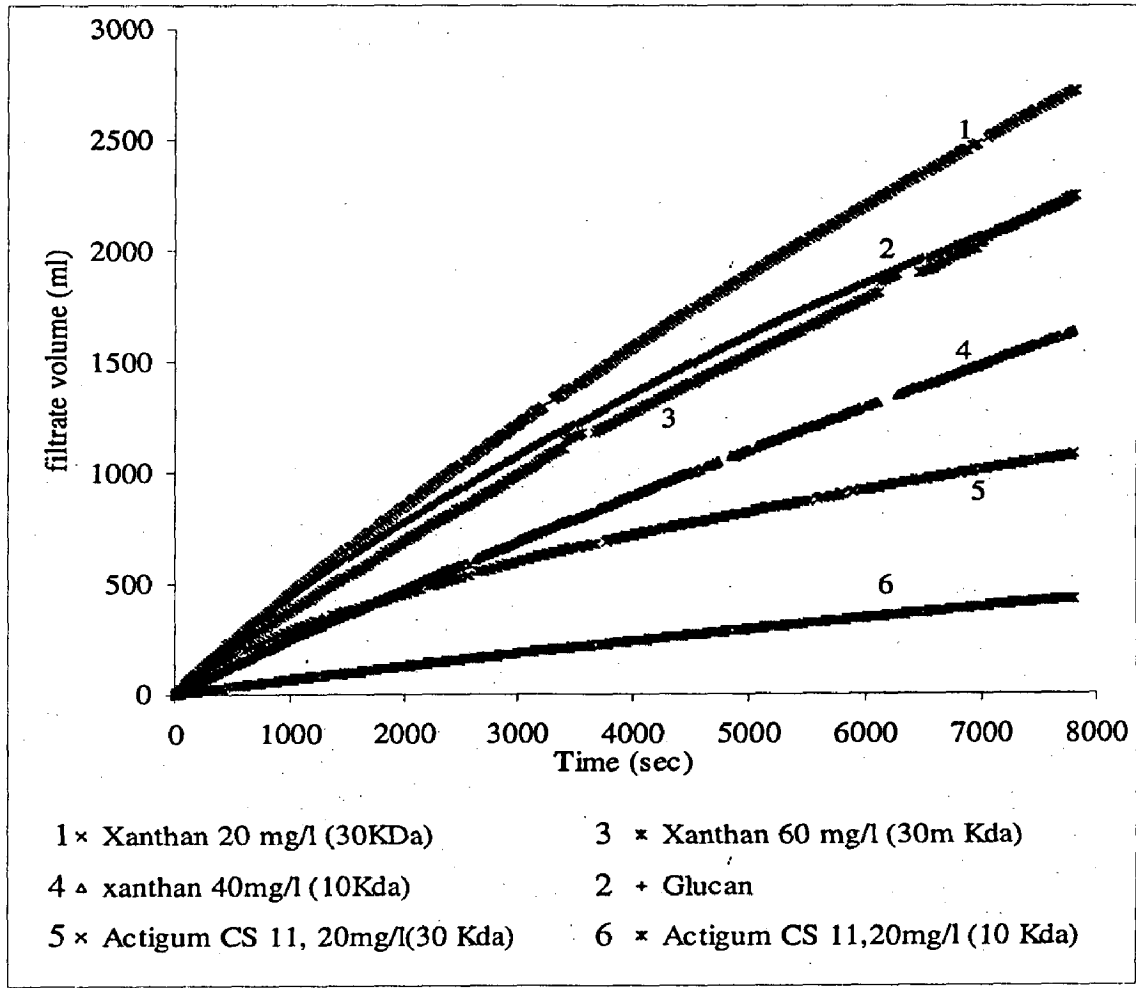
Figure 4-2: volume of filtrate curves as a function of time for crossflow membrane test cell experiments of Xanthan (20, 40, 60 mg/l), Actigum (20 mg/l) and Glucan with cellulose membrane of 30 KDa and 10 KDa.

54

4.1.3 Resistance vs. Time

The filtrate flux data can be used to examine the underlying mechanism by replotting the data in terms of the total resistance as given by resistances in series model Equation 1. The mentioned total resistance is the resistance related to polysaccharide filtration without differentiating between cakes and fouling (pore blocking/pore narrowing) resistance. Figure 4-3 shows the total resistance as a function of time for Xanthan, Actigum CS 11 and Glucan polysaccharide at different concentration using the membrane of MWCO 30 KDa and 10 KDa operated at 1.4 and 1.2 bar respectively.

The total resistance for all polysaccharides increases with a decreasing slope for the entire experiment. The total resistance for 10 KDa membranes is initially large due to the smaller pores and it increases slightly. The total resistance of the 30 KDa membranes starts off much lower, increases at the same rate as that of 10 KDa membranes till the end of experiment. The Glucan obtained directly after fermentation step shows slightly different behavior. Initially, the resistance for 30 KDa membrane operated with Glucan has the similar resistance value as the resistance for the membrane operated with Xanthan (20 mg/l), but exactly after 200 seconds, the resistance for the membrane filtered with liquid polysaccharide increases above the resistance of the membrane fouled with less dilute polysaccharide solution. Table 4-2 shows the total resistance data for different polysaccharide solutions measured after 130 minute of crossflow filtration.

Table 4-2: Total resistance data of different polysaccharides measured after 130 minute of filtration

Polysaccharide	Membrane (MWCO),KDa	Concentration (mg/l)	Total resistance after 130 minute of filtration
Xanthan	20	30	4.4355E+12
Xanthan	40	10	6.70871E+12
Xanthan	60	30	6.38866E+12
Actigum CS 11	20	30	1.43063E+13
Actigum CS 11	20	10	2.30105E+13
Glucan	55	30	6.08896E+12

It should be noted that total resistance depends on experimental conditions i.e., polysaccharide feed concentration, membrane material and pore MWCO. The experimental data clearly shows that the total resistance increases with increasing bulk polysaccharide concentration.

The total resistance (R_t) continues to increase even after 130 minute of filtration for all polysaccharides, indicating the flux never attains a steady state value under the conditions of experiment as seen in figure 4-3. The feed suspension of polysaccharide in the size range of membrane pore size would lead to pore plugging or pore narrowing mechanism indicated by resistance versus time curve of concave upward tendency or by point of inflection where in the fouling shifts from one fouling mechanism to another during the initial stages of filtration experiments. Thus the polysaccharide particle size distribution in feed suspension and MWCO of membrane is of much importance in determining the underlying internal fouling mechanism (pore plugging/pore narrowing) during filtration experiments.

MWCO of membrane has been determined with various standard molecules (polyethylene glycols, dextran). Unfortunately no exact correlation exists between the molecular weight and size of a molecule. The molecular size depends primarily on the structure of the molecule i.e., whether it is more in the shape of a long chain or globular. This results in different ratio of molecular weight to size of standard molecules used for MWCO determination. Hence no exact correlation exists between the MWCO of a membrane and its pore size. As a rule of thumb, it is often assumed that 100 kDa membranes correspond to approximately 10 nm pore diameter[22].

According to this rule, the pore size of membrane (Cellulose 30 KDa and 10 KDa) is approximately not more than 10 nm. The particle size distribution described in the latter section reveals absence of particle size in the range closer to the pore size of membrane. Adding to this, the total resistance behavior with time for all polysaccharide does not contain any point of inflection or concave upward tendency. Moreover for the smaller MWCO membrane, the fouling appears to be due to immediate fouling of the pores and a growing polysaccharide layer on the top surface of the membrane. This is supported by the second derivative of the resistance versus time curve being negative for the entire experiment.

It is hypothesized that Xanthan molecule is of semi flexible nature proposed to be right hand double helix and self association processes in Xanthan solution results in introduction of micro aggregates at low concentration to interact with each other at lower concentration would be theoretically expected[34]. The feed suspension under constant stirring condition during crossflow filtration results in aggregation of polysaccharide over time and the aggregates become large enough to be rejected by the membrane and serve as sites for further deposition of polysaccharide. The aggregate formations are discussed in the dynamic light scattering section. As discussed earlier the second derivative of the resistance versus time curve is then negative. The second derivative was calculated for all resistance versus time curve for all polysaccharide and it was found to be negative for the entire experiment (data not shown in report) showing that fouling appears due to immediate blocking of the pores and growing polysaccharide on the surface of the membrane. The concave down slope of the resistance as a function of time for Actigum CS11 (20 mg/l) filtered with 30 KDa membrane is more pronounced, slightly increasing compared to Xanthan and Glucan. The larger aggregates do not pass the membrane and the fouling is external (cake formation/cake build up). This rejected layer of large aggregates is apparently packed loosely enough to allow polysaccharide to pass through. Thus in the present study, crossflow filtration of different polysaccharide feed suspension, the plots of total resistance (R_t) as a function of time for cellulose membrane all yielded clearly concave down curves as per resistance in series model from beginning till the end of experiments implying that external fouling (i.e., via cake build up) is the main mechanism of fouling.
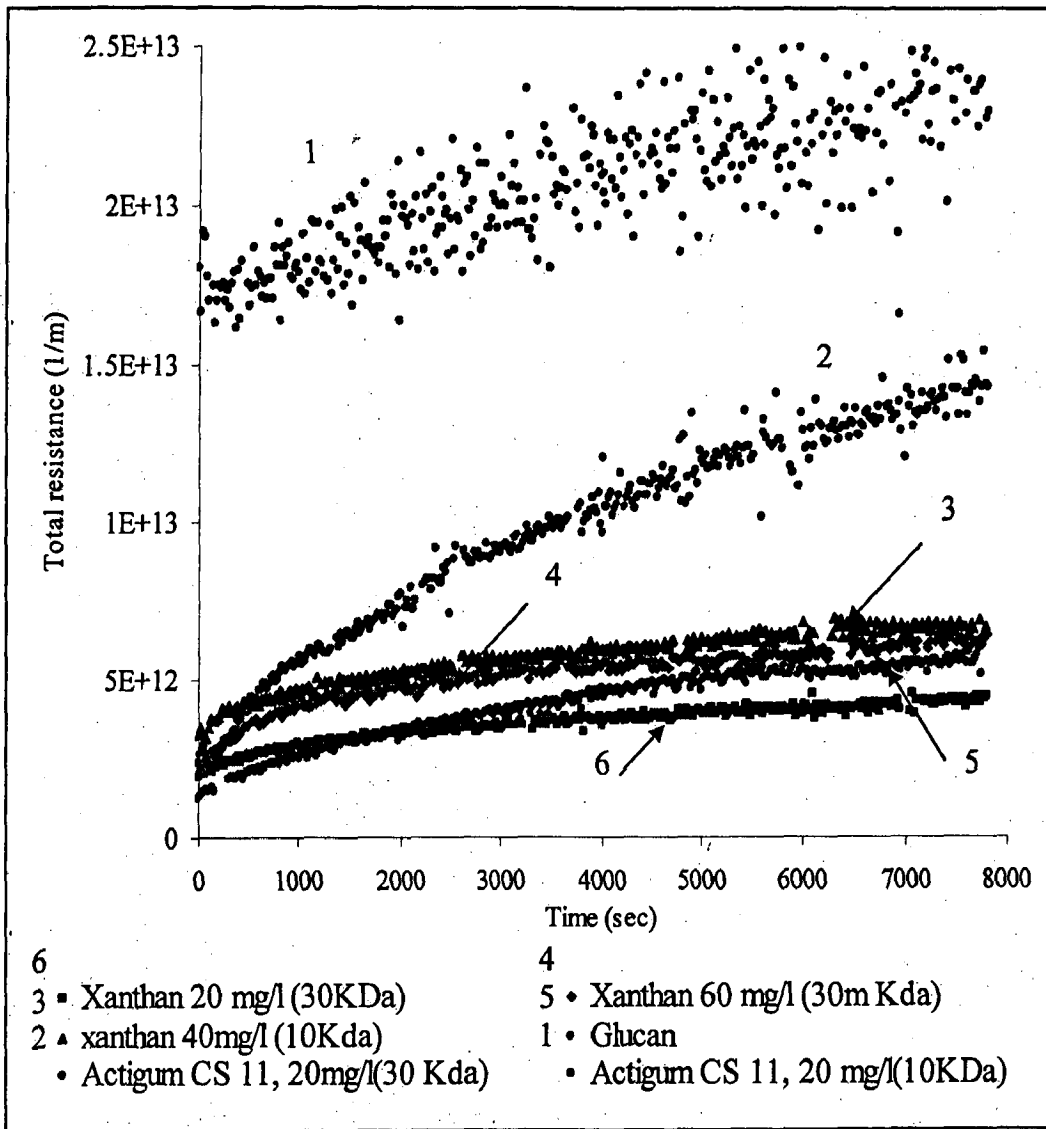
Figure 4-3: Resistance vs. time curves of crossflow membrane test cell experiments for Xanthan (20, 40, 60 mg/l), Actigum (20 mg/l) and Glucan with cellulose membrane of 30 KDa and 10 KDa.

60

4.1.4 Classical Filtration Laws

A more traditional approach to examine the predominant fouling mechanism is to plot the flux data in an appropriate liberalized form using characteristic coordinates developed by Hermia for pore blockage (permeate flux verses permeate volume), pore constriction (filtration time/permeate volume vs. filtration time) and cake formation (filtration time/permeate volume vs. permeate volume) models as discussed in theoretical section (Chapter 2). Figures (4-4 to 4-8) show the graphs using the characteristics coordinates on a crossflow membrane test cell with different polysaccharide and regenerated cellulose membrane (10 KDa and 30 KDa). If the shape of the resulting characteristic coordinate curve is linear in one of the graphs, one can attribute the observed flux decline to the corresponding fouling mechanism. The crossflow membrane test cell experiment conducted with Xanthan (20 mg/l, filtered with 30 KDa membrane) and Actigum CS 11 (20 mg/l, filtered with both membrane) a clear linear relationship exist between t/V versus V (filtration time/permeate volume versus permeate volume) and therefore it is assumed that cake formation is the predominant fouling mechanism. As can be seen from the graphs that these polysaccharides exhibit a t/V versus V plot with very high R^2 value of 0.99 is needed to indicate the predominance of one of the classical fouling mechanisms.

In contrast, no linearization is obtained with the cake formation model for Glucan and Xanthan (40 mg/l and 60 mg/l) crossflow membrane filtration nor can the pore constriction model or the pore blockage model explain the data. This means that either two or more fouling mechanism is relevant e.g. pore constriction and cake formation. Table 4-3 summarizes the result of all crossflow membrane test cell experiments with regard to the R^2 values obtained from linear fits in the characteristics plots for pore blockage, pore constriction and cake formation. The last column indicates the predominant fouling mechanism as given by R^2 value of greater than 0.99. In the case where none of the classical fouling mechanism plots result in a linear relationship "*" is entered for the corresponding crossflow membrane test cell experiment. For polysaccharides at lower concentration (20 mg/l) where one of the classical fouling models can explain the flux decline data, cake formation is the predominant fouling mechanism. In none of the crossflow membrane test cell experiments can the fouling

behavior of the different polysaccharides be described by pore blockage model as can be seen clearly from the filtrate versus volume of filtrate plot in figure 4-8.

*Table 4-3: R^2 values of linear fits of the flux decline data using the characteristic coordinates for the linear blockage, pore constriction and cake formation model, *- fouling mechanism is difficult to detect.*

| Membrane (MWCO)	Polysaccharide	Conc. (mg/l)	Pore constriction R^2 value	Pore Blockage R^2 value	Cake formation R^2 value	Predominant Fouling Mechanism
30	Xanthan	20	0.9753	0.904	0.9901	Cake formation
10	Xanthan	40	0.947	0.864	0.9618	*
30	Xanthan	60	0.9044	0.8033	0.9312	*
30	Glucan	550	0.9645	0.8723	0.9887	*
30	Actigum CS11	20	0.9708	0.7923	0.9995	Cake formation
10	Actigum CS11	20	0.9966	0.7002	0.9988	Cake formation and/or pore constriction
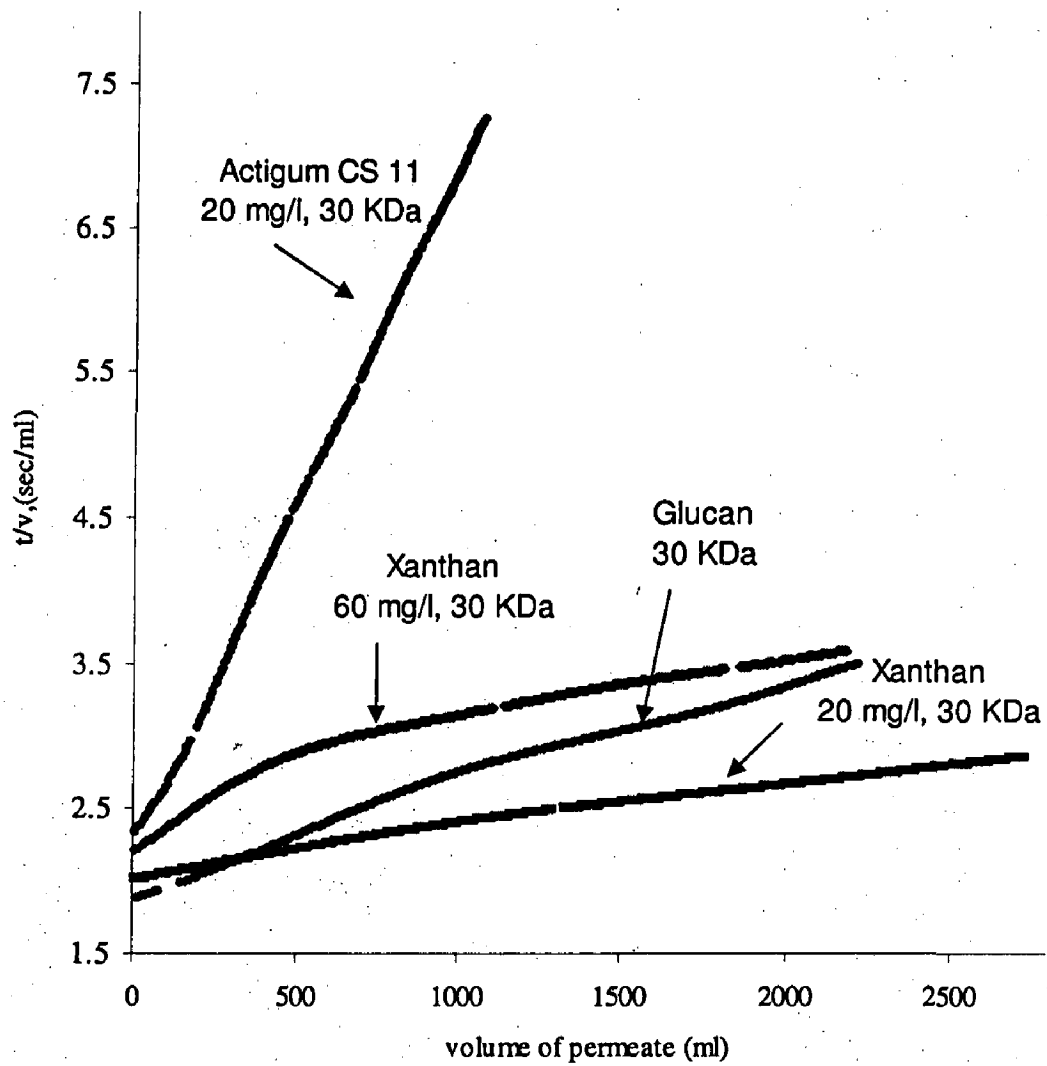
Figure 4-4: Linearized flux data for the regenerated cellulose membrane (30 KDa) filtration using characteristics coordinates for cake filtration.
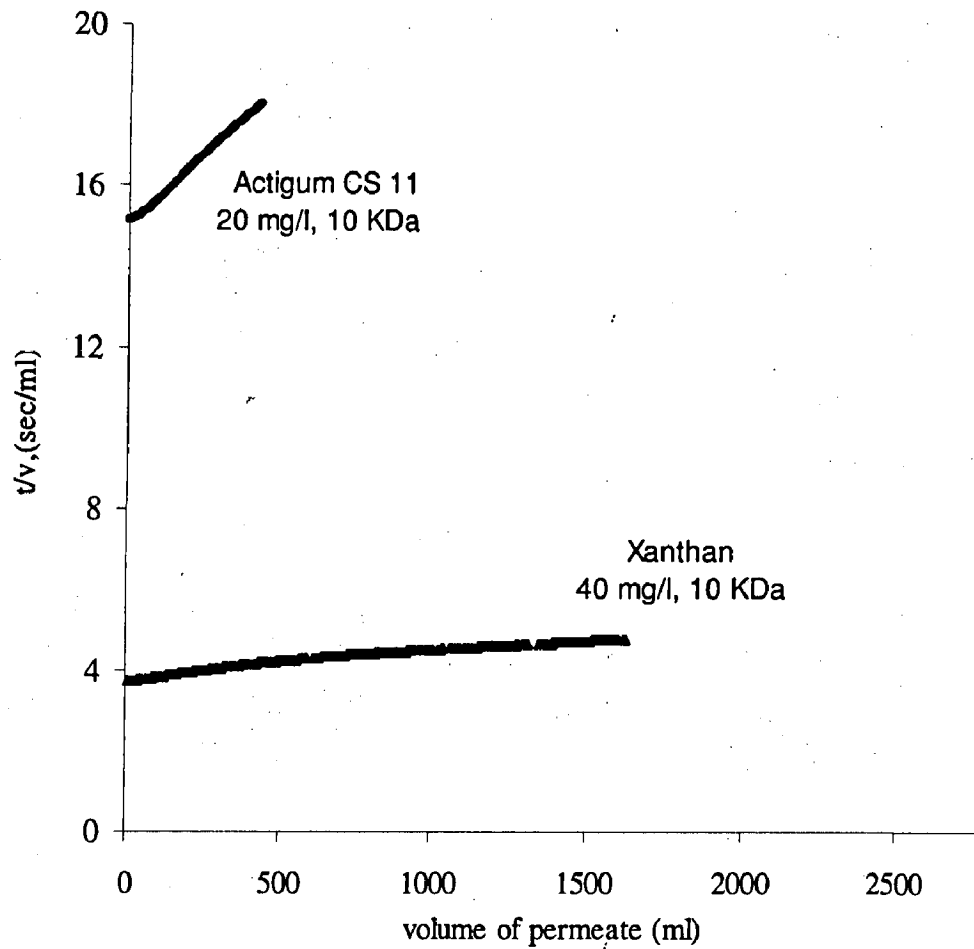
Figure 4-5: Linearized flux data for the regenerated cellulose membrane (10 KDa) filtration using characteristics coordinates for cake filtration.
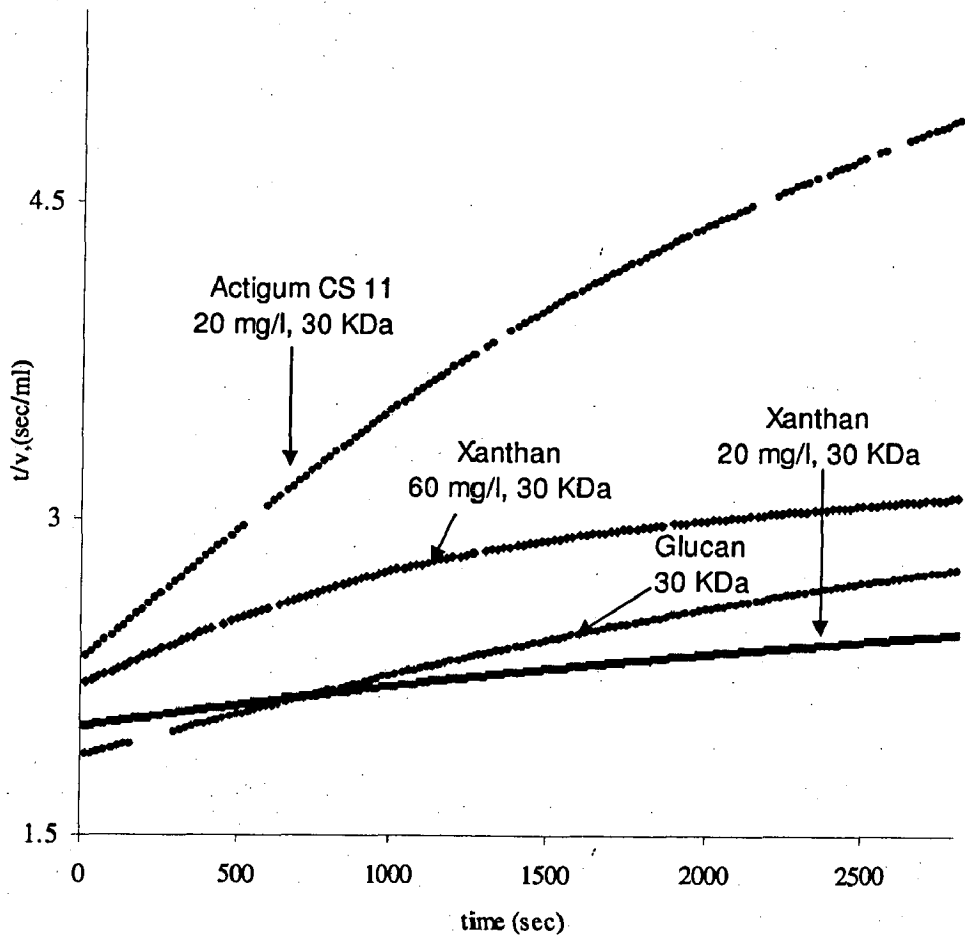
Figure 4-6: Linearized flux data for the regenerated cellulose membrane (30 KDa) filtration using characteristics coordinates for pore constriction.
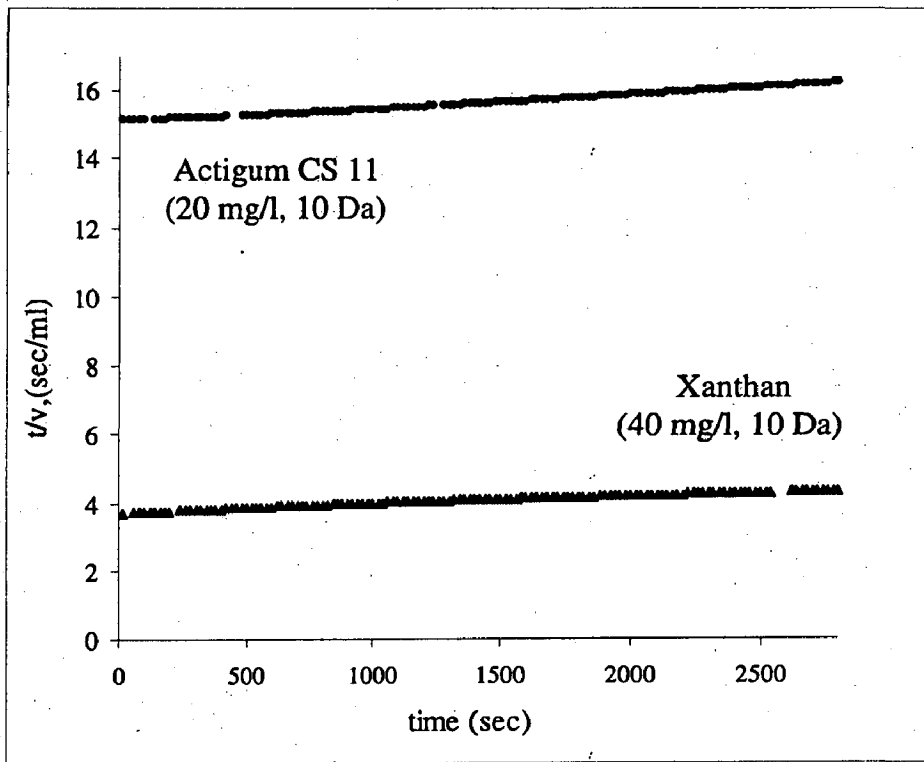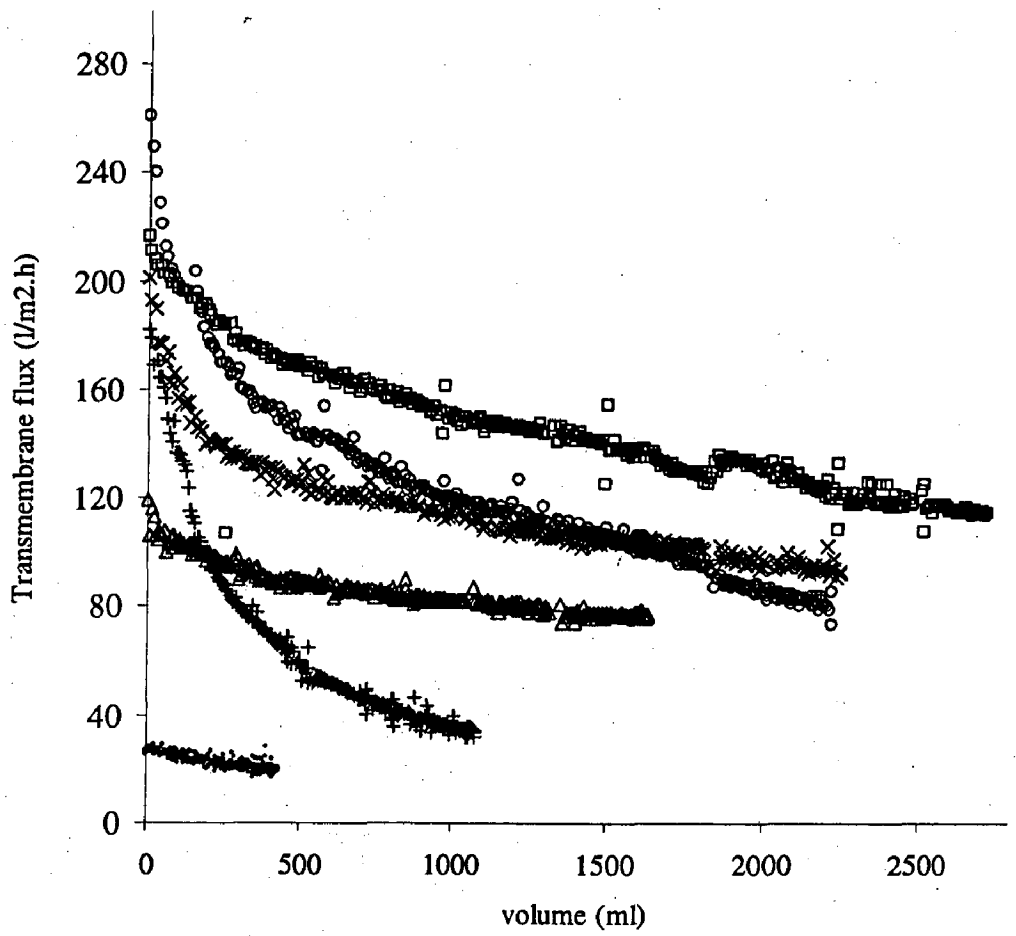
Figure 4-7: Linearized flux data for the regenerated cellulose membrane (10 KDa) filtration using characteristics coordinates for pore constriction.

Figure 4-8: Linearized flux data for the regenerated cellulose membrane (10 KDa) filtration using characteristics coordinates for pore blockage.

4.2 VISCOSITY MEASUREMENTS

The samples collected at different times, 20 minute interval during filtration experiments were simultaneously analysed for viscosity. Figures 4-9 and 4-10 show temporal changes of viscosity of the different polysaccharide suspension with time and permeate volume respectively. In order to maintain accurate measurement all samples had to be analysed in a short period of time. The viscosity was represented as kinematic viscosity in mm^2/s. Viscosity of the permeate for all polysaccharides was almost constant at around 0.9 m.Pa.s (almost similar to that of pure water). The figures 4-9 and 4-10 showed that the different polysaccharide suspension exhibits similar behaviour, all showing slight increases in viscosity with increase in permeate volume. The system under consideration does not contain any microbial source or presence of oxygen transfer to induce reaction within polysaccharides to yield reaction products. Thus increase in viscosity of the suspension could only be possible because of the polysaccharide present in feed suspension. It can be clearly stated that the polysaccharides, which increase viscosity in the feed suspension, are removed from the surface of the membrane and accumulated in the feed tank. The result shows pronounced increase in viscosity value for the Xanthan (60mg/l, 30kDa membrane) conducted at 130 minute of operation. The stirrer employed in feed tank to ensure constant mixing through out filtration experiment was not working during the final stages leading to high viscosity value. The viscosity measurement for Actigum CS 11 (20mg/l, 10 KDa membranes) and Glucan was conducted with rotational viscometer. The data's are not shown in this report since these samples were not suitable for measurement with rotational viscometer.
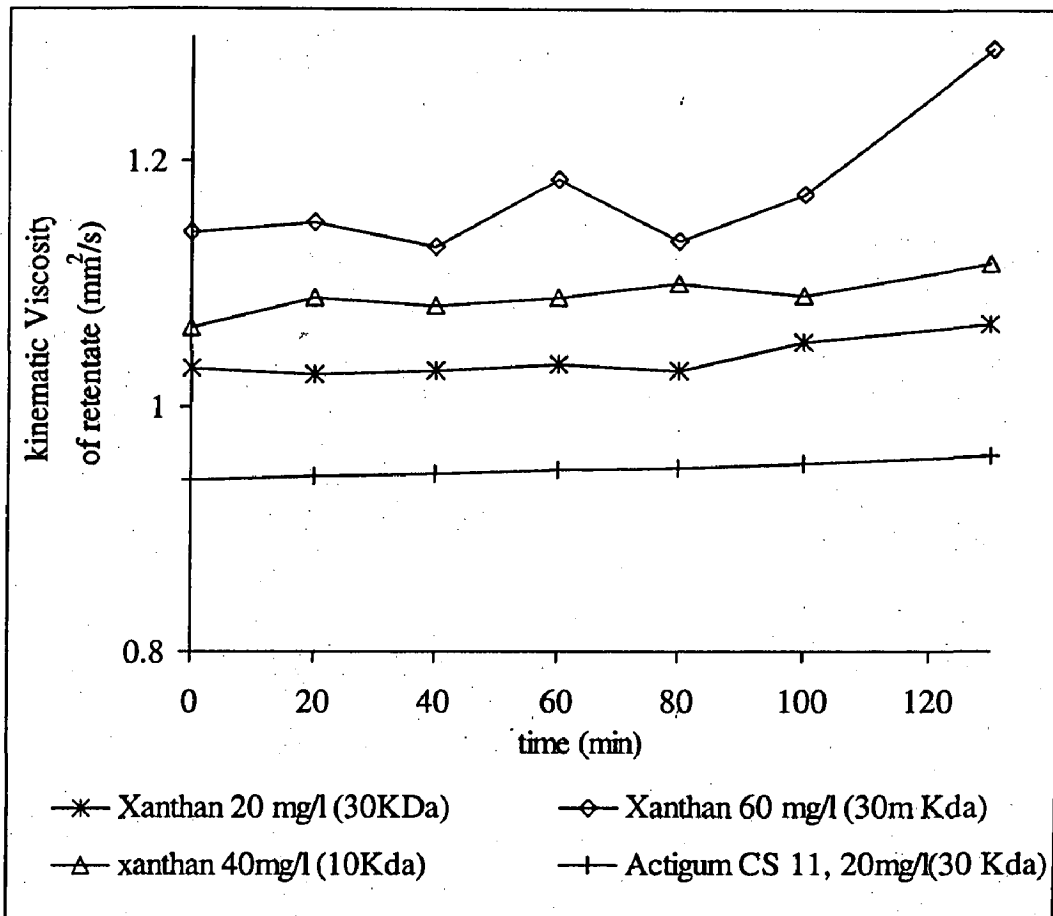
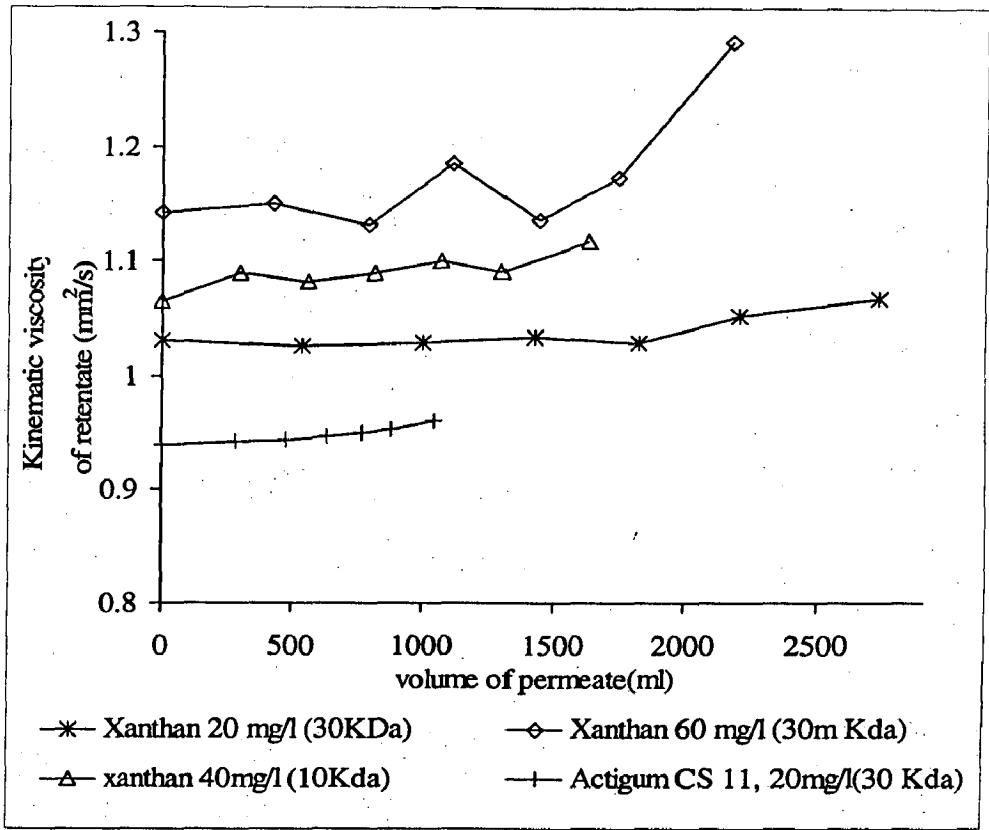*Figure 4-9: Change of Kinematic Viscosity of polysaccharide suspension with filtration time*

Figure 4-10: Change of Kinematic Viscosity of polysaccharide suspension with volume of

permeate

4.3 IR ANALYSIS OF FOULANTS

Attenuated total Reflectance Fourier Transform Infra Red Spectroscopy (ATR-FTIR) has been performed on all membrane after filtration experiments for qualitative information about the foulants and to evidence absorption bands due to polysaccharides deposition on to membrane surface. Both membrane and fouling layer were simultaneously analyzed. FTIR spectra were collected at different positions (five measurements) of the fouled membrane and the resulting spectra showed similar peaks with slightly varying intensity. The possible reason could be the foulants which causes permeate flux decrease may not have evenly deposited over the membrane surface. First the FTIR spectra of the clean membrane were obtained. Then the FTIR spectra for the membrane along with foulants were obtained and subtracted from spectrum of clean membrane to get spectra of foulants only. Figures 4-11 to 4-16 show the FTIR spectrum of components in polysaccharide suspension that fouled regenerated cellulose membrane (the regenerated cellulose membrane spectrum has been digitally subtracted using difference tool in FTIR software).

Polysaccharides are recognized by peaks at wave numbers of 1040 cm^{-1} (C-O bond from alcohol group), 2940 cm^{-1} (C-H stretch) and 3400 cm^{-1} (-OH stretch)[23,42]. Polysaccharides contain a significant number of hydroxyl groups, which exhibit a broad rounded absorption band above 3000 cm^{-1}. The absorption in that region of figure (4-11 to 4-16) has the rounded trait typical of hydroxyl groups[43] which suggest that the foulants are polysaccharides.

The main absorption bands were almost the same for all membranes and the observed bands were a broad band at 3300 cm^{-1}, a sharp peak at 1034 cm^{-1}, a peak at 2950-2850 cm^{-1}. The major peaks in the fingerprint region were assigned as listed in table 4-4.

In the fingerprint region (region below 1500 cm^{-1} where bands characterizes the molecule as a whole), the strongest absorption band is observed at 1034 cm^{-1} followed by a small sharp peak at 1100 cm^{-1}. Absorption in this region (1034 cm^{-1}) is due to C-O or Si-O bonds and is commonly associated with alcohols, ethers, polysaccharides and silicates. A peak at 1030-1040 cm^{-1} could also be indicative for silica although no peak at 2940 cm^{-1} should be detected in this case[43].

Examination of other regions of the spectrum can reveal the foulants deposited onto membrane surface. Further Cho et al.[44] attributed FTIR absorption in this region to polysaccharides or polysaccharide-like membrane foulants. The small sharp peak near 1100 cm^{-1} is an indicative of alcohol groups in carbohydrates probably from polysaccharides. The suspension employed for fouling analysis in our research contains only polysaccharides, absorption band at 1034 cm^{-1} and 1100 cm^{-1} clearly indicates that polysaccharides deposit on to membrane leading to reduction in permeate flow.

Table 4-4: Characteristic IR absorption bands and their attribution[45].

Chemical bond	Wave number (cm^{-1})	Mode
>CH$_2$ - CH	2960-2850 2890-2880	Normally 2-3 bands; (C-H) stretching vibration
>CH$_2$ -CH$_3$	1470-1430	(C-H) deformation vibration
-O-H	1410-1260	(O-H) deformation vibration
-C-OH	1150-1040	(C-O) stretching vibration

Figure 4-11: ATR-FTIR spectra of foulants deposited on membrane with Xanthan feed suspension (20mg/l, 30 KDa regenerated cellulose membrane)
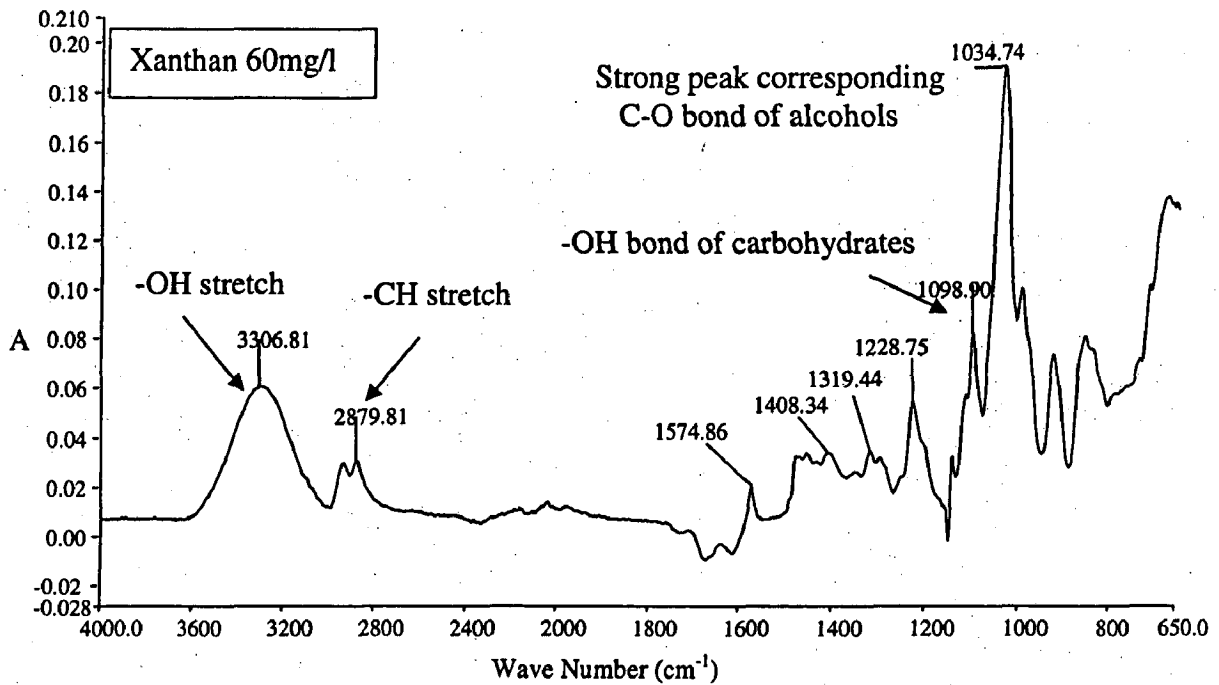
Figure 4-12: ATR-FTIR spectra of foulants deposited on membrane with Xanthan feed suspension (60mg/l, 30 KDa regenerated cellulose membrane)

Figure 4-13: ATR-FTIR spectra of foulants deposited on membrane with Actigum CS 11 suspensions (20mg/l, 30 KDa regenerated cellulose membrane)

Figure 4-14: ATR-FTIR spectra of foulants deposited on membrane with Glucan feed suspension (30 KDa regenerated cellulose membrane)

Figure 4-15: ATR-FTIR spectra of foulants deposited on membrane with Actigum CS 11 feed suspensions (20mg/l, 10 KDa regenerated cellulose membrane)
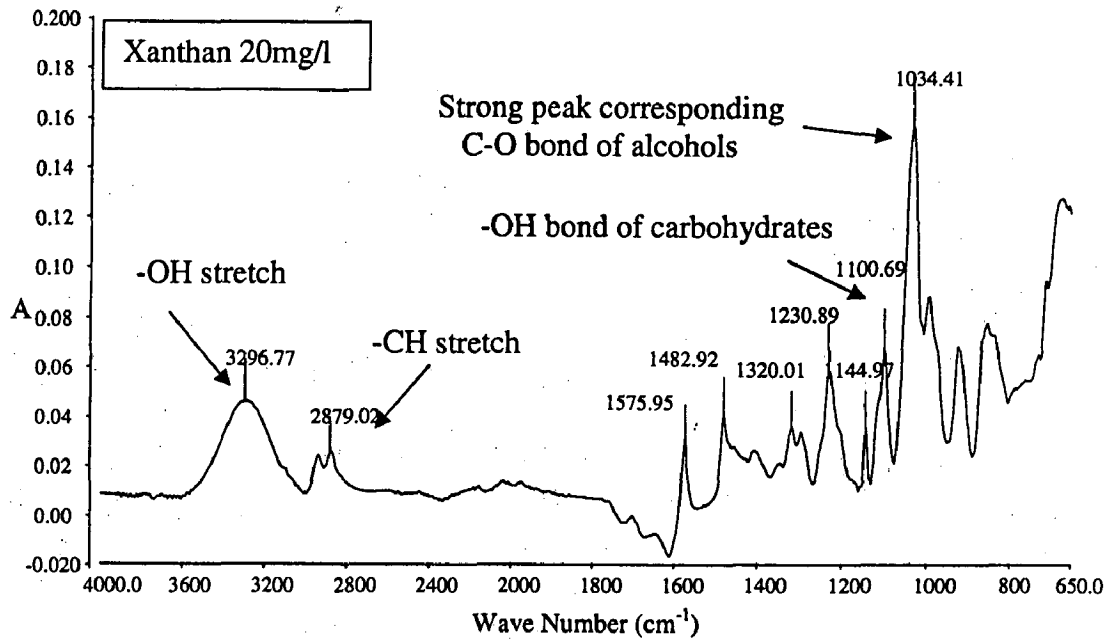

Figure 4-16: ATR-FTIR spectra of foulants deposited on membrane with Xanthan feed suspension (40mg/l, 30 KDa regenerated cellulose membrane).
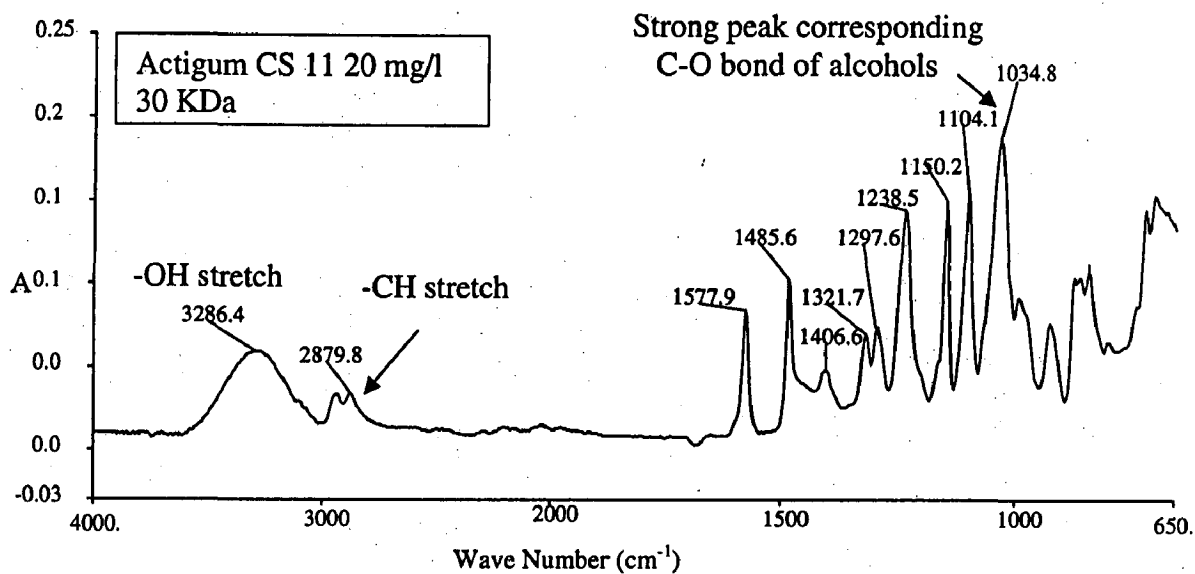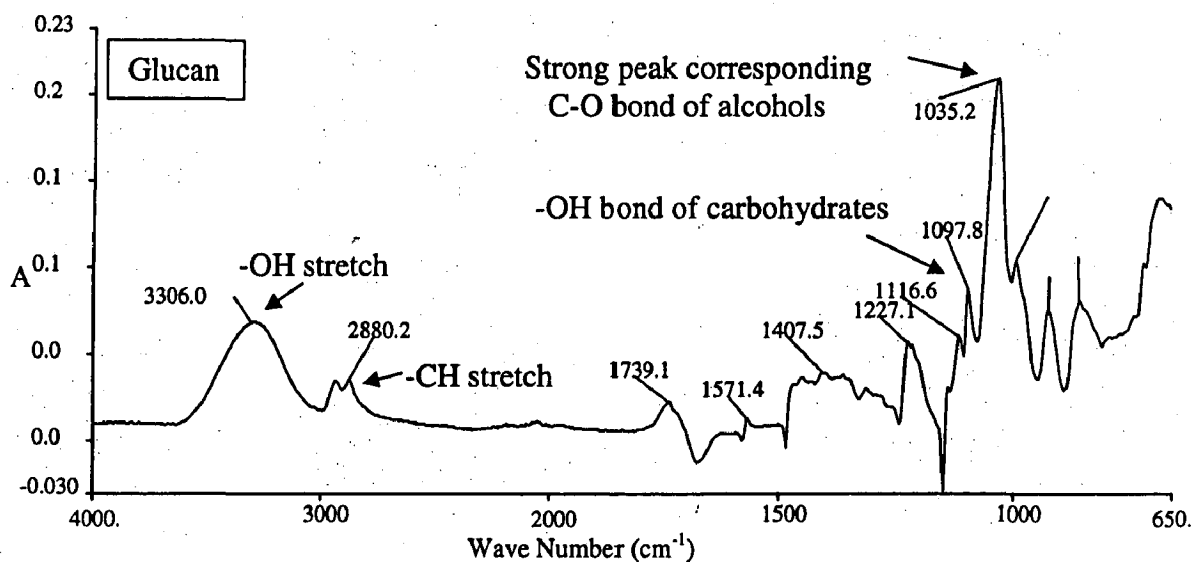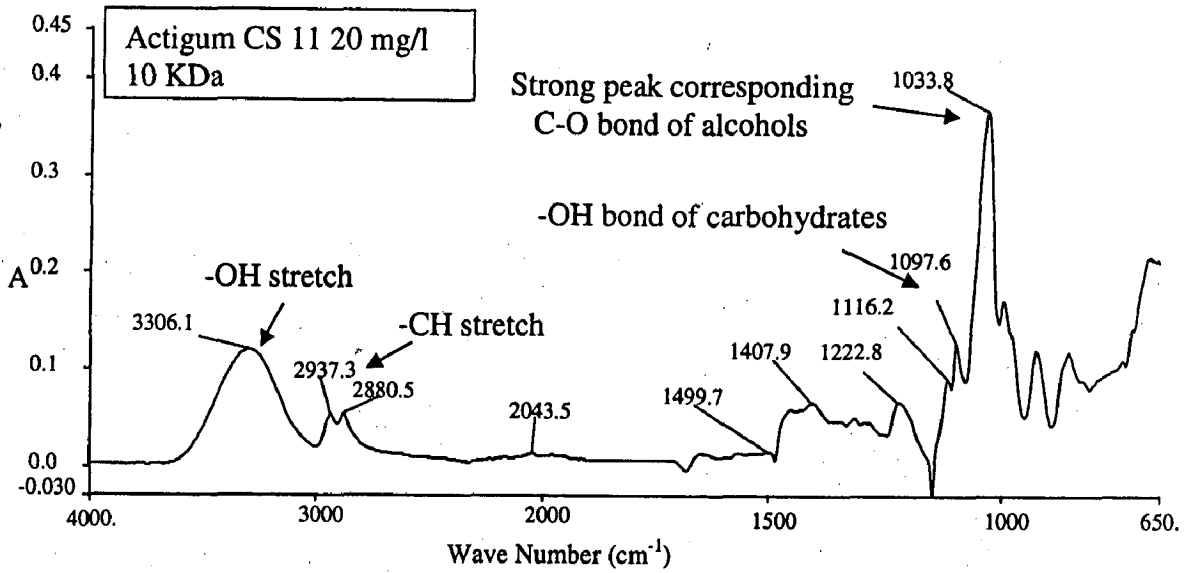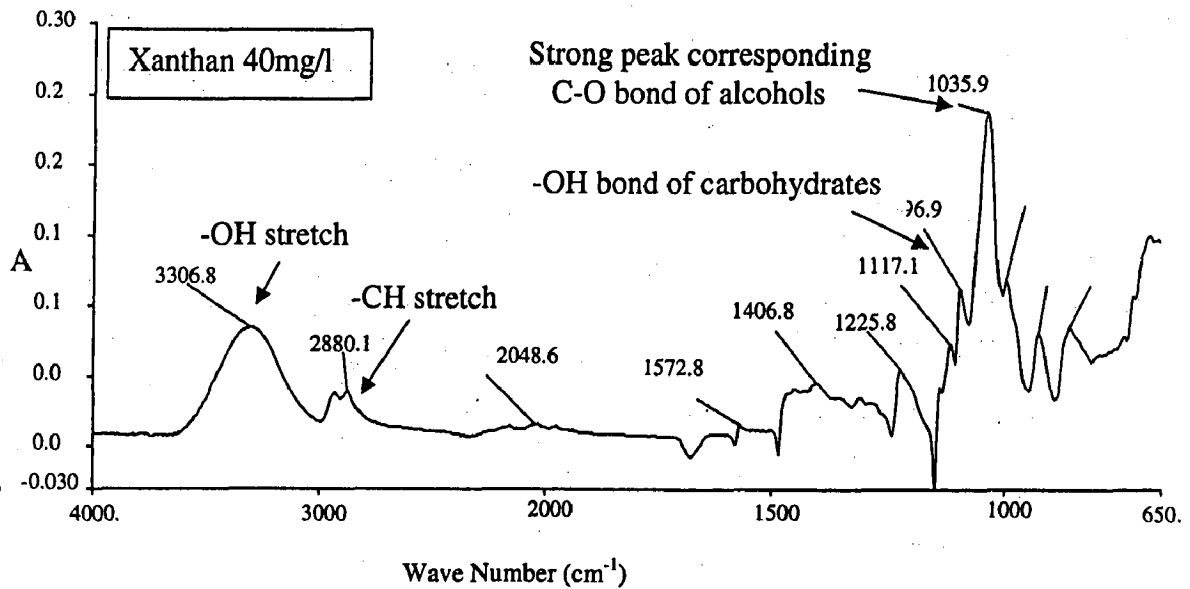
4.4 QUANTIFICATION OF CAKE LAYER MASS

4.4.1 UV Absorbance at 280 nm (UV$_{280}$)

Permeate flux decline, in the present study was attributed to the build up of a concentrated particle cake layer near the membrane surface as described earlier with Xanthan (20 mg/l) and Actigum CS 11 (20 mg/l). The primary aim of this part of experimental study was to determine the accumulation of particles in cake layer expressing in terms of mass of cake layer per unit membrane area. This can be achieved by measuring the change in concentration of the polysaccharide suspension in the retentate line. With the UV absorbance value the corresponding mass of the polysaccharides deposited on the membrane surface can be calculated from a simple mass-balance, using polysaccharide feed concentration values obtained during the filtration runs and by the volume of permeate collected at different time.

Before preparing the standard calibration curve at fixed wavelength a wavelength scan from 200 to 650nm was run for Xanthan polysaccharide at different concentration. And all found to exhibit a broad curve showing a slight peak with maximum absorbance at around 280 nm shown in figure 4-17.

Figure 4-18 shows the retentate polysaccharide concentration as measured by UV absorbance at 280 nm (UV$_{280}$). The values represented by UV absorbance at 280nm (UV$_{280}$) showed a concentration value beyond the maximum concentration that can be maintained in the retentate line. Thus the values depicted does not relate to the actual concentration of polysaccharides in the system under consideration clearly stating that these polysaccharides are not suitable for measurement with UV absorbance at 280 nm. From literature, Xanthan gum solutions undergoing shear stresses, shear forces will dominate Brownian motion at low shear rates, causing molecular alignment, resulting in the solution not being in a state of true random motion[34]. Doi and Edwards[34] show theoretically that under the application of shear forces, rod-like molecules will align in solution and move longitudinally in a constrained tube before molecular interaction occurs. Although Xanthan molecules may not be considered as rod like, their extended form in solution suggests the alignment of molecules in solution may be applied qualitatively. Because of the semi-flexible nature of Xanthan and the tendency for

aggregation or self-association at low concentrations, it is difficult to obtain a measure of concentration where molecules interact when shear is applied. Thus shear stress imposed to the polysaccharide in suspension by the centrifugal pump during filtration run might have caused change in structure of polysaccharide, which could be considered leading to increase in scattering of light. UV absorbance superimposed by the scattering of light suggests thorough structural analysis of the polysaccharide suspension should be examined to justify the cause of increase in concentration.
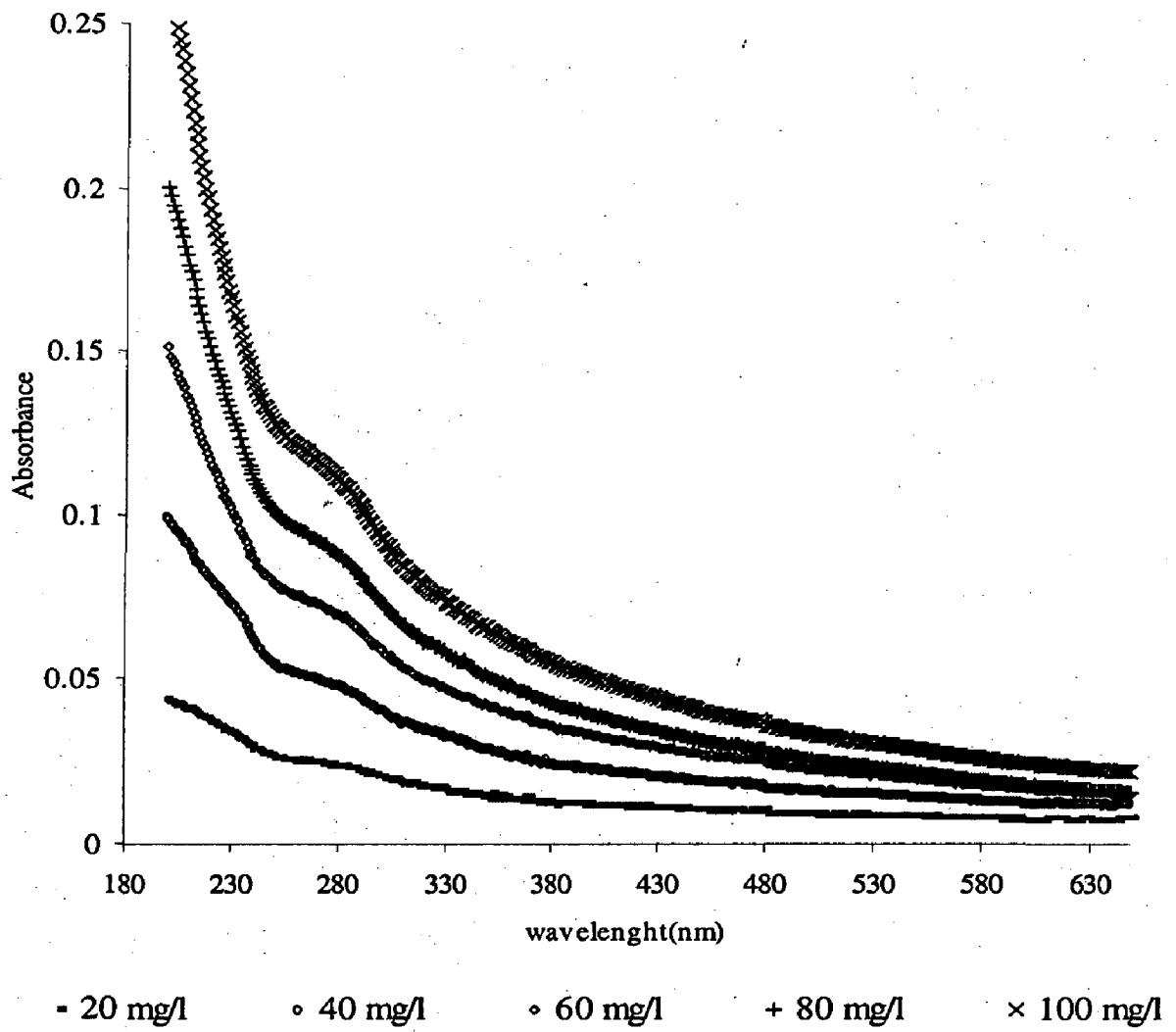
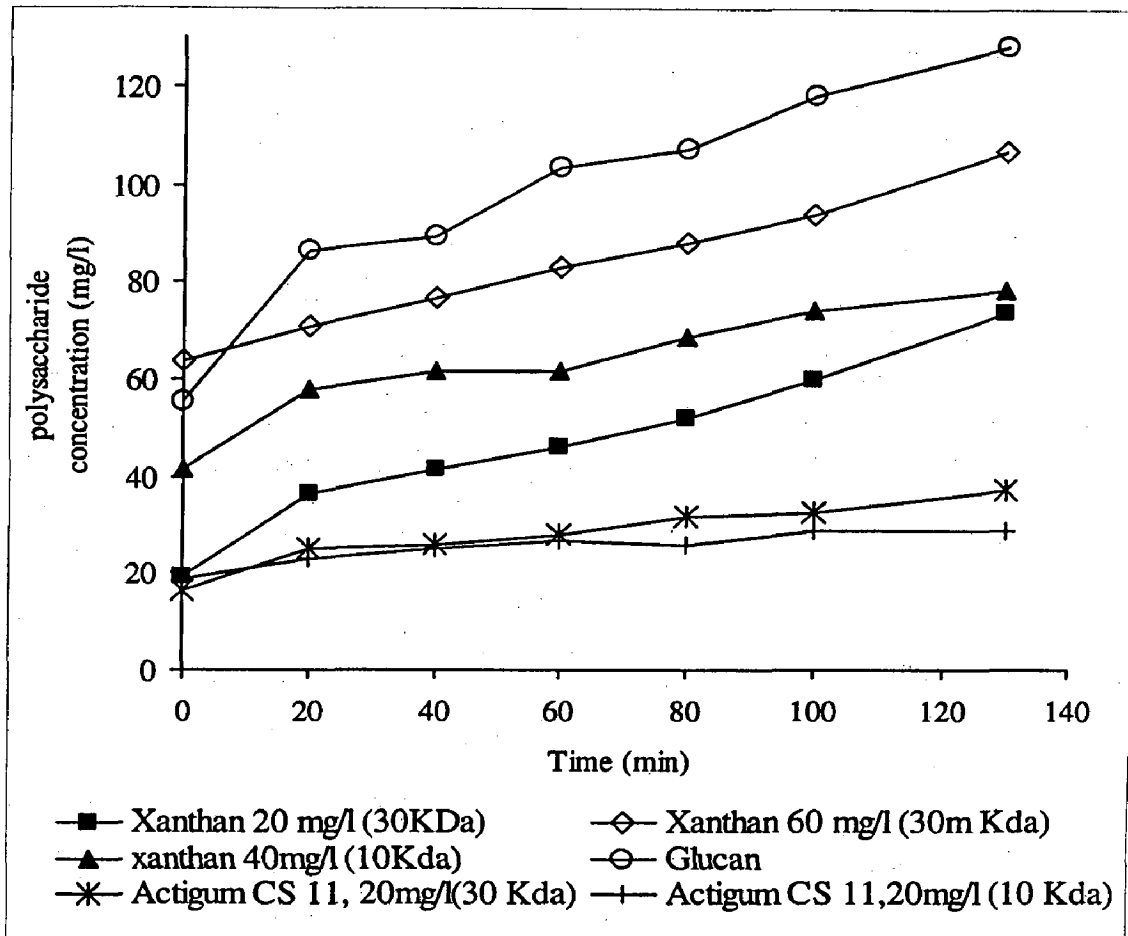*Figure no 4-17: Wavelength scans from 200-650 nm with Xanthan as standard.*

Figure 4-18: Retentate polysaccharide concentration as measured by UV$_{280}$

4.4.2 Colorimetric Determination

In addition to the UV absorbance at 280 nm, a photometric determination of polysaccharides was applied. This method was easier to perform, less expensive and could be carried out in higher frequency. The results of the photometric detection are given as glucose equivalents. In figure 4-19 change in polysaccharide concentration in the retentate line are given over time.

Polysaccharide concentration changes in the retentate line during filtration experiments. The range of concentrations measured in the retentate line by colorimetric detection is quite significant compared to that measured by UV_{280} and cannot be neglected. The colorimetric determination was carried out only for Xanthan (60 mg/l, 30 KDa membranes) and with Actigum CS 11 (20 mg/l and 30 KDa membranes). This method did not really work for Xanthan. For the filtration experiments conducted with 60 mg/l concentration the initial concentration value obtained was only 40 mg/l followed by gradual increase in concentration as can be seen from figure 4-19. Thus these actual concentration measurements for polysaccharides are complicated. And reliable concentration measurements were obtained for Actigum CS 11 polysaccharide.

The evolution of polysaccharide concentration within the crossflow membrane filtration system should give information about the way the polysaccharides behave in the aspect of concentration and its tendency of fouling. Thus this study would permit to demonstrate a link between membrane fouling and polysaccharide concentration. With these results obtained correlation of polysaccharide mass deposited on per unit membrane surface area can be extracted.

We can note that this concentration increases because of the marked accumulation of particle above the regenerated cellulose membrane surface. The reason for difference in concentration measurement with Xanthan by colorimetric determination was searched in literature. Once again structure of Xanthan plays an important role in this. It was hypothesized that the sugar composition of Xanthan is difficult to obtain as the cellulosic backbone is highly too resistant to hydrolysis.

Permeate flux decline, in the present work was attributed to the buildup of a cake layer near the membrane surface. The accumulation of polysaccharides on to membrane surface, expressed in terms of mass of polysaccharide deposited over filtration time is

shown in figure 4-20 for filtration experiments conducted with Xanthan (60 mg/l, 30 KDa) and Actigum CS 11 (20 mg/l, 30 KDa). The mass of the polysaccharide deposited onto membrane surface for the experimental runs, regardless of initial feed polysaccharide concentration, particle size increased with time. These results are consistent with the permeate flux data (figure 4-1) which indicate decline in permeate flux due to increased resistance of the cake layer to permeate flow as polysaccharides accumulate in the cake layer. It is also noted that more mass was deposited in the case of Xanthan at initial feed concentration of 60 mg/l. Thus clearly stating that polysaccharide deposition on to membrane surface increases with increasing bulk feed concentration.
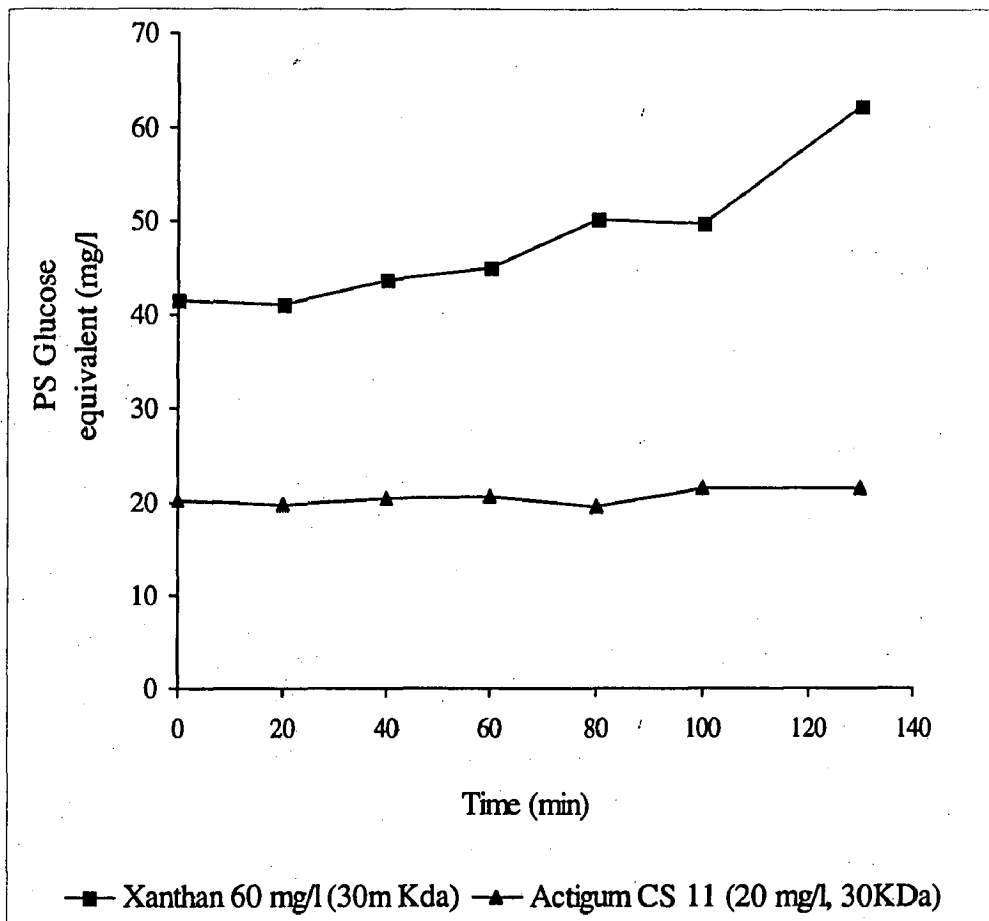
Figure 4-19: Retentate polysaccharide concentration as measured colorimetric determination expressed as PS-Glucose equivalent (mg/l).
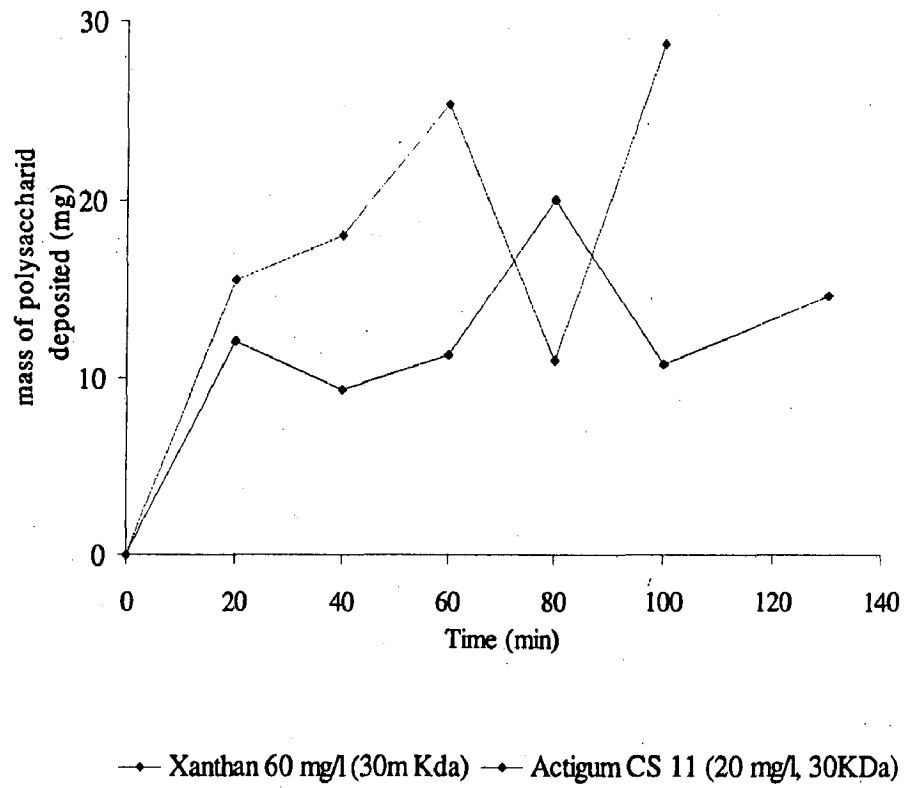
Figure 4-20: Mass of polysaccharide deposited onto membrane surface over filtration time.

98

4.5 DYNAMIC LIGHT SCATTERING RESULTS

The stability of the polysaccharide suspension investigated in the crossflow filtration experiments was determined by measuring changes in particle mean hydrodynamic diameter and particle size distribution with time using Dynamic Light Scattering (DLS). DLS measurements could also reveal information about the link between particle size and its tendency to fouling. With this aim the change in particle size distribution in the retentate line for all polysaccharides collected at different times were monitored and compared with each other during the operation of a cross flow membrane filtration experiments. Totally five measurements were made for all samples and all found to exhibit similar distribution and the distribution with mean Z average diameter was taken for study. The intensity weighted particle size distribution of retentate examined every 20 minute during filtration experiments of Xanthan, Actigum CS 11 and Glucan are shown in figure (4-21) to (4-25).

During the recirculation of retentate, the Z average diameter of Xanthan of initial feed concentration 40 mg/l and 60 mg/l (crossflow filtration experiments conducted with 10 KDa and 30 KDa membrane respectively) dropped at the beginning of operation but showed moderate and gradual decrease after the initial period. At low concentration, 20 mg/l for Xanthan the Z average diameter does not show any change untill 80 minute of operation and after that showed gradual decrease till the end of experiment. The Actigum CS 11 suspension had the largest particles compared to Xanthan and Glucan. Its particle size distribution is of much importance, which does not show any change through out the experiment. Glucan exhibited a totally different phenomenon with particle size continued to decrease right from the initial period till throughout the entire experiment. All these polysaccharide suspension showed different behavior in the aspect of particle size distribution.

The intensity of the scattered light is a strong function of the particle size, with the aggregates causing much more scattering, leading to the large size of the aggregate peak. From literature, light scattering of Xanthan solutions is complicated by the semi flexible nature of the Xanthan molecules proposed to be right hand double helix and the presence of micro aggregates at low concentrations caused by Xanthan gum self association[34].

100

Figure 4-21: Dynamic light scattering results for the scattered intensity as a function of size for Xanthan (20mg/l, 30 KDa membrane) at different time interval
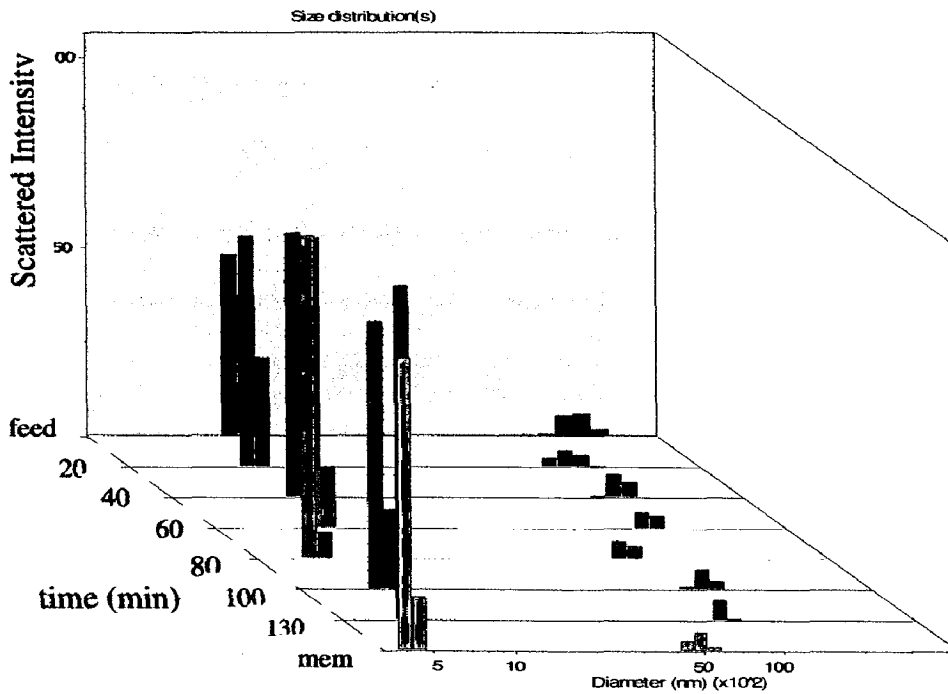
Figure 4-22: Dynamic light scattering results for the scattered intensity as a function of size for Xanthan (60mg/l, 30 KDa membrane) at different time interval

102

Figure 4-23: Dynamic light scattering results for the scattered intensity as a function of size for Actigum CS 11 (20mg/l, 30 KDa membrane) at different time interval

Figure 4-24: Dynamic light scattering results for the scattered intensity as a function of size for Glucan (30 KDa membrane) at different time interval
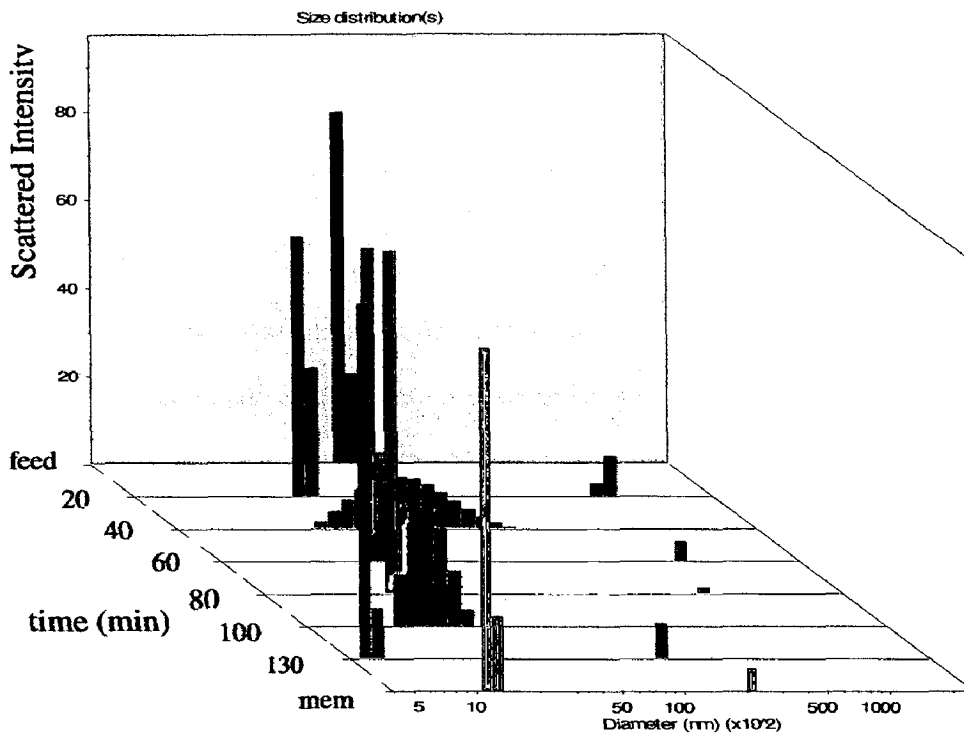
Figure 4-25: Dynamic light scattering results for the scattered intensity as a function of size for Xanthan (40mg/l, 40 KDa membrane) at different time interval
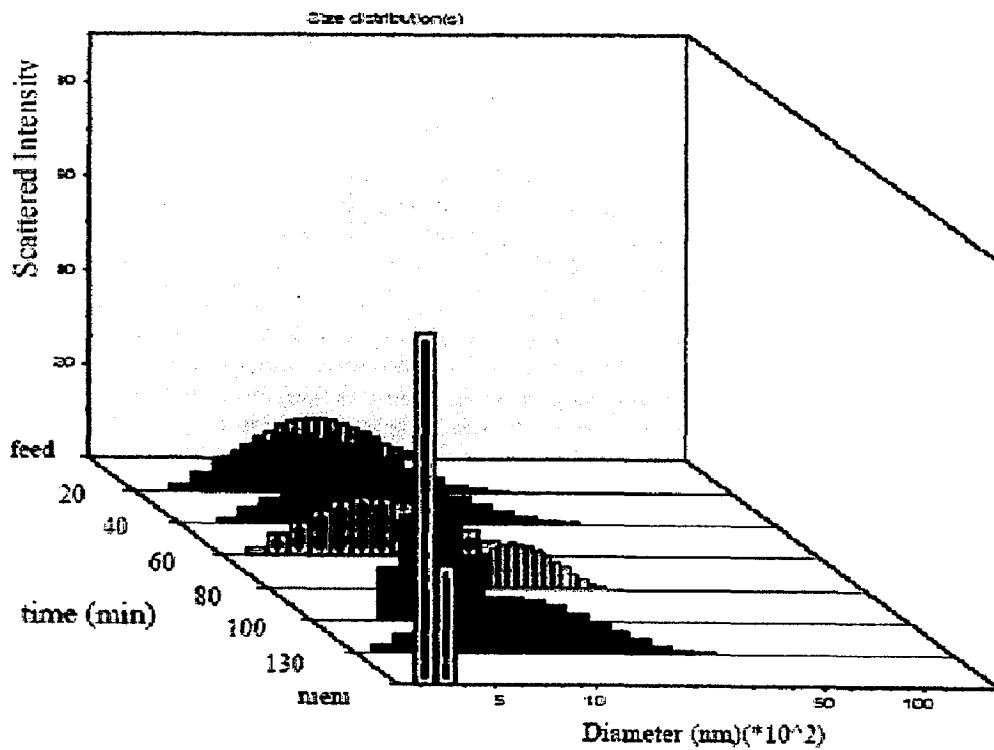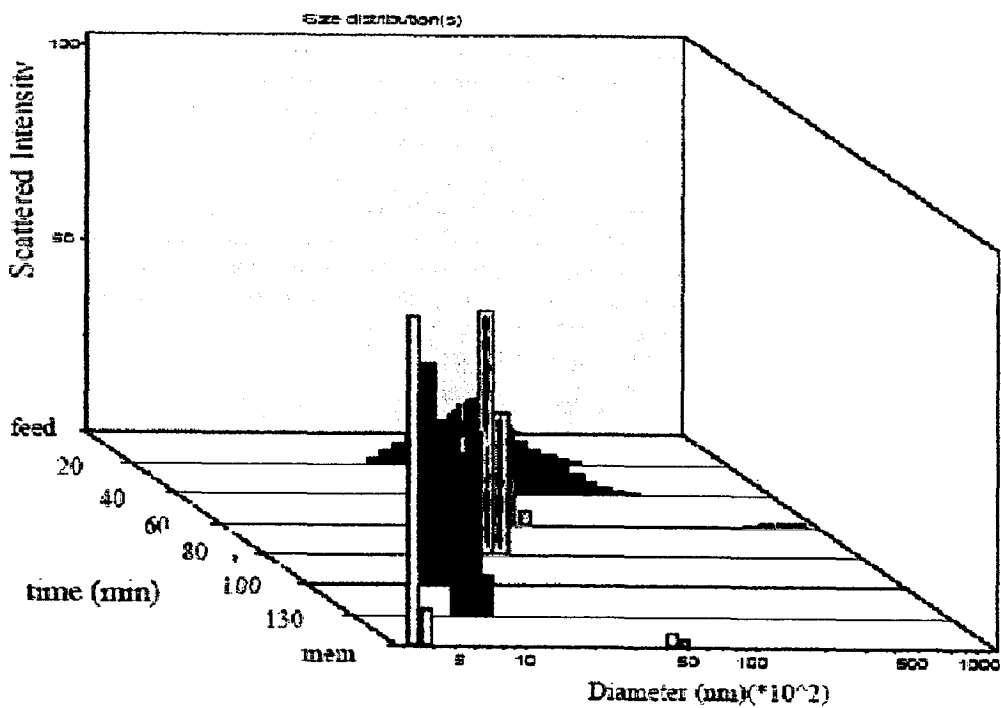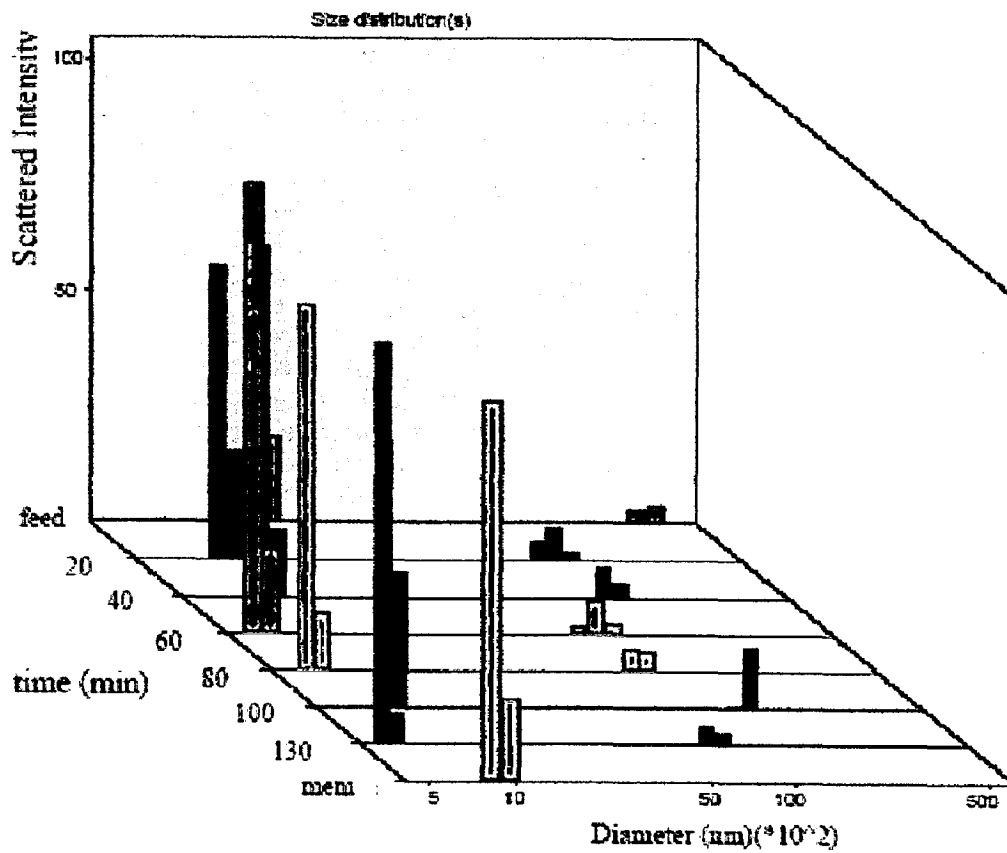
106

The DLS result of Xanthan, figure 4-21, 4-22 and 4-25 shows that they form micro aggregates at very low concentrations. These micro aggregates can be formed during the initial preparation of the polysaccharide solutions, or they may be generated during the filtration process, either by pumps employed in crossflow filtration systems or by the shear rates that exist in the vicinity of the membrane surface or in the membrane pores. The DLS results showed shift in particle size distribution to the lower region and micro aggregates diminished during filtration experiments implying that these change in particle size distribution and membrane fouling are interrelated. This decrease in size of micro aggregates might lead to the flux decrease by formation of a dense cake layer on the membrane surface. It is notable that the pattern of flux figure 4-1 coincides well with the variation in particle size distribution with permeate flux decreases with decreases in particle size distribution. The sharp decline in particle size distribution with Xanthan (40mg/l and 60 mg/l) during initial period of operation clearly reveals the reason for much faster decrease in initial permeate flux when compared to crossflow experiment conducted with Xanthan of 20 mg/l initial feed concentration. Thus the permeate flux decline and the shift in particle size distribution was attributed to the buildup of a concentrated polysaccharide cake layer near the membrane surface. This would also be assigned that the polysaccharide transfer to the membrane surface increases with decrease in particle size and with increase in bulk polysaccharide concentration. This was supported by the DLS results showing decrease in particle size with increase in concentration.

The same phenomenon was obtained for experiments conducted with Glucan, figure 4-24 but with slight variation, the particle size distribution decreases throughout the entire experiment as described earlier. This continuous decrease (shift) in particle size distribution is an evidence that the permeate flux declines much faster for Glucan compared to other polysaccharide suspension. It can be seen clearly in figure 4-1 (Section number 4.1). The non approachability of steady state for concentrated aqueous suspension (Glucan) was supported by continuous shift in particle size distribution revealing that more number of particles is deposited onto membrane surface leading to fouling. The Actigum CS 11 suspension contains bigger particles, which are too large to enter the membrane pores and they are accumulated on the membrane surface in a

growing cake layer. The PSD (figure 4-23) results showed that no preferential deposition of particle was taking place. No change in PSD occurred with Actigum CS 11, but still it showed higher flux decline. This is solely because of larger particles that are not sufficient enough to pass through the membrane pores. The similar PSD also reveals that only few numbers of particles are involved in fouling with a thin cake layer formation.

The particles that are deposited onto membrane surface were also analyzed with DLS for all experiments. The particles were removed gently by spatula and subsequently dissolved in about 60 ml of deionized water. This volume of water was arbitrarily chosen to remove completely the particles attached over membrane. The particle adhered due to Glucan polysaccharide over membrane surface was easily removed; visible dense cake layer was noticed. The PSD of material removed from the membrane surface was intermediate, varying with narrow size distribution.

Permeate collected during filtration experiments were also analyzed for PSD. During PSD measurements the intensity of the scattered was too low, count rate obtained was less than 30 Kcounts/sec indicating that the permeate had few polysaccharides in it. Permeate hardly contained particles in it. Thus the polysaccharides that are responsible for membrane fouling are retained on the membrane surface and large enough to pass through the membrane pores.

CONCLUSION

This study permits to demonstrate a link between membrane fouling and polysaccharide concentration. Polysaccharide deposition on regenerated cellulose membranes during crossflow filtration experiments leads to several flux decline behaviors, influence suspension filterability and the membrane performance. The polysaccharide analyzed in this study remained in suspended soluble state during filtration experiments. With high polysaccharide concentration the membrane fouls more than for a low one. Under conditions of dilute solutions (20 mg/l - 60 mg/l), for membrane of 30 KDa and 10 KDa MWCO the total resistances as a function of time are examined as per resistance in series model. All yielded concave downward curves that are clearly indicative of external fouling, i.e. cake formation is the main mechanism of fouling. Further, mathematical analysis of the membrane test cell experiments carried out in this research clearly revealed cake formation as predominant fouling mechanism for polysaccharide suspension with very low concentration (20 mg/l). With higher concentration of polysaccharide feed suspension predominant fouling mechanism was difficult to detect with assumed model prediction indicating fouling could be because of combination of two or more fouling mechanism. It was shown for the two polysaccharide suspension.

Viscometry analysis results showed that polysaccharide accumulated both in retentate and removed from the membrane, which might have caused an increase in the viscosity of the suspension. Thus this viscometry studies suggests the importance of the viscosity during the operations. Concentration analysis results showed that the main portion of the polysaccharide remains in suspension and only little amount leads to major flux decline.

Investigation of membrane after filtration experiments by ATR-FTIR spectrometry revealed a vibration band associated with the polysaccharides could be clearly distinguished from those of the membrane material. The polysaccharides on these membranes produced relatively sharp absorption bands.

Dynamic light scattering intensity distributions reveal presence of micro aggregates, concentration of these micro aggregates decrease with time during filtration runs clearly indicating that these aggregates are deposited onto membrane surface leading to fouling. This is well supported by shift in particle size distribution towards lower region and this is more pronounced for the experiments conducted with aqueous polysaccharide suspension (Glucan).

REFERENCES

[1] Koros, W.J., Ma, Y.H., Shimidzu, T., "Terminology for membranes and membrane processes; IUPAC recommendations", Journal of Membrane Science, 120 (2000) 149–159.

[2] Evenblij, H., and Van Der Graaf, J.H.J.M., "Occurrence of EPS in activated sludge from a membrane bioreactor treating municipal wastewater" Water Science and Technology, 50 (2004) 293-300.

[3] Laspidou, C. and Rittmann, B., "A unified theory for extracellular polymeric substances, soluble microbial products, and active and inert biomass", Water Research, 36 (2002) 2711-2720.

[4] Barker, D.J. and Stukey, D.C., "A review of soluble microbial products (SMP) in waste water systems", Water Research, 33 (1999) 3063-3082.

[5] Azeredo. J., Rosario, Valentina, "A New Method for extraction of exopolymer from Activated sludges", Water Science and Technology, 37 (1998) 0367- 370.

[6] Chang, I.S., Clech, I.L., Jefferson, B., and Judd, S., "Membrane Fouling in Membrane Bioreactors for Wastewater Treatment", Journal of Environmental Engineering, 128 (2002) 1018-1029.

[7] Bura, R., Cheung et al., "Composition of extracellular polymeric substances in the activated sludge matrix.", Water Science and Technology, 37 (1998) 325-333.

[8] Chang, I.S., and Lee, C.H., "Membrane filtration characteristics in membrane coupled activated sludge system—the effect of physiological states of activated sludge on membrane fouling", Desalination, 120 (1998) 221–233.

[9] Nagaoka, H., "Nitrogen removal by submerged membrane separation activated sludge process", Water Science and Technology, 39 (1999) 107-114.

[10] Nagaoka, H., Ueda, S., and Miya, A., "Influence of bacterial extracellular polymers on the membrane separation activated sludge process", Water Science and Technology, 34 (1996) 165–172.

[11] Nagaoka, H., Yamanishi, S., and Miya, A., "Modeling of biofouling by extracellular polymers in a membrane separation activated sludge", Water Science and Technology, 38(1998) 497–504.

[12] Kim, J. S., Lee, C. H., and Chun, H.D., "Comparison of ultrafiltration characteristics between activated sludge and BAC sludge", Water Research, 32 (1998) 3443–3451.

[13] Dignac, M. F., Urbain, V., Rybacki, D., Bruchet, A., Snidaro, D., and Scribe, P., "Chemical description of extracellular polymers: Implication on activated sludge floc structure", Water Science and Technology, 38 (1998) 45–53.

[14] Hodgson, P.A., Leslie, G.L., Schneider, R.P., Fane, A.G., Fell, C.J. D., and Marshall, K.C., "Cake resistance and solute rejection in bacterial microfiltration: The role of the extracellular matrix", Journal of Membrane Science, 79 (1993) 35–53.

[15] Zhang, X., Bishop, P.L., and Kupferle, M.L., "Measurement of Polysaccharides and proteins in biofilm Extracellular polymers" Water Science and Technology, 37 (1998) 345–348.

[16] Rosenberger, S., Kraume, M., "Filterability of Activated Sludge", Desalination, 151 (2002), 195-200.

[17] Kim, J. S., Lee, C. H., and Chang, I. S., "Effect of pump shear on the performance of a crossflow membrane bioreactor", Water Research, 35 (2002) 2137–2144.

[18] Hong, S., Faibish, R.S., and Elimelech, M., "Kinetics of permeate flux in crossflow Membrane Filtration of colloidal Suspensions", Journal of colloid and Interface science, 196 (1997) 267-277.

[19] Tarabara, V.V., Hovinga, R. M., and Wiesner M.R., "Constant Transmembrane Pressure Vs. Constant Permeate Flux: Effect of particle size on crossflow membrane Filtration", Environmental Engineering Science, 19 (2002) 343- 355.

[20] Faibish, R.S., Elimelech, M., and Cohren, Y., "Effect of Interparticle Electrostatic Double Layer Interactions on Permeate flux Decline in Crossflow Membrane Filtration of Colloidal Suspensions: An Experimental Investigation" Journal of Colloid and Interface Science, 204 (1998) 77-86.

112

[21] Mulder, M., (1991) "Basic Principles of Membrane Technology" Kluwer Academic Publishers, Dordrecht, The Netherlands.

[22] Claudia Laabs (2004): Fouling of low-pressure membranes by municipal wastewater: Identification of principal foulants and underlying fouling mechanisms, Ph.D. thesis, Process Engineering, Technical University Berlin, Germany, 2004.

[23] Ye., Y., Clech, P.L., Chen, V., Fane, A.G., Jefferson, B., "Fouling mechansisms of alginate solutions as model extracellular polymeric substances", Desalination 175 (20005) 7-20.

[24] Judd, S., "A review of fouling of membrane bioreactors in sewage treatment", Water Science and Technology, 49 (2004) 229-235.

[25] Chang, I.S., Bag, S.O., Lee, C.H., "Effect of membrane fouling on solute rejection during membrane filtration of activated sludge", Process Biochemistry, 36 (2001) 855-560.

[26] Bowen, W. R., Calvo, J. I., and Hernandez, A., "Steps of membrane blocking in flux decline during protein microfiltration", Journal of Membrane Science, 101 (1995) 153–165.

[27] Wessling, M., "Two dimensional stochastic modeling of membrane fouling", Separation and Purification Technology, 24 (2001) 375-387.

[28] Tracey, E.M., and Davis, R.H., "Protein fouling of track-etched polycarbonate Microfiltration membranes", Journal of Colloid and Interface Science, 167 (1994) 104-116.

[29] Hermia, J., "Constant pressure blocking filtration laws - application to power-law non- Newtonian fluids", Transactions of the Institution of Chemical Engineers, 60 (1982) 183-187.

[30] Madaeni, S.S., Fane, A.G., and Grohmann, G.S., "Virus removal from water and wastewater using membranes", Journal of Membrane Science, 102 (1995) 65-75.

[31] Lojkine, M.H., Field, R.W., Howell, J.A., "Crossflow microfiltration of cell suspensions review of models with emphasis on particle size effects", Transitions in Chemical Engineering, 70 (1992) 149-164.

[32] Wu, C., "Light scattering characterization of the MWD of some intractable polymers", Polymers for Advanced Technologies, 8 (1996) 177-183.

[33] Dubois, M., Gilles, K.A., Hamilton, J.K., Rebers, P.A., and Smith, F., "Colorimetric method for Determination of Sugars and related substances", Analytical Chemistry, 28 (1956) 350-356.

[34] Rodd, A.B., Dunstan, D.E., Boger, D.V., "Characterization of Xanthan Gum Solutions using Dynamic Light Scattering and Rheology", Carbohydrate Polymers, 42 (2000) 159-174.

[35] Richter, S., Boyko, V., Matzker, R., Schröter, k., "A Thermo reversible Gelling System: Mixtures of Xanthan and Locust- Bean Gum", Macromolecular Rapid Communications, 25 (2004) 1504-1509.

[36] Sutherland, I.W., "Microbial exopolysaccharides-structural subtleties and their consequences", Pure & Applied Chemistry, 69 (1997) 1911-1917.

[37] Podolsak, A.J., Tiu, C., "Rheological Properties and some Applications for rhamsan and Xanthan Gum Solutions", Polymer International, 40 (1996) 40, 155-167.

[38] Holzwarth, G., "Molecular weight of Xanthan polysaccharide", Carbohydrate Research, 66 (1978) 173-186.

[39] Homme, R.K.P., Froiman, G., and Hoagland, D.A., "Molecular-size Determination of Xanthan polysaccharide, Carbohydrate Research, 106 (1982) 225-233.

[40] Coviello et al., "Scleroglucan: A Versatile Polysaccharide for Modified Drug Delivery", Molecules, 10 (2005) 6-33.

[41] Vuppu, A.K., et al. "Tapping Mode Atomic Force Microscopy of Scleroglucan Networks", Biopolymers, 42 (1997) 89-100.

[42] Cetin, S., and Erdincler, A., "The role of carbohydrate and protein parts of extracellular polymeric substances on the dewaterability of biological sludges", Water Science and Technology, 5 (2004) 49-56.

[43] Howe, K.J., Ishida, K.P., Clark, M.M., "Use of ATR/FTIR spectrometry to study fouling of microfiltraion membranes by natural waters", Desalination, 147 (2002) 251-255.

[44] Cho, J., Amy, G., Pellegrino, J., and Yoon, Y., "Characterization of clean and natural organic matter (NOM) fouled NF and UF membranes, and foulants characterization", Desalination, 118 (1998) 101-108.

[45] Nakanishi, K. (1962), Infrared Absorption Spectroscopy, Holden Day, San Francisco.

APPENDIX I

Derivation of Characteristic Equations

Cake Filtration Model

Assumptions:

1) The particles are hard and that the resulting cake is incompressible (i.e., the cake porosity and resistance are independent of pressure drop). The particle type (hard or soft) has a great effect on cake formations. Hard particles will form a cake similar to balls in a box. The particles will be touching, but there will be unused space around the particles for fluid to flow. As a result, the filter's differential pressure will increase slowly and steadily as the cake builds. On the other hand, deformable particles will cause a different outcome. Initially, the soft particles will act like hard particles. However, as the cake builds, the particles will deform due to the increasing differential pressure across the cake and membrane. As the particles deform, the cake compresses and reduces the volume between the particles that is available for flow. This increases the system's differential pressure and further compresses the cake in a disastrous cycle leading to plugging. Soft particles are extremely difficult to model, so for this model, it is assumed that the particles are hard and the cake is incompressible.

2) The fluid is Newtonian (viscosity is independent of shear)

3) All particles are retained on the surface and no other plugging mechanism occurs (i.e., no particles enter the pore and plug)

Development:

The basis for the cake formation model is given by Darcy's equation. This equation states that the volume of filtrate passing through the membrane is related to the system pressure and the resistance the membrane. This is shown in equation (1):

$$\frac{dV}{dt} = \frac{\Delta P A}{\mu R_{ini}}$$

Eqn.10

116

At some future time t, equation (1) can be revised as follows:

$$\frac{dV}{dt} = \frac{\Delta PA}{\mu R_t}$$

Eqn.2

In equation (2), R_t is the sum of the membrane resistance and the resistance of the built-up particulate cake. A formulation for R_t is shown in equation (3).

$$R_t = \frac{\alpha CV}{A_m} + R_m$$

Eqn.3

Substitution of equation (3) into equation (2) leads to the following equation:

$$\frac{dV}{dt} = \frac{\Delta PA}{\mu\left(\dfrac{\alpha CV}{A_m} + R_{ini}\right)}$$

Eqn.4

For constant pressure systems, equation (4) can be solved to yield the following characteristic equation:

$$\frac{t}{V} = \frac{\alpha C\mu}{2\Delta pa^2}V + \frac{\mu R_m}{\Delta PA} = \frac{\alpha C\mu}{2\Delta PA^2 V} + \frac{1}{M_o}$$

Eqn.5

Complete Pore Plugging Model

Assumptions:

1) Each particle participates in the plugging process by sealing one pore, and once a pore as been sealed, other particles do not enter that pore and superimpose on that particle.

2) Cake Formation is not allowed

3) The fluid is Newtonian (i.e., viscosity is independent of shear).

Development:

117

The basis for the complete pore plugging model is Poiseuille's law. The volume of filtrate is related to the membrane's pressure drop and physical properties as shown in equation (6):

$$\frac{dV}{dt} = \frac{\Pi \Delta P}{8\mu L} r_p^4 N_p \qquad \text{Eqn.6}$$

However, the number of open pores is a function of the initial number of open pores and of the number of plugging particles per unit volume of filtrate as shown in equation (7):

$$N_p = N_{po} - K_2 V \qquad \text{Eqn.7}$$

For constant pressure systems, substitution of (7) into (6) yields the following equation (10):

$$\frac{dV}{dt} = \frac{\Pi \Delta P A}{8\mu L} r_p^4 N_p^1 - \frac{\Pi \Delta P}{8\mu L} r_p^4 K_2 V \qquad \text{Eqn.8}$$

Integrating the volume with respect to time leads to the following characteristic equation:

$$V = \frac{N_{po}}{K_2}(1 - e^{-bt}) \qquad \text{Eqn.9}$$

Where

$$b = \frac{\Pi r_p^4 \Delta P K_2}{8\mu L} \qquad \text{Eqn.10}$$

Gradual Pore Plugging Model

Assumptions:

1. The fluid is Newtonian (i.e., viscosity is independent of shear).

Development:

Similar to the complete pore plugging model, the basis for the gradual pore plugging model is a modified Poiseuille's law (equation (6)). In this case, however, as the particles enter and adsorb to the pore walls, the pore diameter r_p decreases while the number of

pores remains constant. To determine the pore diameter reduction, a mass balance can be performed on a single pore. This can then be multiplied by the number of pores to relate the total mass of particles deposited to the reduction in pore diameter. The resulting mass balance is shown in equation (11):

$$CdV = -\rho_s L N_p 2\Pi r dr$$

Eqn.11

Integration of equation (114) yields the following:

$$CV = \rho_s \Pi LAN_p^1 (r_o^2 - r_p^2)$$

Eqn.12

For constant pressure systems, substitution of equation (12) into (6) and integration of the result leads to the following characteristic equation:

$$\frac{t}{V} = Gt + \frac{1}{M_0}$$

Eqn.13

Or

$$V = \frac{M_o t}{1 + M_o Gt}$$

Eqn.14

Where

$$G = \frac{C}{\Pi L \rho_s} \left(\frac{\Pi}{8 \mu L} \right)^{\frac{1}{2}} \left(\frac{\Delta P}{M_o N_p} \right)^{\frac{1}{2}}$$

Eqn.15

119

APPENDIX II

Analysis of Polysaccharides

Reagents

- 5 % phenol solution (Distilled H_2O)
- 95-97 % Sulphuric acid

Vials (Double Measurements)

- 1 ml of sample
- 1 ml of phenol solution, mix in whirli mixer
- 5 ml of conc. H_2SO_4 add in a stream to have good mixing (do not mix in Whirli mixer)
- leave 10 minutes at room temperature
- shake with hand and mix in Whirli mixer (cover vials)
- leave 30 minutes at room temperature
- Read absorption at 490 nm against standard in UV/VIS spectral photometer, program, "PS 5-100 mg/l". Concentrations are given in mg glucose equivalent/l